ABSTRACT

The concept of building concrete pressure vessels for gas-cooled nuclear reactors originated in France in the early 1960's. Shortly thereafter, prestressed concrete reactor vessels (PCRVs) began to be developed in this country, and recognition of this as a highly specialized field requiring particular expertise resulted in authorization in 1966 from the U.S. Atomic Energy Commission for Oak Ridge National Laboratory (ORNL) to conduct investigations in this area. A review of available literature on containments utilized for water-cooled reactors (i.e., pressurized-water and boiling-water reactors) initiated this activity. Following this review, various aspects of prestressed concrete pressure vessels were investigated with respect to reliability, structural performance, constructability, and economy. These investigations were conducted under the U.S. Department of Energy's (DOE) High-Temperature Gas-Cooled Reactor (HTGR) and Gas-Cooled Fast Breeder Reactor (GCFR) Programs. The overall objectives of these programs were to: (1) provide technical support to ongoing PCRV design activities, (2) contribute to the overall technological database, and (3) supply independent review and evaluation. Activities under these programs addressed many aspects of concrete technology and included investigations of high-strength and fibrous concrete materials; design, fabrication, testing, and analysis of models ranging in intricacy from a reinforced concrete beam to a cavity closure for a complete PCRV; development and evaluation of analytical methods to predict performance; evaluation of concrete behavior at elevated temperature and under multiaxial stress states; development and assessment of concrete embedment instrumentation systems; and reviews of relevant technology. ORNL's pilot work in this area contributed to the design and construction of the first U.S. gas-cooled reactor to use a prestressed concrete pressure vessel – Fort St. Vrain Nuclear Generating Station in Platteville, Colorado, which started operation in 1976. Concrete pressure vessel research in support of HTGRs ended when the concept of a modular HTGR started to be developed. Due to the smaller size of modular HTGRs, the concrete pressure vessels lost their size advantage and pressure vessel designs turned to steel. The PCRV-related research was followed by two additional DOE-sponsored programs - feasibility of use of prestressed concrete pressure vessels for coal gasification plants and evaluation of concrete behavior at elevated temperature in support of the Clinch River Breeder Reactor Project. Prestressed concrete pressure vessel designs were developed for two coal gasification processes: Synthane and Hygas. In support of the Clinch River Breeder Reactor, normal and lightweight concrete mix designs were developed and concrete mechanical and physical properties determined at temperature to 621 C. Prestressed concrete pressure vessel activities then shifted to studies sponsored by the U.S. Nuclear Regulatory Commission (NRC) addressing containments and other safety-related structures for light-water reactors. Activities included evaluations of Regulatory Guides addressing containment inspections, and aging management of safety-related concrete structures and containment pressure boundary components. Primary program accomplishments under the concrete aging program include formulation of a Structural Materials Information Center that contains data and information on the time variation of material properties under the influence of pertinent environmental stressors and aging factors for 144 materials, an aging assessment methodology to identify critical concrete structures and degradation factors that can potentially impact their performance, guidelines and evaluation criteria for use in condition assessments of reinforced concrete structures, and a reliability-based methodology for current condition assessments, estimations of future performance, and development of in-service inspection/maintenance strategies for reinforced concrete nuclear power plant structures. In addition, in-depth evaluations were conducted of several nondestructive evaluation and repair-related technologies to develop guidance on their applicability. Containment pressure boundary component-related activities include development of a degradation assessment methodology; reviews of techniques and methods for inspection and repair of containment metallic pressure boundaries; evaluation of candidate techniques for inspection of inaccessible regions of containment metallic pressure boundaries; establishment of a methodology for reliability-based condition assessments of steel containments and liners; and fragility assessments of steel containments with localized corrosion. The aging work for the NRC is currently ongoing. Although activities address nuclear power plant concrete structures, almost all of the results are applicable to general civil engineering structures.

Since initiation of the Concrete and Containment Technology Program at ORNL, over 350 technical reports or papers have been prepared. Program personnel also have been actively involved in National and International technical committees with program results forming the basis for several documents published by these committees. Contained in the balance of this report is a summary of activities that have taken place under this program.

ORNL/TM-2002/213

OAK RIDGE
NATIONAL LABORATORY

MANAGED BY UT-BATTELLE
FOR THE DEPARTMENT OF ENERGY

ACTIVITIES UNDER THE CONCRETE AND CONTAINMENT TECHNOLOGY PROGRAM AT ORNL

December 2002

D. J. Naus

UT-BATTELLE

ORNL-27 (4-00)

DOCUMENT AVAILABILITY

Reports produced after January 1, 1996, are generally available free via the U.S. Department of Energy (DOE) Information Bridge:

Web site: http://www.osti.gov/bridge

Reports produced before January 1, 1996, may be purchased by members of the public from the following source:

National Technical Information Service
5285 Port Royal Road
Springfield, VA 22161
Telephone: 703-605-6000 (1-800-553-6847)
TDD: 703-487-4639
Fax: 703-605-6900
E-mail: info@ntis.fedworld.gov
Web site: http://www.ntis.gov/support/ordernowabout.htm

Reports are available to DOE employees, DOE contractors, Energy Technology Data Exchange (ETDE) representatives, and International Nuclear Information System (INIS) representatives from the following source:

Office of Scientific and Technical Information
P.O. Box 62
Oak Ridge, TN 37831
Telephone: 865-576-8401
Fax: 865-576-5728
E-mail: reports@adonis.osti.gov
Web site: http://www.osti.gov/contact.html

This report was prepared as an account of work sponsored by an agency of the United States Government. Neither the United States government nor any agency thereof, nor any of their employees, makes any warranty, express or implied, or assumes any legal liability or responsibility for the accuracy, completeness, or usefulness of any information, apparatus, product, or process disclosed, or represents that its use would not infringe privately owned rights. Reference herein to any specific commercial product, process, or service by trade name, trademark, manufacturer, or otherwise, does not necessarily constitute or imply its endorsement, recommendation, or favoring by the United States Government or any agency thereof. The views and opinions of authors expressed herein do not necessarily state or reflect those of the United States Government or any agency thereof.

ORNL/TM-2002/213

Metals and Ceramics Division

ACTIVITIES UNDER THE CONCRETE AND CONTAINMENT TECHNOLOGY PROGRAM AT ORNL

D. J. Naus

December 2002

Prepared by the
OAK RIDGE NATIONAL LABORATORY
Oak Ridge, Tennessee 37831
managed by
UT-BATTELLE, LLC
for the
U.S. Department of Energy
under Contract No. DE-AC05-00OR22725

CONTENTS

Page

LIST OF FIGURES v

LIST OF TABLES ix

ACKNOWLEDGMENTS xi

ABSTRACT xiii

1. INTRODUCTION 1

2. CONCRETE PRESSURE VESSELS 3
   2.1 PRESTRESSED CONCRETE REACTOR VESSELS (PCRVS) 3
   2.2 CONCRETE CONTAINMENT VESSELS (CCVS) 3

3. CONCRETE RESEARCH STUDIES 5
   3.1. CONCRETE CONTAINMENT VESSELS FOR NUCLEAR REACTORS 6
   3.2. APPLICATION OF PRESTRESSED CONCRETE PRESSURE VESSELS TO COAL GASIFICATION PLANTS 6
   3.3 ELEVATED-TEMPERATURE BEHAVIOR OF CONCRETE AND THE CONCRETE-STEEL REINFORCING BAR BOND 7
      3.3.1 Concrete Behavior at Elevated Temperature 7
      3.3.2 Concrete-Steel Reinforcing Bar Bond 7
      3.3.3 Clinch River Breeder Reactor Elevated Temperature Concrete Properties 8
      3.3.4 Time-Dependent Deformations Under Elevated Temperature and Multiaxial Loadings 11
   3.4 MODEL TESTING 12
      3.4.1 Size Effect 12
      3.4.2 Thermal Cylinder Experiment 12
      3.4.3 PCRV Head Failures 13
      3.4.4 Moisture Migration 13
      3.4.5 PCRV Concrete Closure Plugs 14
      3.4.6 Grouted vs Nongrouted Tendons 17
         3.4.6.1 Grouted-nongrouted tendon behavior 17
         3.4.6.2 Evaluation of selected "new" material systems 18
         3.4.6.3 Bench-scale corrosion tests 20
         3.4.6.4 Acoustic emission evaluation 22
   3.5 MATERIALS EVALUATION AND TESTING 24
      3.5.1 Development of High-Strength Concrete Materials and Model Testing Techniques 24
         3.5.1.1 High-strength concrete materials 24
         3.5.1.2 Model testing techniques 27
      3.5.2 Testing of Thermal Barrier Hard Ceramic Pad Materials 28
   3.6 STATE-OF-THE-ART STUDIES AND TECHNOLOGY ASSESSMENTS 29
      3.6.1 Major PCRV Components 29
         3.6.1.1 Concrete properties in a nuclear environment 29
         3.6.1.2 Steel reinforcement and post-tensioning systems 30
         3.6.1.3 Liner, insulation and cooling systems 31
      3.6.2 Concrete Embedment Instrumentation Studies 33
         3.6.2.1 General gage performance 34
         3.6.2.2 Gage performance in "simulated" PCRV environment 36
         3.6.2.3 Gage performance under extreme operating conditions 37
      3.6.3 Optimized PCRV for HTGR/SC Plant 39
      3.6.4 Pebble-Bed-Fueled vs Prismatic-Fueled HTGRs 39
      3.6.5 Pressure Vessel Concepts for HTGR Modular Reactor Systems 40

Page

3.7 U.S. NUCLEAR REGULATORY COMMISSION-RELATED ACTIVITIES 40
3.7.1 In-Service Inspections of Greased Tendons in Prestressed Concrete Containments 40
3.7.2 Evaluation of Containment Leak-Rate Testing Criteria 41
3.7.3 Aging Management of Safety-Related Concrete Structures 42
3.7.3.1 Concrete containment aging program 45
3.7.3.2 Structural aging program 46
3.7.3.3 Concrete aging conclusions 57
3.7.4 Aging Management of Containment Pressure Boundary Components 58
3.7.4.1 Steel containment/liner assessment and root-cause resolution practices 60
3.7.4.2 Reliability-based condition assessment 69
3.7.4.3 Application of results 74
3.8 TECHNICAL COMMITTEE ACTIVITIES 74

4. REFERENCES 77

LIST OF FIGURES

Figure		Page
1	Cross-section of PCRV for HTGR.	3
2	Examples of reinforced and prestressed concrete nuclear power plant containments	4
3	Basic program activities.	5
4	Cross section of Fort St. Vrain PCRV for 330 MW(e) HTGR	5
5	Conceptual designs for coal gasification prestressed concrete vessels.	6
6	Test specimen	7
7	Effect of temperature and thermal cycling	7
8	Concrete-rebar bond test setup	8
9	Bond slip and unconfined compression test results	8
10	Open-hot test setup and residual compressive strength results	9
11	Unconfined compressive strength test setup	9
12	Shear test furnaces during specimen heating	9
13	Concrete-rebar bond test setup	10
14	Sustained load test setup	10
15	Hanging wire method for length change	10
16	Dilatometer-based apparatus	10
17	Experimental setup for measuring thermal diffusivity and conductivity	11
18	Oil bath for cooling test	11
19	Schematic of creep test setup	11
20	Effect of radial stress on axial creep strain	11
21	Prototype and model types	12
22	Thermal cylinder model	12
23	Head failure model being prepared for test	13
24	Model post-test: end-slab flexure failure	13
25	Schematic of moisture migration model showing instrumentation locations	14
26	Moisture distribution at end of testing	14
27	GCFR PCRV cross section showing closure plug locations	14
28	Schematic of closure plug model test fixture	15
29	Model prior to placement into test fixture for pressurization	15
30	GCFR PCRV closure plug model test facility	15
31	Model after pressurization to 75.84 MPa	16
32	Model after sectioning	16
33	Post-test view of inner and outer failed sections of half-thickness model	16
34	Central core cavity closure prototype	17
35	Model after pressurization to 79.3 MPa	17
36	Setup for testing beams in flexure	18
37	Effect of post-tensioning level	18
38	Bond transfer length test specimen	18
39	Relative bond transfer length results	18
40	Bond pull-out tensioning fixture	19
41	Bond pull-out test specimen	19
42	Bond pull-out test setup	19
43	Relative load-slip	19
44	Structural and fibrous concrete load versus deflection behavior	20
45	Stressed wire time to failure test setup	20
46	Nonstressed tendon NH_4NO_3 and $NaC\ell$ exposure test setup	20
47	Effect of percent failure load on failure time: $H_2S + H_2O$ environment	21
48	Effect of flaw size on time to failure, tendon stressed to 60% failure: $H_2S + H_2O$ environment	21
49	AE test setup: concrete cylinders	22
50	Acoustic emission test results: medium-strength concrete	23
51	AE test setup: flexure	23
52	AE multi-channel source-location system	23
53	Beam load-deflection compared to AE results	24
54	Nongrouted tendon AE results showing good correlation to crack locations	24

Figure		Page

55 Grouted tendon AE results showing effect of increased cracking 24
56 PCRV for HTGR steam cycle/cogeneration 25
57 Optimum cementitious materials test results: 9.5-mm maximum size aggregate 25
58 Optimum cementitious materials test results: 38-mm maximum size aggregate 25
59 Effect of partial cement replacement with fly ash: 9.5-mm maximum size aggregate 26
60 Effect of partial cement replacement with fly ash: 38-mm maximum size aggregate 26
61 Effect of age and fly ash content on compressive strength 26
62 Effect of age and fly ash content on modulus of elasticity 27
63 PCRV plain concrete model post-test 28
64 PCRV fibrous concrete model post-test 28
65 Ceramic pad test setup 28
66 Schematic of test fixture 28
67 Data reported in the literature on the effects of elevated temperature on concrete compressive strength for specimens tested either after returning to room temperature (cold) or tested at temperature (hot) 30
68 Data reported in literature on effects of radiation on concrete compressive strength and modulus 30
69 Simultaneous stressing of multistrand post-tensioning systems 31
70 Schematics of hot- and cold-liner concepts 32
71 Liner, insulation, and cooling system for HTGR-SC plant 33
72 Vibrating-wire strain gages 34
73 Calibration test specimen 35
74 Calibration results: VWSG Type G, specimen 1 35
75 Reinforcement cage used to maintain gage alignment during specimen fabrication 36
76 Gage stability test specimen 36
77 Gage stability test results: unbonded wire resistance meters 36
78 Insulated test specimen: "simulated" PCRV environment 37
79 Example of results for "simulated" PCRV environment 37
80 Alkaline-water immersion test setup 38
81 Elevation view of PCRV and containment structure for gas-reheat HTGR-SC plant 39
82 Example of tolerance band for prestress 41
83 Nuclear power plant initial operating license expiration 42
84 Concrete containment under construction 44
85 Examples of environmental stressor-related degradation 44
86 LWR concrete component problem areas 45
87 Structural materials information center 46
88 Long-term concrete compressive strength results 47
89 Summary of the study reviewing and assessing service life models 47
90 Grease leakage at Trojan Plant 48
91 Coring to obtain grease migration samples 48
92 Degradation assessment methodology 49
93 Location of steel reinforcement 49
94 Mean degradation functions of one-way slab 53
95 Failure probability of one-way slab 53
96 Comparison of measured and calculated shear strength 54
97 Mean degradation function of wall in shear without repair 56
98 Failure probability of wall in shear without repair 56
99 Hazard function of wall in shear without repair 56
100 Cross-section of BWR MK I steel containment 58
101 Containment pressure boundary corrosion examples 59
102 Degradation assessment methodology based on ASME Section XI, Subsection IWE 61
103 Examples of NDE methods 62
104 Simulation scenario for steel liner-reinforced concrete containment 65
105 Simulation scenario for steel containment 65
106 Experimental results evaluating defect geometry and depth 66
107 Experimental results evaluating interface conditions and test setup 66
108 Magnetostrictive sensor test setup used to generate and detect wave 67
109 Schematics of plate specimens used to benchmark several aspects of guided wave inspection 67
110 Experimental results using horizontal shear waves 68

Figure **Page**

111 Experimental results using Lamb guided waves 69
112 Time-dependent reliability of steel cylindrical shell: effect of corrosion and load rate 72
113 Containment fragilities for postulated corrosion 73

LIST OF TABLES

Table		Page
1	General embedment strain meter performance characteristics.	34
2	Results of alkaline-water immersion test	38
3	Statistical properties of strength and load	54
4	Statistical data for steel cylinder	71

ACKNOWLEDGMENTS

Research described in this report was sponsored by the U.S. Department of Energy and the Office of Regulatory Research of the U.S. Nuclear Regulatory Commission. The findings and opinions expressed in this report are those of the author and do not reflect the views of either the U.S. Department of Energy or U.S. Nuclear Regulatory Commission.

The author would like to thank the many participants who have contributed to the Concrete and Containment Technology Program over the years. In particular, the author would like to acknowledge the many contributions of C.B. Oland and J.M. Corum of Oak Ridge National Laboratory, J. P. Callahan of Albuquerque, New Mexico, and Bruce Ellingwood of the Georgia Institute of Technology.

ABSTRACT

The concept of building concrete pressure vessels for gas-cooled nuclear reactors originated in France in the early 1960's. Shortly thereafter, prestressed concrete reactor vessels (PCRVs) began to be developed in this country, and recognition of this as a highly specialized field requiring particular expertise resulted in authorization in 1966 from the U.S. Atomic Energy Commission for Oak Ridge National Laboratory (ORNL) to conduct investigations in this area. A review of available literature on containments utilized for water-cooled reactors (i.e., pressurized-water and boiling-water reactors) initiated this activity. Following this review, various aspects of prestressed concrete pressure vessels were investigated with respect to reliability, structural performance, constructability, and economy. These investigations were conducted under the U.S. Department of Energy's (DOE) High-Temperature Gas-Cooled Reactor (HTGR) and Gas-Cooled Fast Breeder Reactor (GCFR) Programs. The overall objectives of these programs were to: (1) provide technical support to ongoing PCRV design activities, (2) contribute to the overall technological database, and (3) supply independent review and evaluation. Activities under these programs addressed many aspects of concrete technology and included investigations of high-strength and fibrous concrete materials; design, fabrication, testing, and analysis of models ranging in intricacy from a reinforced concrete beam to a cavity closure for a complete PCRV; development and evaluation of analytical methods to predict performance; evaluation of concrete behavior at elevated temperature and under multiaxial stress states; development and assessment of concrete embedment instrumentation systems; and reviews of relevant technology. ORNL's pilot work in this area contributed to the design and construction of the first U.S. gas-cooled reactor to use a prestressed concrete pressure vessel – Fort St. Vrain Nuclear Generating Station in Platteville, Colorado, which started operation in 1976. Concrete pressure vessel research in support of HTGRs ended when the concept of a modular HTGR started to be developed. Due to the smaller size of modular HTGRs, the concrete pressure vessels lost their size advantage and pressure vessel designs turned to steel. The PCRV-related research was followed by two additional DOE-sponsored programs - feasibility of use of prestressed concrete pressure vessels for coal gasification plants and evaluation of concrete behavior at elevated temperature in support of the Clinch River Breeder Reactor Project. Prestressed concrete pressure vessel designs were developed for two coal gasification processes: Synthane and Hygas. In support of the Clinch River Breeder Reactor, normal and lightweight concrete mix designs were developed and concrete mechanical and physical properties determined at temperature to 621 C. Prestressed concrete pressure vessel activities then shifted to studies sponsored by the U.S. Nuclear Regulatory Commission (NRC) addressing containments and other safety-related structures for light-water reactors. Activities included evaluations of Regulatory Guides addressing containment inspections, and aging management of safety-related concrete structures and containment pressure boundary components. Primary program accomplishments under the concrete aging program include formulation of a Structural Materials Information Center that contains data and information on the time variation of material properties under the influence of pertinent environmental stressors and aging factors for 144 materials, an aging assessment methodology to identify critical concrete structures and degradation factors that can potentially impact their performance, guidelines and evaluation criteria for use in condition assessments of reinforced concrete structures, and a reliability-based methodology for current condition assessments, estimations of future performance, and development of in-service inspection/maintenance strategies for reinforced concrete nuclear power plant structures. In addition, in-depth evaluations were conducted of several nondestructive evaluation and repair-related technologies to develop guidance on their applicability. Containment pressure boundary component-related activities include development of a degradation assessment methodology; reviews of techniques and methods for inspection and repair of containment metallic pressure boundaries; evaluation of candidate techniques for inspection of inaccessible regions of containment metallic pressure boundaries; establishment of a methodology for reliability-based condition assessments of steel containments and liners; and fragility assessments of steel containments with localized corrosion. The aging work for the NRC is currently ongoing. Although activities address nuclear power plant concrete structures, almost all of the results are applicable to general civil engineering structures.

Since initiation of the Concrete and Containment Technology Program at ORNL, over 350 technical reports or papers have been prepared. Program personnel also have been actively involved in National and International technical committees with program results forming the basis for several documents published by these committees. Contained in the balance of this report is a summary of activities that have taken place under this program.

1. INTRODUCTION

The ability of concrete to meet the requirements of the function for which it was intended depends on a variety of factors, such as selection of the aggregates, cement, water, and admixtures used to make it; mixing and placing of the concrete; correct curing; and proper design and reinforcement detailing. Concrete is strong in compression but has relatively low tensile strength so it is necessary to add reinforcing steel or to use steel tendons to "prestress" it for certain uses, such as pressure vessels. Concrete, whose strength, durability, and comparatively low cost make it one of the most important building materials used in construction today, offers a number of attractive design and engineering features for construction of containment and process vessels used in nuclear and non-nuclear energy systems. Concrete vessels can be fabricated in virtually any size and shape, they perform well from an operational safety standpoint, and they are easily fabricated on site with relatively inexpensive materials.

2. CONCRETE PRESSURE VESSELS

Concrete pressure vessels are essentially spaced steel structures since their strength is derived from a multitude of linear steel elements made up of deformed reinforcing bars or a combination of deformed steel bars and prestressing steel. Nuclear power plant containments house the primary circuit and have a relatively passive function under normal operating conditions. The primary purpose of a nuclear power plant containment is to prevent the release of fission products to the environment and to provide a shield against radiation (i.e., separate the reactor and other safety significant systems and equipment from outside environment). As such, the containment is designed for a series of postulated incidents or accidents including leakage and even rupture of the primary cooling system and its consequences. The containment is also designed to provide protection against severe extreme events (e.g. earthquakes, floods, tornados, and missile impact). In the unlikely event that severe overpressurization should occur causing the concrete containment to begin to fail, it does so in a slow, predictable manner, by cracking vertically in the side wall and slowly venting the excess pressure. Even when a concrete vessel cracks, it is still a very significant structure in terms of safety, and continues to have the capability to contain whatever is inside. In addition to design considerations, nuclear power plant containments are constructed, operated, and controlled in such a way as to reduce the consequences of an accident to an acceptable level.

2.1 PRESRESSED CONCRETE REACTOR VESSELS (PCRVs)

The design of PCRVs for high-temperature gas-cooled reactor systems is based on the integral concept (i.e., the entire pressurized gas circuit composed of the reactor core, primary coolant system, and portions of the secondary coolant system is contained within a single vessel). Prestressed concrete pressure vessels used for High-Temperature Gas-Cooled Reactor (HTGR) systems are generally massive, thick-walled, right circular cylinders having flat heads. Initially they were single-cavity, but have evolved to incorporate a multi-cavity design. In the multi-cavity design the reactor is located within a large central cavity that is surrounded by smaller cylindrical cavities containing the primary cooling system and housing auxiliary cooling loops or pressure relief wells (Figure 1). The steam generators and helium circulators are located in the primary cooling system cavities that are connected at the top and bottom to the central core cavity by radial ducts and are sealed at the upper end by plugs that support the helium circulators. A continuous welded steel liner is attached to the walls of each cavity and serves to contain the primary coolant while the concrete vessel supports the liner and provides resistance to the coolant pressure loading. A thermal barrier and network of cooling tubes are attached to the liner to maintain the specified temperature (≤65 C) at the liner-concrete interface during normal full-power operation.

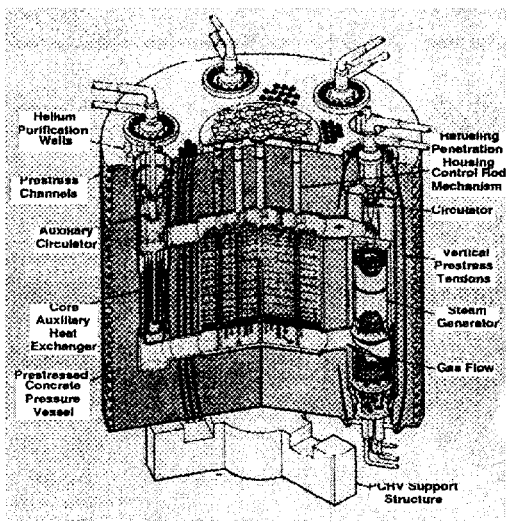

Figure 1. Cross-section of PCRV for HTGR.

2.2 CONCRETE CONTAINMENT VESSELS (CCVs)

Containments for light-water reactor plants are shell-type concrete structures, reinforced, or more frequently prestressed, usually cylindrical in shape, with varying dimensions depending of the type of nuclear power plant and the specific features of the containment (e.g., either single- or double-wall construction). Leaktightness is generally provided by a mild steel liner that is integral with, attached to, and supported by the concrete vessel at its inner surface. Containments are complex structures considering that they have numerous penetrations ranging in size from a few centimeters to several meters in diameter, the magnitudes and numbers of loads imposed, and the specific regulations and associated inspections performed. Figure 2 presents examples of reinforced and post-tensioned concrete containments.

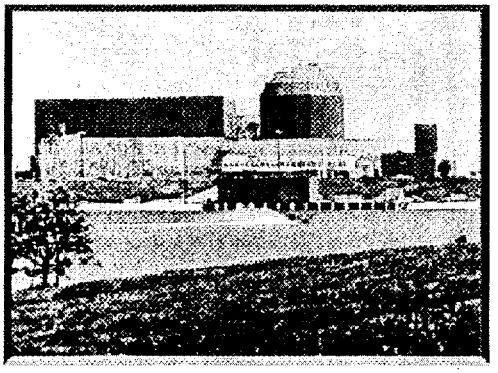

Reinforced Concrete Containment

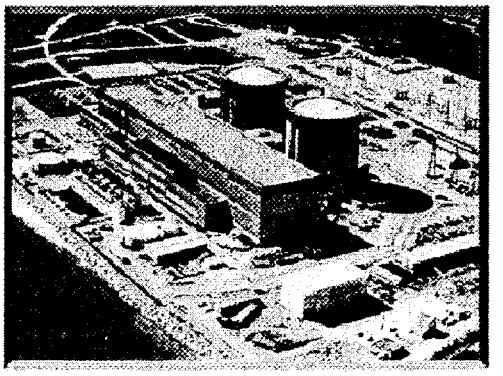

Prestressed Concrete Containment

Figure 2. Examples of reinforced and prestressed concrete nuclear power plant containments.

3. CONCRETE RESEARCH STUDIES

The concept of building concrete vessels for gas-cooled nuclear reactors originated in France in the early 1960's. Shortly thereafter, prestressed concrete reactor vessels (PCRVs) began to be developed in this country, and recognition of this as a highly specialized field requiring particular expertise resulted in authorization in 1966 from the U.S. Atomic Energy Commission for ORNL to conduct investigations in this area. A review of available literature on containments utilized for water-cooled reactors (i.e., pressurized-water and boiling-water reactors) initiated this activity. Following this review, various aspects of prestressed concrete pressure vessels were investigated with respect to reliability, structural performance, constructability, and economy. These investigations were conducted under the High-Temperature Gas-Cooled Reactor (HTGR) and Gas-Cooled Fast Breeder Reactor (GCFR) Programs. The overall objectives of these programs were to: (1) provide technical support to ongoing PCRV design activities, (2) contribute to the overall technological database, and (3) supply independent review and evaluation. The basic activities and their interaction for meeting these objectives are shown in Fig. 3. Primary areas of interest were finite-element analysis methods development, materials and structural behavior tests, instrumentation evaluation and development, and structural model tests. ORNL's pilot work in this area contributed to the design and construction of the first U.S. gas-cooled reactor to use a prestressed concrete pressure vessel–the Public Service Company of Colorado's Fort St. Vrain Nuclear Generating Station in Platteville, Colorado, which started operation in 1976 (Figure 4).♦

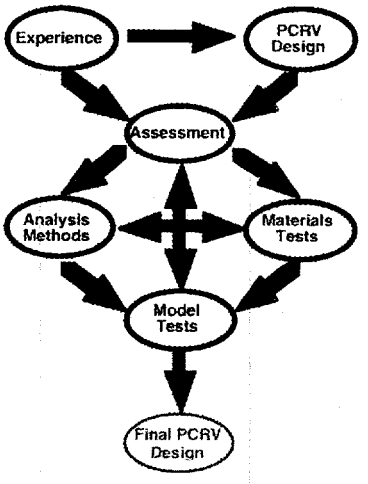

Figure 3. Basic program activities.

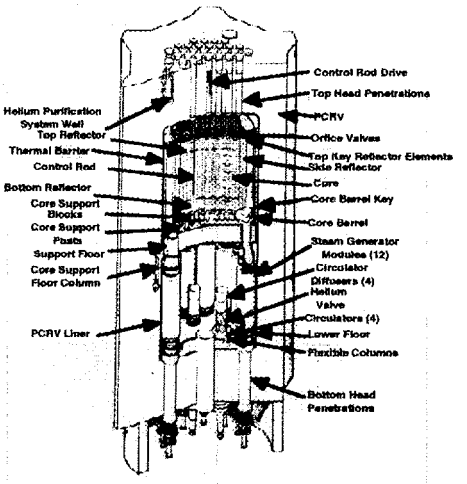

Figure 4. Cross section of Fort St. Vrain PCRV for 330 MW(e) HTGR.

Concrete pressure vessel research in support of HTGRs ended in the early 1980s when the concept of a modular HTGR started to be developed. Due to the smaller size of modular HTGRs, the concrete pressure vessels lost their size advantage and pressure vessel designs turned to steel. The PCRV-related research was followed by programs assessing the feasibility of use of prestressed concrete pressure vessels for coal gasification plants and evaluation of concrete behavior at elevated temperature in support of the Clinch River Breeder Reactor Project. Prestressed concrete pressure vessel designs were developed for two coal gasification processes: Synthane and Hygas. In support of the Clinch River Breeder Reactor, normal and lightweight concrete mix designs were developed and concrete mechanical and physical properties determined at temperatures to 621 C. Following this, prestressed concrete pressure vessel activities shifted to studies primarily addressing containments for light-water reactors. Primary activities included evaluations of U.S. Nuclear Regulatory Commission Regulatory Guides and aging of nuclear power plant containments and other safety-related structures. This work is currently ongoing.

To date, over 350 technical reports or papers have been prepared under the Concrete and Containment Technology Program at ORNL. Program personnel also have been actively involved in National and International technical

---

♦ Public Service Company of Colorado is now Excel Energy. Nuclear power operations at Fort St. Vrain came to a close in 1989 due to series of problems at the plant. Plant decommissioning was completed in 1992.

committees with program results forming the basis for several documents publishedby these committees. More detailed information on several of the research activities conducted under this program is provided below.

3.1 CONCRETE CONTAINMENT VESSELS FOR NUCLEAR REACTORS

Initial work under the concrete program addressed a review of then current practices in the design and construction of prestressed and reinforced concrete secondary containments for water-cooled nuclear reactors. The review included the identification of a wide range of design and construction factors, including [1,2]:

- different types of concrete containments;
- criteria used in the design of concrete containments;
- predicted environmental and service conditions likely to be encountered, along with an evaluation of the effects of these conditions on structural behavior;
- modes of failure and the possibility of using models to study actual behavior;
- problems in earthquake- and tornado-resistant designs and in missile protection;
- material properties and methods of selecting critical materials for service in environments of interest;
- need and importance of quality assurance in both design and construction;
- codes and standards applied in concrete technology, and areas where these standards appear to require augmentation or revision; and
- need for developing operational testing requirements for concrete containments.

3.2 APPLICATION OF PRESTRESSED CONCRETE PRESSURE VESSELS TO COAL GASIFICATION PLANTS

Utilization of PCRVs for commercial-size coal gasification systems was evaluated. Problem areas were identified, and a test program defined for concept verification, and performance examination and demonstration. Conceptual designs were developed for two gasifier vessels to provide vehicles for assessment: two-train plants based on the Hygas and Synthane processes (Fig. 5). These systems require pressure vessels 47 to 82 meters high with an internal diameter of

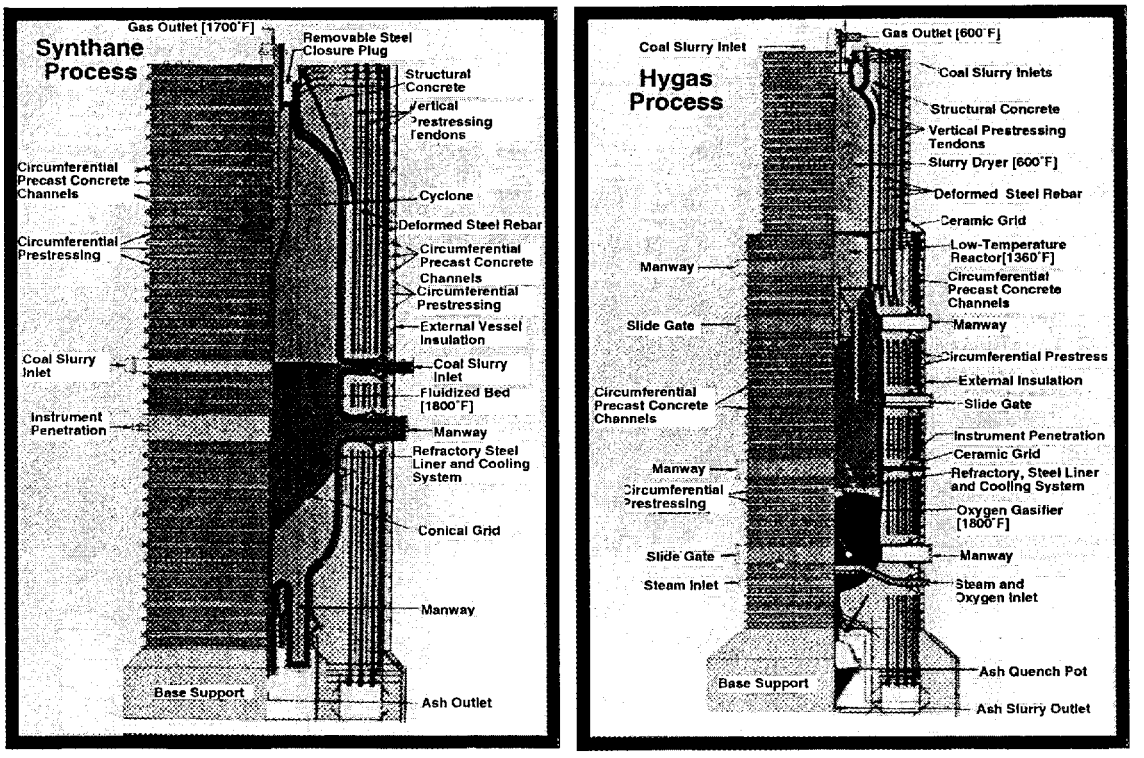

Figure 5. Conceptual designs for coal gasification prestressed concrete vessels.

8 to 10 meters. In preparing these designs, extensive use was made of developments for gas-cooled nuclear reactor containment vessels. Because of the harsh environment that they contain, gasifier vessels must also be accessible for routine maintenance and repair. Results of these studies indicated that the use of prestressed concrete pressure vessels in applications where large, heavy-walled steel vessels were formerly utilized is both technically and economically feasible. A follow-up study was outlined to develop supporting design data, but was not implemented. More detailed information on design of the prestressed concrete pressure vessels, and their insulation and liner systems, is available [3].

3.3 ELEVATED-TEMPERATURE BEHAVIOR OF CONCRETE AND THE CONCRETE-STEEL REINFORCING BAR BOND

Studies have been conducted to determine the effects of elevated temperature on concrete materials and on the concrete-reinforcing bar (rebar) bond.

3.3.1 Concrete Behavior At Elevated Temperature

A study was conducted to determine the influence of thermal exposures on the mechanical characteristics of concrete and to evaluate associated instrumentation, testing and sealing techniques. Tests were conducted on 15.2-by 45.7-cm long sealed concrete cylinders (Fig. 6) to determine the effect of the following on the stress-strain relationship of concrete: (1) sustained temperature of 149 C, (2) number of thermal cycles from 21 to 149 to 21 C (Fig. 7), (3) influence of permitting moisture to escape freely from the concrete during heat treatment as compared to the case where the moisture was contained by the presence of a sealing jacket, and (4) influence of testing the concrete at 149 C versus permitting the specimens to cool to 21 C prior to testing. Results showed that: (1) the instrumentation, sealing and testing techniques developed were successful; (2) thermal coefficient of expansion of concrete increased with a decrease in rate of heating; (3) when moisture was not permitted to escape freely, significant residual expansion was observed after the first thermal cycle and this expansion increased with number of cycles and/or duration of exposure; and (4) when the moisture was contained within the specimen, the compressive strength was affected significantly with the longer the duration of exposure at 149°C the lower the concrete strength and stiffness [4].

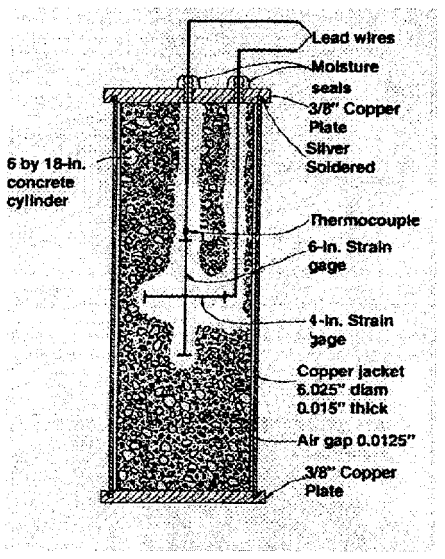

Figure 6. Test specimen.

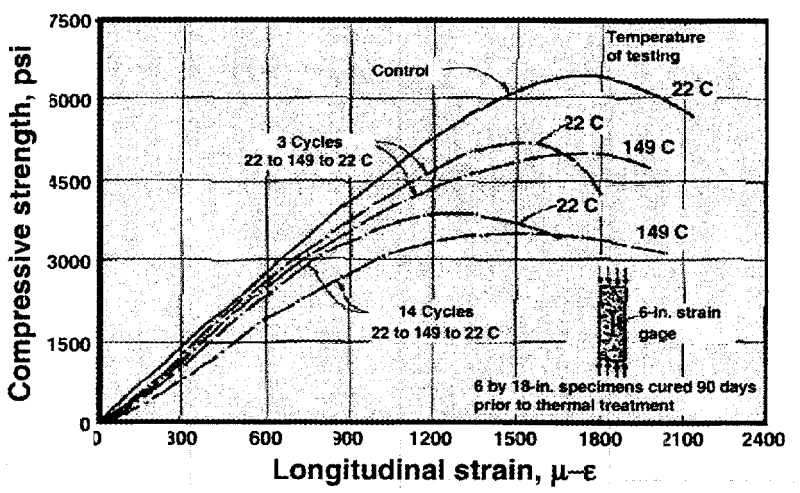

Figure 7. Effect of temperature and thermal cycling.

3.3.2 Concrete-Steel Reinforcing Bar Bond

A series of bond pull-out tests was conducted to determine the effect of elevated temperature on the bond strength between concrete and deformed steel reinforcement. In the tests 15.9 cm concrete cubes with a No. 6 deformed reinforcing bar centrally located and extending through the cubes were cast using a 27.6 MPa limestone aggregate concrete. The specimens were moist cured 90 days prior to heating. Two sets of three specimens each were heated at a rate of 17 C per hour to temperatures of 66 and 149 C, respectively. Each specimen was permitted to thermally stabilize

at the specified temperature for 14 days and then transferred, while still hot, to a universal testing machine and evaluated according to ASTM C 234 which provided the test specifications for comparing concretes on the basis of bond developed with reinforcing steel (Fig. 8). Results indicated little difference in bond strength between specimens tested at 24 and 149 C; however, the bond strengths of specimens thermally stabilized at 66 C were consistently below the comparable 24 C value (Fig. 9) [5].

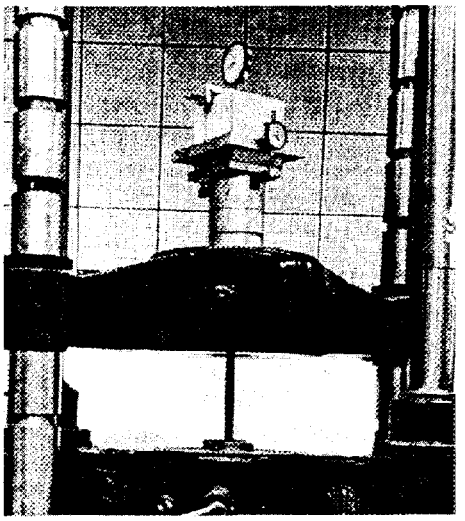

Figure 8. Concrete-rebar bond test setup.

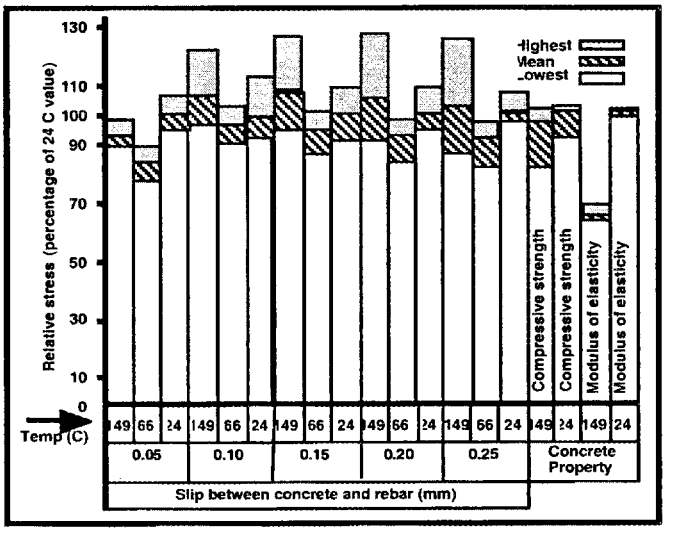

Figure 9. Bond slip and unconfined compression test results.

3.3.3 Clinch River Breeder Reactor Elevated Temperature Concrete Properties

In support of the design of the Clinch River Breeder Reactor with respect to postulated accident conditions, two test programs have been conducted: (1) uniaxial compressive strength at temperatures reaching 760 C, and (2) variations in mechanical and thermal properties at temperatures reaching 621 C.

A limited testing program was conducted as part of an ongoing investigation of the effects of elevated temperature on mature limestone aggregate concrete compressive strength and modulus of elasticity. Twenty-four 15.2 by 30.5 cm cylindrical test specimens were supplied by the Tennessee Valley Authority. The specimens having a design compressive strength of 27.6 MPa had been cast during construction of the Watts Bar Nuclear Power Plant and varied in age from 263 to 587 days at time of test. Prior to testing, the specimens were continuously moist cured. Two sets of conditions were employed to determine the response of the concrete to sustained elevated temperature: (1) open-hot (tested at temperature, moisture free to leave concrete) and (2) closed-cold (tested at room temperature, moisture loss restricted). These conditions were selected to provide upper and lower bounds, respectively, on compressive strength. Each open-hot specimen was contained within its own electrical resistance furnace. The closed-cold apparatus was designed to simulate the moisture environment existing in mass concrete when a portion of the structure is subjected to localized heating and subsequent cooling. For this test condition either two or three cylinders were sealed in stainless steel pressure vessels. A pressure relief valve and condenser were used to control moisture. Both the open-hot and closed-cold specimens were heated at a rate of 14 C/hr to the specified heat soak temperature (i.e., 177, 371, 566, and 760 C) where the temperature was maintained for 14 days. At conclusion of the heat-soak period, the open-hot specimens while in their furnace were moved to the testing machine and tested in compression until failure (Fig. 10). Axial strain was determined using a quartz rod-based system. Upon completion of the 14-day sustained heating period, the closed cold specimens were permitted to cool to room temperature at a rate that did not exceed 14 C/hr. The cylinders were instrumented with wire-resistance strain gages and tested to failure in compression. As noted in Fig. 10, both the open-hot and closed-cold specimens exhibited a steady decrease in compressive strength with increasing exposure temperature. Modulus of elasticity results exhibited a similar trend [6].

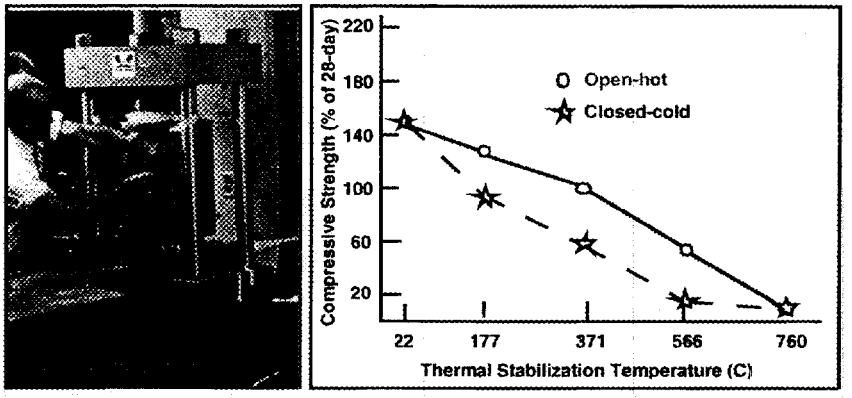

Figure 10. Open-hot test setup and residual compressive strength results

The second test program examined the variations in mechanical and thermal properties of a structural limestone aggregate and a lightweight insulating concrete exposed to elevated temperatures up to 621 C. Because of the temperature exposure of interest, the program required the development of specialized test methods and instrumentation systems. Five test series were conducted under this program: (1) unconfined compression, (2) "modified" shear, (3) concrete-steel reinforcement bond, (4) sustained load, and (5) physical properties. Cylindrical test specimens 0.30 by 0.15–m-diameter were used for the control (reference), unconfined compression, and sustained load test series. "S"-shaped parallelepiped specimens were used for the "modified" shear tests and 0.3 m cube concrete specimens containing a No. 11 steel reinforcing bar embedded vertically were used for the concrete-steel reinforcement bond tests. Either prismatic or cylindrical test specimens were used for the physical property tests. Structural limestone aggregate specimens cured in a lime-saturated water solution were used for all test series, with a minimum of three test specimens tested for each test condition. Lightweight concrete specimens cured in a lime-saturated water solution for 28 days, followed by storage in an environmental chamber until testing, were evaluated only in the unconfined compression test series. Each compression test specimen was contained within its own electrical resistance furnace. After installing thermocouples, specimens were heated at 17 C/hr to their designated thermal stabilization temperatures, which ranged up to 621 C. After maintaining the thermal stabilization temperature for 14 days (28-days in some cases), the furnace containing a test specimen was positioned in the testing machine, instrumentation calibrated, and the specimen loaded in compression while at temperature until failure occurred (Fig. 11). Compressive strength, modulus of elasticity, and Poisson's ratio data were determined for each specimen. Specimen preparation, heatup, and thermal stabilization procedures for the "modified" shear test series were similar to those for the unconfined compression test series. After 14-days thermal stabilization, the furnace containing the specimen (Fig. 12) was positioned in the testing machine and the specimen loaded in compression to failure. Relative shear strength was evaluated by dividing the maximum load by the area of

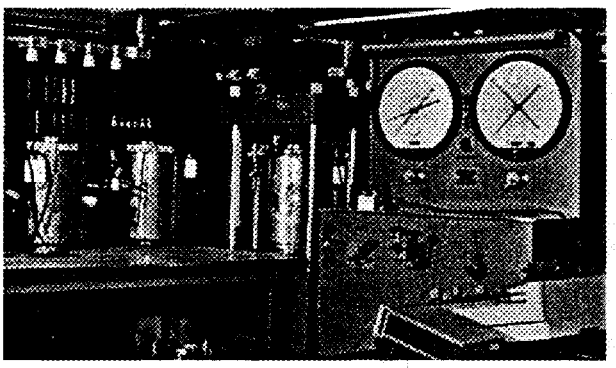

Figure 11. Unconfined compressive strength test setup.

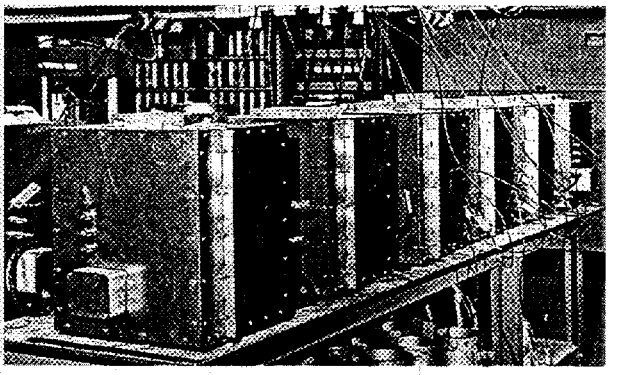

Figure 12. Shear test furnaces during specimen heating.

the pre-designated shear plane. The concrete-steel reinforcement bond test setup is shown in Fig. 13. The test procedure consisted of placing the cubical test specimen containing a No. 11 steel rebar and several thermocouples into the test furnace-platen assembly, heating the specimen at a rate of 17 C/hr to the thermal stabilization temperature, maintaining the temperature for 14 days, calibrating the instrumentation, and loading the steel rebar while the concrete was constrained. A continuous record of load vs. concrete-rebar displacement was obtained during each test. Sustained load tests were conducted using the test setup shown in Fig. 14. The testing procedure consisted of placing the cylindrical

test specimens containing thermocouples in their furnace-platen assemblies, loading the specimens to either 20 or 50% their reference design compressive strength, heating the specimens at a rate of 17 C/hr to their scheduled thermal stabilization temperature, and maintaining the temperature for 60 days followed by permitting the specimens to slowly cool to ambient. Specimen load, length change, and temperature were continuously monitored throughout the testing sequence. Due to the temperature levels of interest, test methods had to be developed for determining the

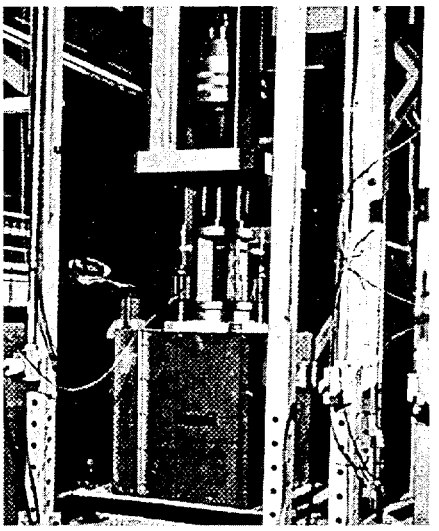

Figure 13. Concrete-rebar bond test setup.

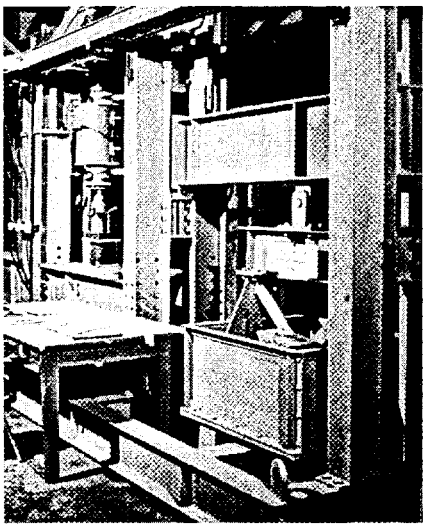

Figure 14. Sustained load test setup.

physical properties of the structural and lightweight concretes. Physical properties determined for these concretes included total length change due to thermal effects and coefficients of thermal diffusivity and conductivity. Figure 15 presents a schematic of the hanging wire method used for measuring length change of the lightweight insulating concrete. A fused-silica dilatometer test fixture was used for determining length change of the structural limestone aggregate concrete (Fig. 16). Coefficients of thermal diffusivity and conductivity were determined using a variable state

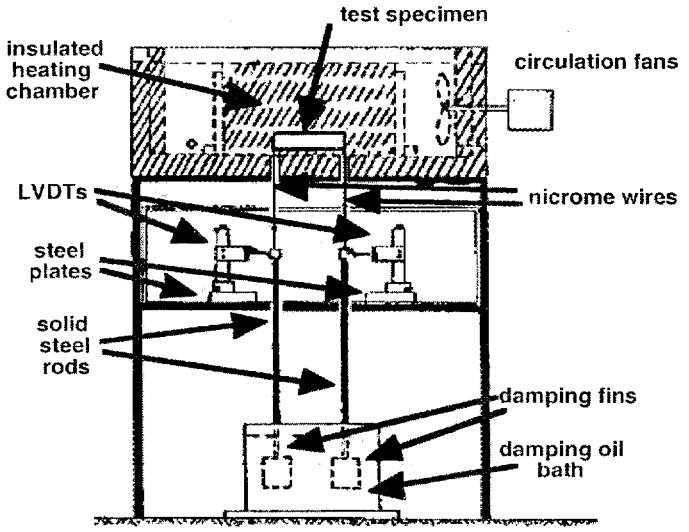

Figure 15. Hanging wire method for length change.

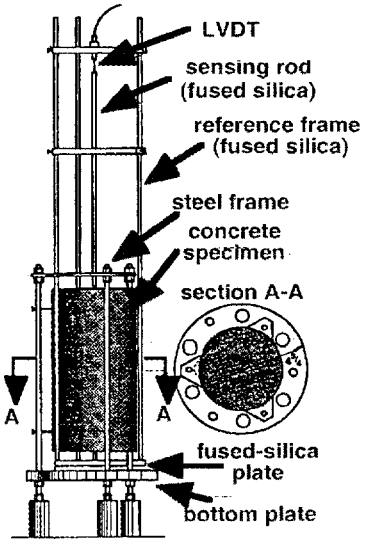

Figure 16. Dilatometer-based apparatus.

method developed by Harmathy. The test setup is shown schematically in Fig. 17. Coefficients of thermal diffusivity were also determined using the cooling test method shown in Fig. 18. Additional details on the testing procedures as well as mechanical and physical property test results from this program are available [7,8].

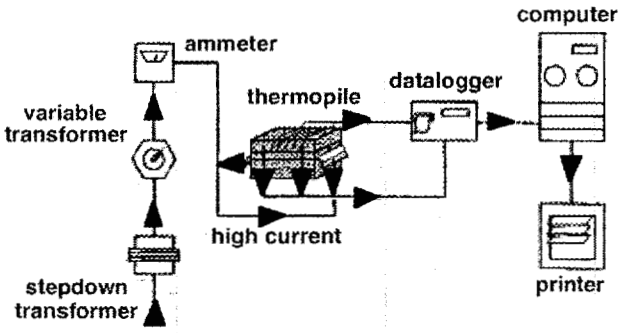

Figure 17. Experimental setup for measuring thermal diffusivity and conductivity.

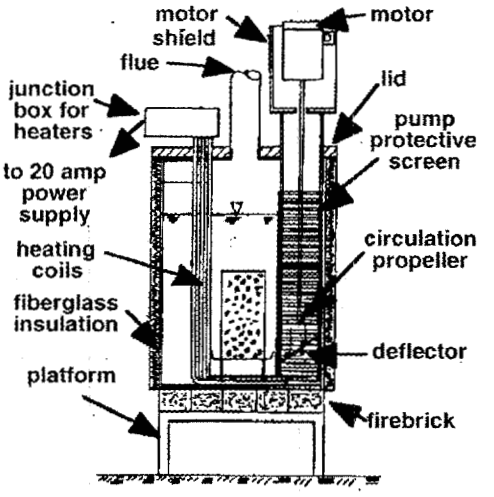

Figure 18. Oil bath for cooling test.

3.3.4 Time-Dependent Deformations Under Elevated Temperature and Multiaxial Loadings

The time-dependent deformation of concrete was investigated by subjecting 15.2-cm diameter by 40.6 cm cylindrical specimens to various stress conditions and elevated temperatures (Fig. 19). Variables included temperature (23.9 and 65.6 C), age at loading (90, 183 and 365 days), a variety of axial and radial load combinations from 0 to 24.8 MPa, and two curing histories (air-dried and as-cast). Strains were measured using vibrating wire gages. In the investigation it was found that compressive and tensile total creep strains were generally larger for: (1) a test temperature of 65.6 C than for 23.9 C, (2) an air-dried concrete than an as-cast concrete (except for low tensile creep), (3) increased time after loading and (4) higher stresses for uniaxial and biaxial states of stress (Fig. 20) [9,10].

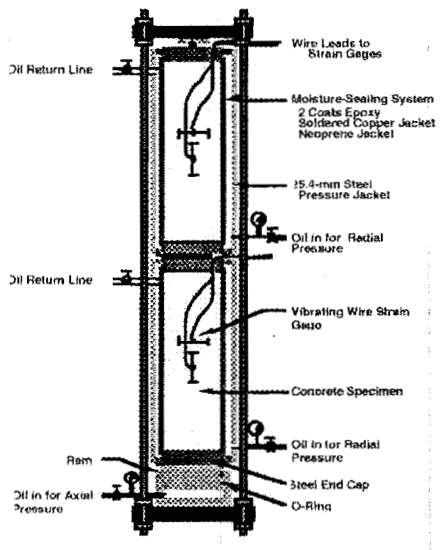

Figure 19. Schematic of creep test setup.

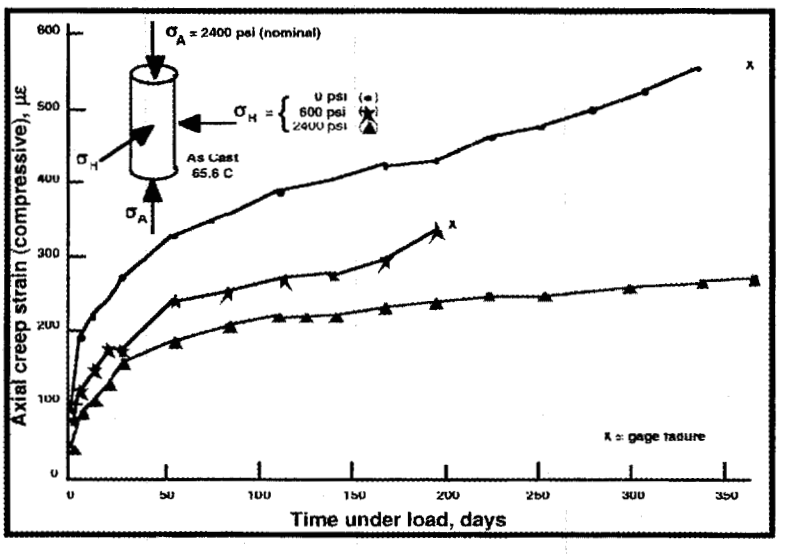

Figure 20. Effect of radial stress on axial creep strain.

3.4 MODEL TESTING

A variety of tests have been conducted using scale models of either an entire concrete pressure vessel or a portion of the vessel.

3.4.1 Size Effect

A series of small PCRV models was designed, analyzed, constructed, and tested to investigate the suitability of small-scale (≤ 1:20) mortar and epoxy models for determining elastic stress distributions, cracking, and failure modes. The primary objective of these tests was to demonstrate the adequacy and relative accuracy of two- and three-dimensional elastic finite-element structural analyses when applied to relatively complex vessel shapes.

Five models were studied. The first was a small concrete vessel that served as the prototype for the other four. The other four models consisted of two 1:2.75-scale mortar models; a 1:5-scale prestressed epoxy model; and a 1:5-scale idealized, unprestressed, axisymmetric epoxy model (Fig. 21). Each model was extensively instrumented, and the test results were compared with finite-element predictions. The prototype and one mortar model were pressurized hydraulically but, to examine possible differences in structural behavior, the other mortar model was tested pneumatically. The epoxy models were tested in the elastic range only. Structural behavior of the small-scale mortar models closely duplicated that of the concrete prototype, and the behavior characteristics of the two mortar models indicated that failure, whether caused by either pneumatic or hydraulic pressure, was gradual and not catastrophic. The elastic stress distributions, load-deformation responses at higher pressures, modes of cracking and pressure levels at which they occur, and even the number and location of major cracks, were essentially the same in both the prototype and the models. The models were analyzed elastically by using both two-dimensional (axisymmetric and plane) and three-dimensional finite-element stress analysis computer programs developed for PCRV's. Comparison of the predicted behavior with test results showed reasonably good agreement for most areas of the vessels, even with the two-dimensional analyses. The more involved three-dimensional analyses predicted the elastic stresses and deflections in the heterogeneous vessels quite well. The close agreement between model and prototype behavior points out the potential for use of small-scale models for studying PCRV behavior. Further, the good agreement between the test results and the analytical predictions of the model's elastic behavior demonstrated the effectiveness and reliability of the finite-element computer analyses used to evaluate PCRVs [11].

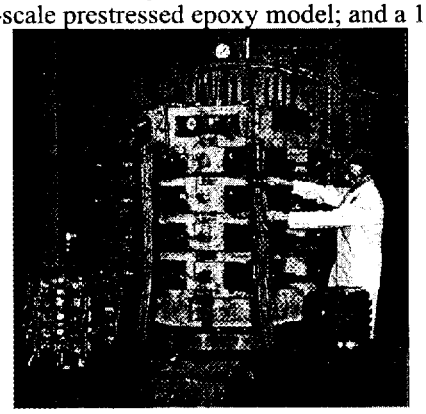

Figure 21. Prototype and model types.

3.4.2 Thermal Cylinder Experiment

The thermal cylinder experiment was designed for two purposes. The first was to provide information for evaluating the ability of analytical methods to predict the time-dependent stress-strain behavior of a one-sixth scale model of the barrel section of a single-cavity PCRV. The second goal was to demonstrate structural behavior under both design and off-design thermal conditions. The model was a thick-walled cylinder having a height of 1.22 m, thickness of 0.46 m, and an outer diameter of 2.06 m (Fig. 22). It was prestressed both axially and circumferentially and subjected to 4.83 MPa internal pressure together with a thermal crossfall imposed by heating the inner surface to 65.6 C and cooling the outer surface to 24 C. Since the model was designed to study the behavior of the

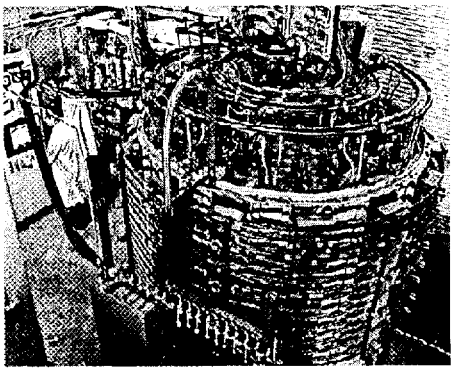

Figure 22. Thermal cylinder model.

barrel section of a massive concrete structure, all exposed surfaces were sealed to prevent loss of moisture, and the ends of the cylinder were insulated to prevent heat flow in the axial direction. The experimentutilized information developed from previous studies of concrete material properties, triaxial creep, instrumentation, analysis methods, and structural models. The initial 460 days of testing was divided into time periods that simulated prestressing, heat-up, reactor operation, and shutdown. At the conclusion of the simulated operating period, the model was repressurized and subjected to localized heating at 232 C for 84 days to produce an off-design hot-spot condition. Comparisons of experimental data with calculated values obtained using the SAFE-CRACK finite-element computer program showed that it was capable of predicting time-dependent behavior in a vessel subjected to normal operating conditions [12].

3.4.3 PCRV Head Failure Studies

A series of head failure model tests was conducted to provide input for development of a method to permit reliable calculations of the strength of PCRV end-slabs. Thirty-eight small-scale cylindrical vessels with flat end–slabs were pressurized to failure (Fig. 23). The vessels were prestressed circumferentially and longitudinally, and the end-slab contained no additional reinforcement. Experimental variables were the end-slab thickness, size and arrangement of penetrations in the end-slab, and concrete strength. The penetrations, which were not reinforced by sleeves or liners, were closed by steel plates at the pressurized surface of the end-slabs. Each vessel was pressurized to failure over a period of approximately three hours (Fig. 24). The range of attained maximum pressures was from 12.4 MPa to 26.0 MPa. End slabs of test vessels tended to fail in shear so failures could be violent despite the use of fluid pressure.

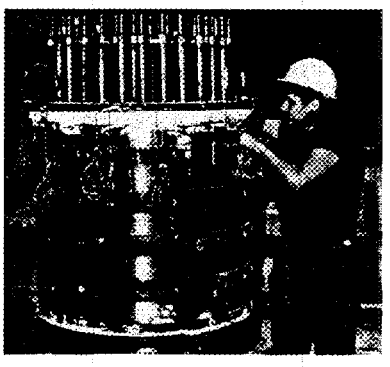

Figure 23. Head failure model being prepared for test.

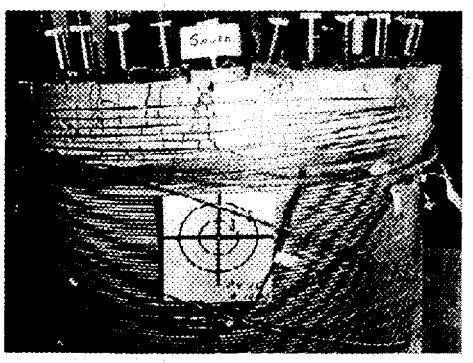

Figure 24. Model post-test: end-slab flexure failure.

The failure pressures indicated decisively the effects of changes in slab thickness and concrete strength. However, end-slab strength was relatively insensitive to changes in the amount of cross-section removed by the penetrations. An axisymmetric nonlinear finite-element model was developed to simulate the behavior of the physical models. The finite-element model was successful in indicating the observed changes in (a) internal stress paths, (b) internal strains, and (c) slab deflections as well as the observed strength of the test vessels. A significant feature of the analytical model was that it used a very simple failure criterion for the concrete (i.e., Mohr in compression and limiting strain in tension). Close agreement between experimental and analytical results confirmed that the overall nonlinear response phenomena in thick end-slabs of prestressed concrete pressure vessels may be estimated satisfactorily without the necessity of detailed information on the responses of concrete subjected to a three-dimensional stress field. Shear strength of the test vessels was calculated successfully without any "calibration" constants derived from test results for the vessels. Required input data were limited to information on the geometry of the vessel, effective prestress forces, compressive strength of the concrete, and type of loading [13,14].

3.4.4 Moisture Migration

In an effort to obtain information regarding the nature of moisture movement and rate of moisture loss in a PCRV, an experimental study of moisture migration in a pie-shaped specimen representing the flow path through a cylindrical wall in a PCRV was conducted. The test specimen was 2.74 m in length with cross-section dimensions of 0.61 by 0.61 m on one end and 0.61 by 0.81 on the other end (Fig. 25). The specimen was sealed against moisture loss on the small end (interior) and along the lateral surfaces, and exposed to the atmosphere on the other end (exterior). After monitoring the temperature distribution for 17 months, a temperature gradient of 44 C was applied to the specimen and the measurements continued for one year. At the end of the test, with the exception of zones nearest the ends or the

specimen, moisture contents were fairly constant. Moisture contents for the two stations nearest the specimen ends were approximately 15% less than the average moisture content for the remaining stations (Fig. 26). Based on this it was concluded that moisture migration in thick sections of concrete, such as a PCRV, is a slow process and is not likely to be a significant factor with a temperature difference of 44 C or less [15].

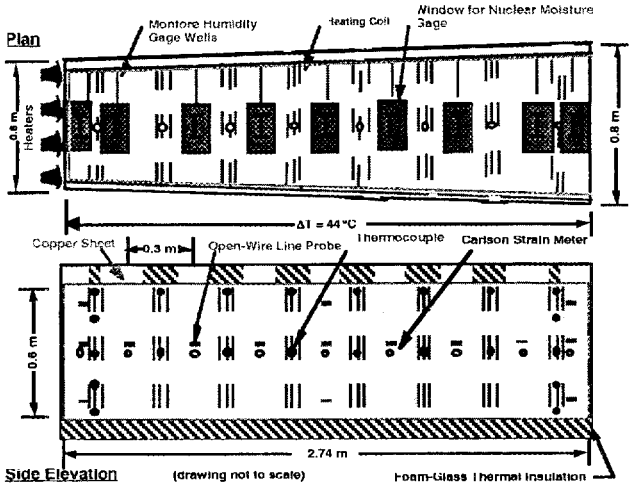

Figure 25. Schematic of moisture migration model showing instrumentation locations.

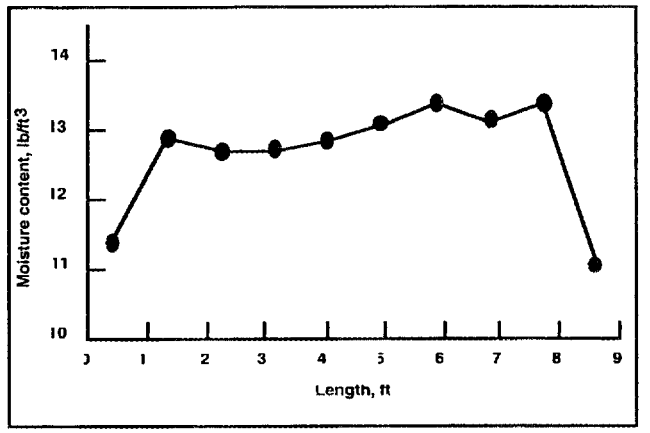

Figure 26. Moisture distribution at end of testing.

3.4.5 PCRV Concrete Closure Plugs

Under the Gas-Cooled Fast-Breeder Reactor (GCFR) Program model tests have been conducted to verify the design of the closures for the steam generator and central core cavities of the PCRV for a 300 MW(e) GCFR. Three small-scale model tests have been conducted: (1) 1:15-scale steam generator cavity full-thickness closure model, (2) 1:15-scale steam generator cavity half-thickness closure model, and (3) 1:20-scale central core cavity closure model. The vertical cross-section view of the PCRV for the 300 MW(e) GCFR shown in Fig. 27 indicates the relative size, location, and principal features of the closures. The design maximum cavity pressure is 10.08 MPa. Concrete in the closure plugs is confined on the side and bottom surfaces by a relatively thin steel liner. A ring forging is attached to the top of the side liner and serves to transfer resulting pressure loadings from the closure plugs to adjacent axial prestressing tendons of the PCRV. Load transfer is accomplished by two-force members (i.e., toggles) that are inclined from the vertical and induce radial compression loading into the ring forgings at the top of the side liner wall; thus, together with the lateral pressure of the coolant, they produce a circumferential prestress on the plugs that remains directly proportional to the pressure loading induced by the reactor coolant. Materials having similar properties to those proposed for use in construction of the prototype closure plugs were used for fabrication of the models (e.g., reinforcing steel was simulated by extruding, heat treating, and deforming low alloy 2 1/4 CR-1 Mo stock wire; concrete was simulated using a mortar mixture developed in the laboratory). Each model was instrumented to provide axial and radial displacements, and strain distributions in the liner and concrete. Strain and displacement data were recorded by a data acquisition system as a function of pressure. Figure 28 presents a cross section of the test fixture containing the full-thickness steam generator cavity closure plug model and shows some of the instrumentation used to provide axial

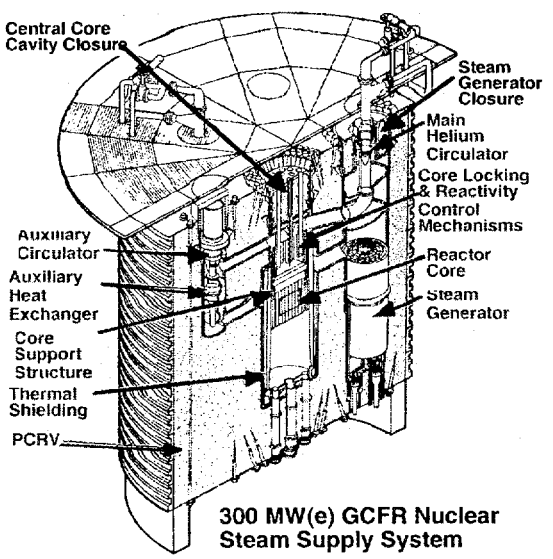

Figure 27. GCFR PCRV cross section showing closure plug locations.

and radial displacements, and strain distributions in the liner and concrete. Strain and displacement data were recorded by a data acquisition system as a function of pressure. A view of the test fixture just prior to insertion of the 1:15-scale steam generator cavity closure model for testing is shown in Fig. 29.

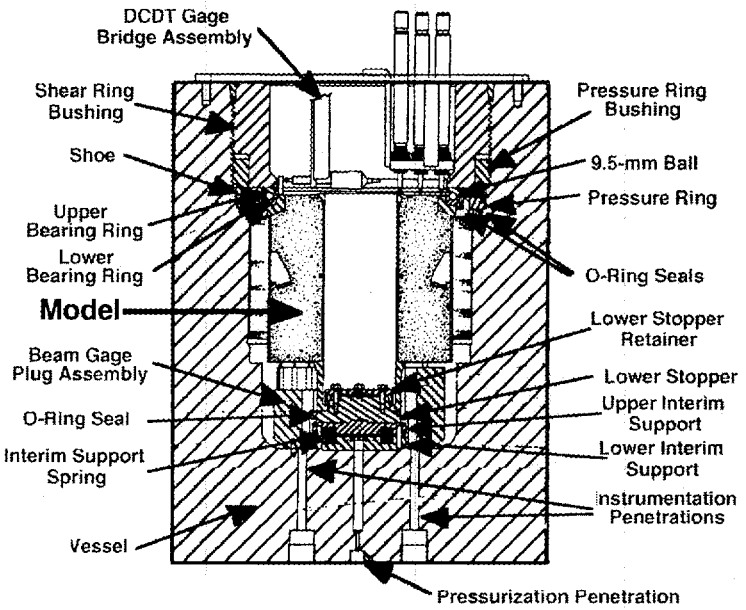

Figure 28. Schematic of closure plug model test fixture.

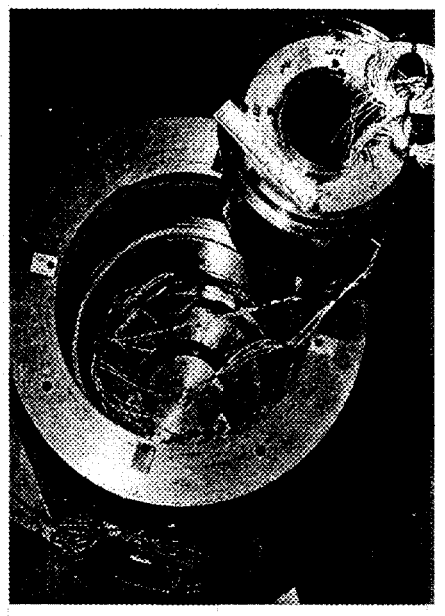

Figure 29. Model prior to placement into test fixture for pressurization.

The test fixture was fabricated from a modified HY-100 forging, designed to permit pressurization to 138 MPa, and contained penetrations in the bottom of the vessel to permit pressurization and entry for up to 24 (three-wire) channels of instrumentation. A threaded bushing assembly was used to secure the models in the test fixture with sealing accomplished by using elastomeric O-ring seals. Figure 30 presents a schematic of the test facility where the closure plug models were tested.

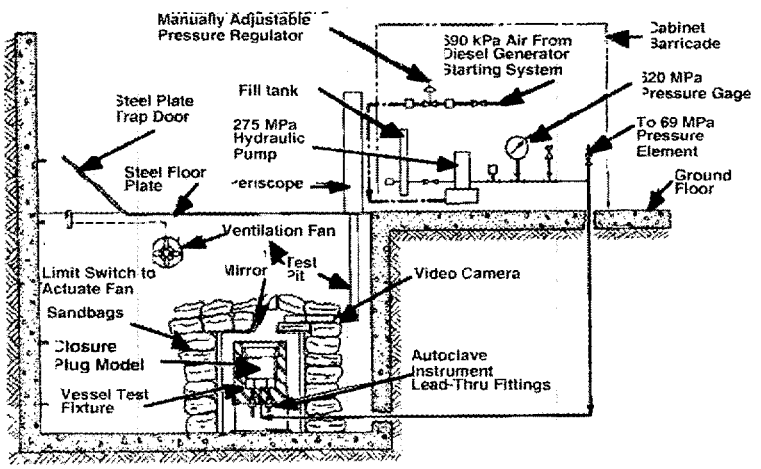

Figure 30. GCFR PCRV closure plug model test facility.

The 1:15-scale full-thickness steam generator cavity closure plug model was initially subjected to ten pressurization cycles to 10.08 MPa. After each cycle the pressure was reduced to 2 MPa. The eleventh cycle was to continue pressurization in steps until the ultimate capacity of the model was reached; however, the test was stopped at 75.84 MPa, which was about 7.5 times the prototype design pressure. Although the ultimate capacity had not been reached, displacement gages were exhibiting significant nonlinearity and several strain gages on steel components inferred that significant yielding had occurred. Figure 31 presents the model following pressurization to 75.84 MPa, and Fig. 32 shows a view of the 0 to 180° cross section of the model after sectioning. Neither visual cracking nor gross distortion were evident. Localized voids could be seen in the concrete underneath the inner and outer

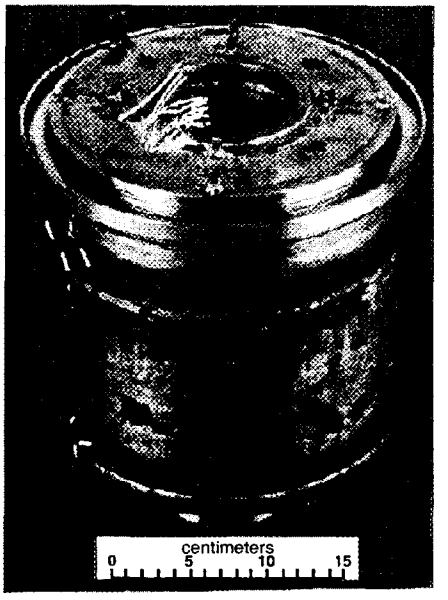

Figure 31. Model after pressurization to 75.84 MPa.

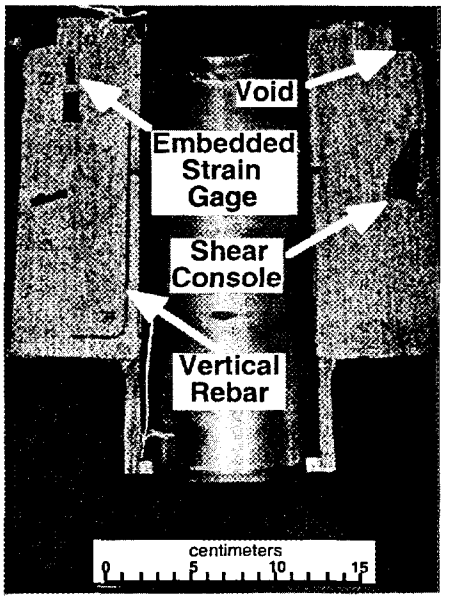

Figure 32. Model after sectioning.

ring forgings, and minor porosity was evident throughout the model. However, good embedment was evident at the top embedment strain gage and at the shear console. The only detectable sign of distress in the model was a banding on the slanted surface of the outer ring forging contact surface [16].

The second model represented a redesign of the steam generator cavity closure plug to a thickness of one-half that of the original model. The primary purpose of this test was to demonstrate structural performance and ultimate load capacity of the redesigned model [17]. Secondary objectives included obtaining data on crack development and propagation, and mode of failure of the composite structure. After ten pressurization cycles to 10.08 MPa, the model was pressurized to failure. No visual indications of distress were evident prior to failure, although strains recorded by the embedded concrete gages were approximately 1%, and the steel components exhibited high inelastic strains. Failure occurred by abrupt punching shear at approximately 99.3 MPa (about 9.9 times maximum cavity pressure), thereby expelling the central section with considerable force. The failure surface was a truncated cone (Fig. 33).

Figure 33. Post-test view of inner and outer failed sections of half-thickness model.

The GCFR central core cavity closure plug differed from the steam generator cavity closure plug in that it contained fifty-five small diameter closely-spaced penetrations, and the penetrations were pressurized during testing [18]. Figure 34 presents the prototype design for the central core cavity closure plug. In fabricating the 1:20-scale model, all physical features of the prototype were scaled by a factor of 20 except for the tubes for which the scale factor was 19.3. It was intended to pressurize the model until failure, but pressurization was interrupted at 38.2 MPa due to an excessively leaking fitting on the pressurization line. After repairing the fitting, pressurization was resumed. Pressurization was again interrupted at 41.3 MPa by an excessively leaking autoclave instrument penetration fitting on the test vessel. A complete rework of the seal without loss of instrumentation would have required removal of the model from the fixture. Rather than proceed along this costly and time-consuming route, the decision was made to isolate the leads to this fitting, repair the seal, and utilize spare leads on other fittings where possible. After these modifications, pressurization

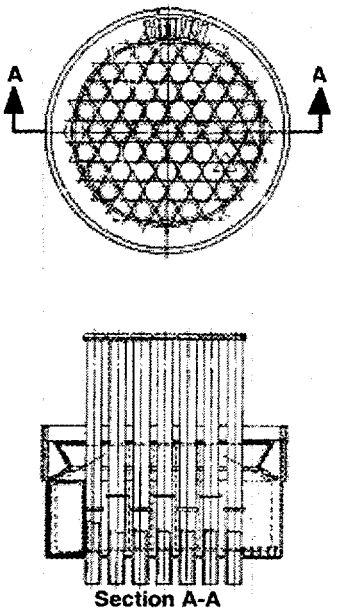

Figure 34. Central core cavity closure prototype.

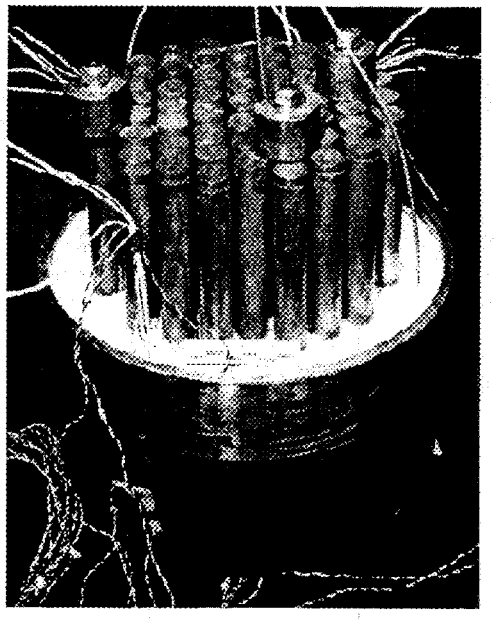

Figure 35. Model after pressurization to 79.3 MPa.

was resumed. At 48.3 MPa pressurization was interrupted by the failure of an end-cap braze joint. Remedial work to repair the joint was implemented and pressurization resumed. However, at a pressure of 58.4 MPa (pressure cycle 14) seals in the pressure intensifier failed. Following repair of the intensifier, one final attempt was made to pressurize the model to failure. At a pressure of 79.3 MPa the end-cap in another penetration tube partially failed to relieve the pressure. Because at this point no practical way existed of ensuring the avoidance of further end-cap failures, the test was terminated. In addition, considerable strain was evident in other tubes and a pressure level of almost eight times maximum cavity pressure had been attained. Removal of the model from the test vessel showed no visible distress except for some tube straining and the end-cap failures (Fig. 35).

3.4.6 Grouted vs Nongrouted Tendons

Nongrouted tendons are predominantly used in this country as the post-tensioning system for prestressed concrete pressure vessels because they are more easily surveyed to detect reductions in prestressing level and distress such as would result from corrosion, should it occur, and they offer the potential for replacement, if required. However, grouted tendon systems, in which a cement-based material is used to fill the ducts of stressed tendons, offer advantages that may make them cost effective for pressure vessel applications. Literature was reviewed to (1) provide insight on the behavior of grouted tendon systems, (2) establish performance histories for structures utilizing grouted tendons, (3) examine corrosion protection procedures for prestressing tendons, (4) identify arguments for and against using grouted tendons, and (5) aid in the development of the experimental investigation. The experimental investigation was divided into four phases [19]: (1) grouted-nongrouted tendon behavior, (2) evaluation of selected "new" material systems, (3) bench-scale corrosion studies, and (4) preliminary evaluation of acoustic emission as a potential technique for monitoring grouted tendons in PCRVs. Summarized below are activities conducted under the experimental investigation.

3.4.6.1 Grouted-nongrouted tendon behavior

Grouted-nongrouted tendon behavior was evaluated using reinforced concrete flexural specimens 0.15-m wide by 0.30-m deep by 3.1-m long containing a single seven-wire strand that had been post-tensioned to either 50, 60, or 70% its ultimate strength. Figure 36 presents the test setup. A comparison of results for grouted and nongrouted tendon flexural members for three different prestressing levels is presented in Fig. 37. Results of this series of tests indicate that grouted tendon beams develop more cracks, but crack widths are smaller, which results in smaller localized strains and less chance of penetration by corrosive environments; for the range of prestressing levels investigated, as the level of prestressing increased, the first cracking and ultimate load values increased; and ultimate loads for grouted tendon beams were larger than for nongrouted beams at the same level of prestressing.

Figure 36. Setup for testing beams in flexure.

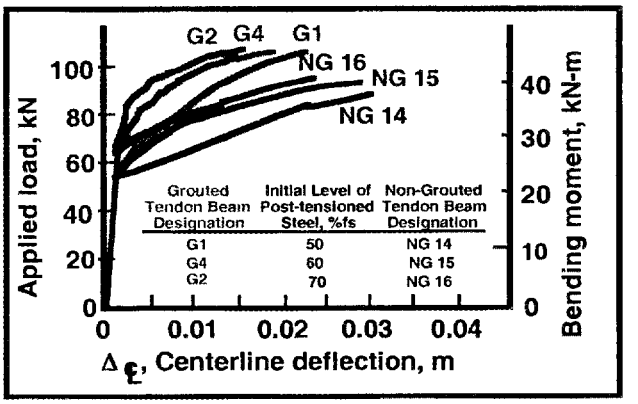

Figure 37. Effect of post-tensioning level.

3.4.6.2 Evaluation of selected "new" material systems

Materials evaluated for potential PCRV applications included polymer-silica and shrinkage-compensating cements as grout materials and steel-fiber reinforced concrete as a structural material. The polymer-silica cement (inorganic corrosion-resistant material) was selected because it was nonshrink, exhibited good bond to minerals, and had high-temperature capabilities. Shrinkage-compensating cement was selected because it eliminates or reduces shrinkage and its associated problems such as cracking or incomplete filling of voids for grout applications. Fibrous concrete was evaluated because it has increased flexural strength, ductility (energy absorption), and resistance to penetration relative to conventional concrete. The polymer-silica and shrinkage-compensating cements were tested to indicate prestressing strand bond transfer lengths and prestressing strand pull-out bond strengths relative to a conventional grout material. The bond transfer lengths were evaluated by fabricating 0.15-m wide by 0.30-m deep by 3.1-m long reinforced concrete beam specimens that contained grouted prestressing wire strands (Fig. 38). The bond transfer length was evaluated by determining the distance along the beam required for the tendon to achieve maximum stress after a simulated anchor failure (i.e., $\leq 40\ \mu\varepsilon$ change). The simulated tendon failure was induced by slowly cutting the prestressing strand at the bracket shown in Fig. 38. For the test conditions evaluated, results indicated that the polymer-silica and shrinkage-compensating cements exhibited improved bond to the prestressing steel relative to conventional grout material (i.e., required 39 and 53% the length required for commercial grout to develop complete prestressing-transfer length) (Fig. 39).

The pull-out test specimens were fabricated using 152-mm-OD by 737-mm-long cast iron pipes that had been filled with concrete and contained a centrally-located seven-wire prestressing strand that ran the length of the specimen and had been stressed to either 50, 60, or 70% the strand strength. Figure 40 presents the tensioning fixture for the bond pull-out specimens and Fig. 41 presents a specimen after removal from the tensioning fixture. The relative performance of the

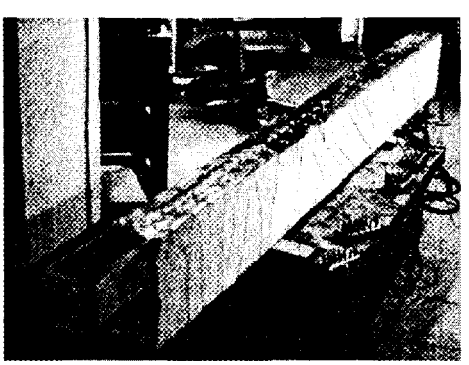

Figure 38. Bond transfer length test specimen.

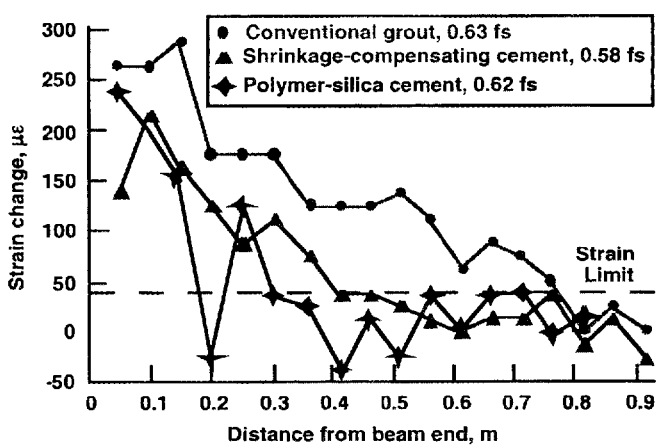

Figure 39. Relative bond transfer length results.

three grout materials was evaluated using an apparatus and procedures similar to those found in ASTM C 234, "Test for Comparing Concretes on the Basis of the Bond Developed with Reinforcing Steel." Figure 42 presents the bond pull-out test setup and Fig. 43 presents an example of results obtained. In general, results indicated that the bond developed by the polymer-silica cement was superior to that developed by the shrinkage-compensating cement and the commercial grout materials.

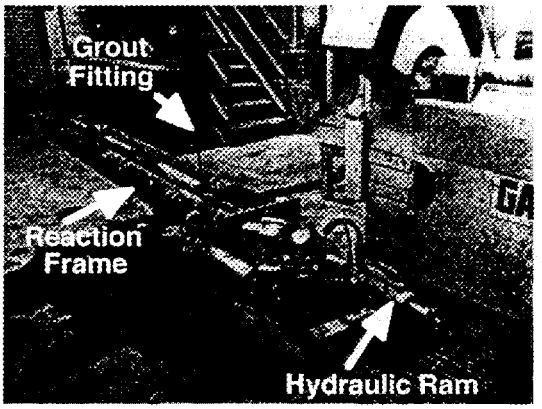

Figure 40. Bond pull-out tensioning fixture.

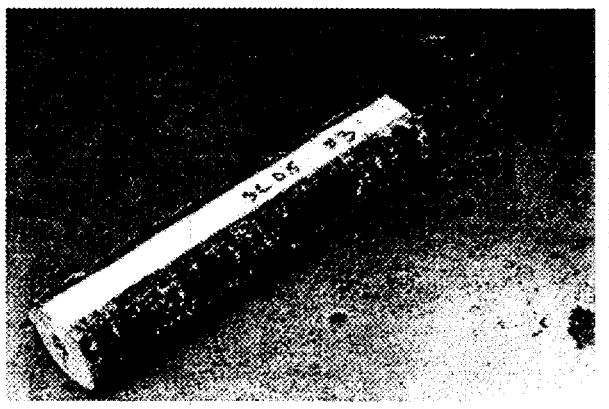

Figure 41. Bond pull-out test specimen.

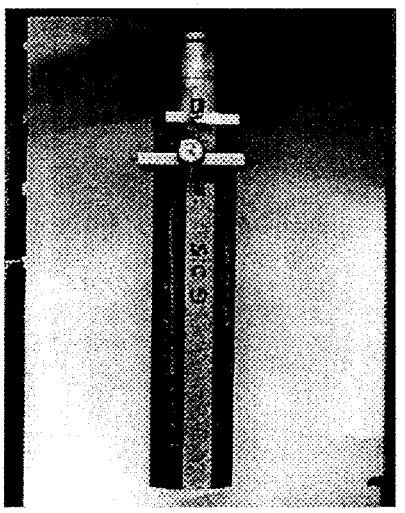

Figure 42. Bond pull-out test setup.

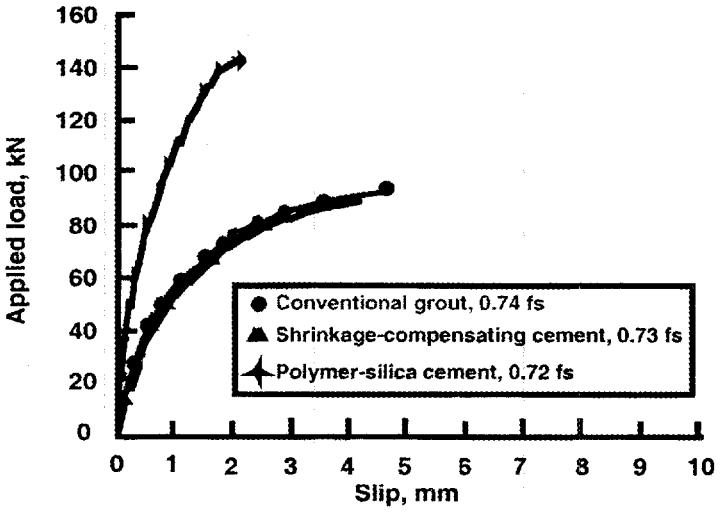

Figure 43. Relative load-slip

Fibrous concrete structural members 0.15-m wide by 0.30-m deep by 3.1-m long containing 1.5 % (by volume) steel fibers (25.4-mm long) were fabricatedand tested using the test setup shown in Fig. 36. The beams were post-tensioned to either 50, 60, or 70% the steel ultimate strength with the tendons either grouted or nongrouted. Figure 44 presents results for grouted and nongrouted fibrous concrete and structural concrete beams. Results showed little difference between the load-centerline deflection curves for the fibrous and structural concrete beams when comparing grouted and nongrouted beams at the same level of prestressing. The primary differences were that both the grouted and nongrouted fibrous concrete beams exhibited more ductility than their structural concrete counterparts, indicating that they had increased toughness, and the first crack load was generally greater for the fibrous concrete beams.

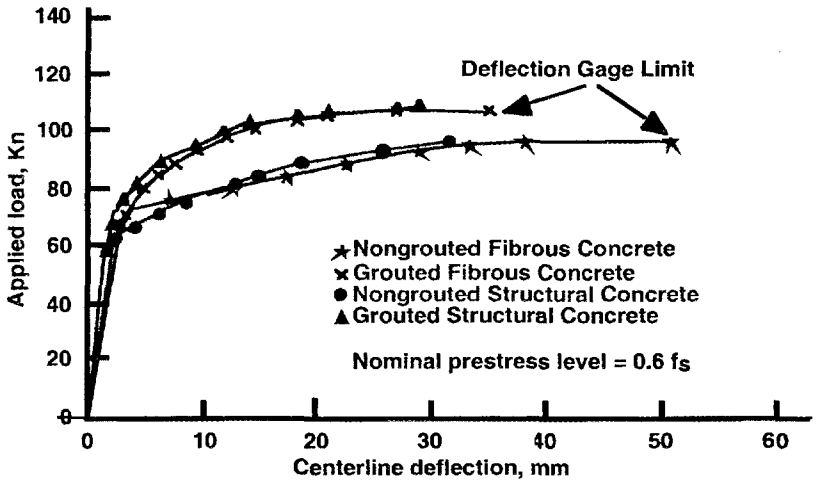

Figure 44. Structural and fibrous concrete load versus deflection behavior.

3.4.6.3 Bench-scale corrosion tests

Bench-scale tests were conducted to investigate the corrosion behavior of a high-strength steel (ASTM A416 Grade 270), typical of that used as tendon material in prestressed concrete pressure vessels [20]. The primary purpose of the tests was to demonstrate the protection afforded by coating the steel with commercial organic petrolatum-based greases or portland cement-based grout. Concentrations of the deleterious substances used were much higher than normally would be encountered. The study utilized 305-mm-long wire segments obtained from the center, straight wire of a seven-wire prestressing strand. Variables in the investigation were stress level [0 to 90% of wire ultimate tensile strength (UTS)], coating materials (none, cement grout, selected commercial products), time of exposure, and environment [hydrogen-sulfide saturated water at room temperature (3000 ppm, pH ~ 4), *0.2 M* NH_4NO_3 at 66°C, and *0.1 M* NaCℓ at room temperature]. Two basic test series were conducted – stressed and unstressed. In the stressed test series, two test types were employed. The first type utilized unprotected specimens that had been stressed to different percentages of their UTS while in contact with water containing H_2S. In the second type grout- or grease-protected specimens were loaded to 60% UTS while exposed to water containing H_2S, Fig. 45. In the second test series unstressed, protected or unprotected, tendon wires were exposed to water containing H_2S, *0.2 M* NH_4NO_3 at 66°C, and *0.1 M* NaCℓ for relatively long periods of time and then strained to failure. Figure 46 presents the test setup for exposing the unstressed tendon wires to the NH_4NO_3 and NaCℓ environments. The greases used in these tests were commercially available petrolatum-

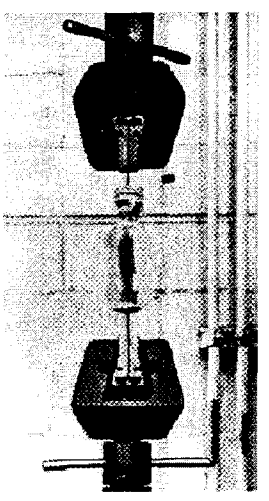

Figure 45. Stressed wire time to failure test setup.

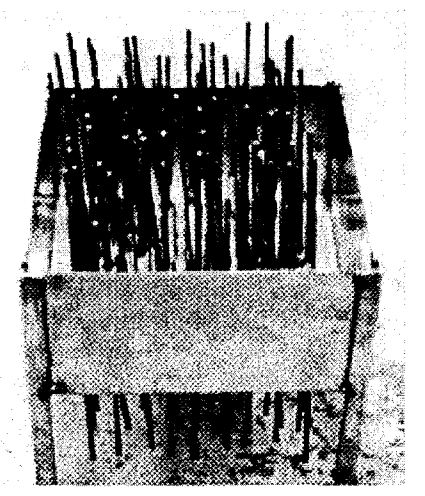

Figure 46. Nonstressed tendon NH_4NO_3 and NaCℓ Exposure test setup.

based corrosion inhibitors with polar agents to facilitate wetting of the wires and displacement of moisture. They were applied according to the manufacturers' recommendations to a thickness of about 1 mm. Test specimens protected by grout were prepared by casting 16-mm-diameter by 38-mm-long grout cylinders around the wires. The area of the wires not coated with grease or grout that could be contacted by the test solutions was covered with a polyurethane insulating paint. In some cases the effect of flaws in the coatings was evaluated. Flaws were placed in the organic coatings by scraping the wire to which the coating had been applied with a similar wire so that a thin strip of unprotected wire resulted. In some cases the wires with flaws were permitted to stand 30 days prior to exposure to evaluate "self-healing" characteristics of the greases. Flaws ranging in width from 0.1 to 3.2 mm were cast in the grout by using plastic shim stock that was removed after the grout hardened. Figure 47 presents average times to failure and ranges in times to failure for the uncoated wires tensioned to different percentages of their UTS. For protected specimens loaded to 60% UTS while exposed to a corrosive environment, no failures occurred during the six-day exposure period and subsequent tensile tests showed no degradation in load capacity or ductility. The organic corrosion inhibitors containing flaws exhibited failure times ranging from 14 to 66 h; however, specimens that were allowed to "self-heal" prior to exposure exhibited no property degradation due to exposure. Figure 48 presents the effect of grout flaw size on time to failure. Protected, unstressed wires exposed to H_2S for 77 days indicated no detrimental effects of corrosion; however, unprotected specimens exhibited an 8% decrease in load capacity and a 60% loss in ductility. After 120 days exposure, the unprotected wires exhibited decreases in load capacity of 11% and ductility of 70%, the grease-protected wires experienced decreases in load capacity from 0 to 14% and decreases in ductility from 70 to 75%, and grout-protected specimens exhibited no loss of load capacity but a 12% decrease in ductility. For unstressed wires exposed to NH_4NO_3 at 65 C, the unprotected wires lost 14% in UTS and 66% in ductility after 43 days with no further changes noted for

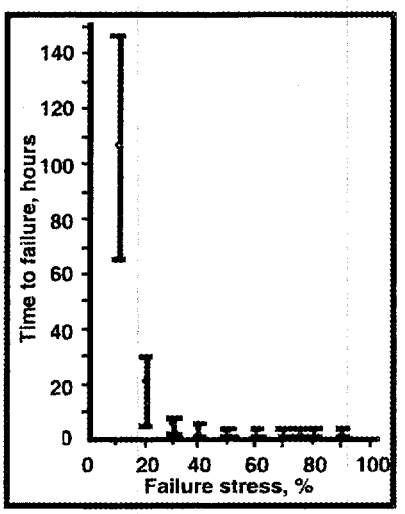

Figure 47. Effect of percent failure load on failure time: $H_2S + H_2O$ environment.

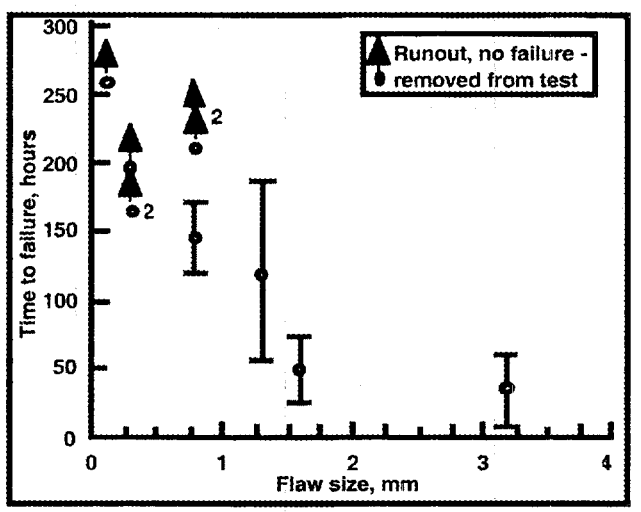

Figure 48. Effect of flaw size on time to failure: tendon stressed to 60% failure: $H_2S + H_2O$ environment.

the remainder of the 132-day test duration. The grease protected wires exhibited no loss of strength or ductility during the 132 day duration of the test; however, after 87 days exposure the portland cement-based grout protected specimens started to exhibit degradation of the grout with associated decreases in the wire strength and ductility. For unstressed wires subjected to $NaC\ell$, after 107 days exposure the grease-and grout-protected wires exhibited strength losses up to 6% and 4%, respectively. Ductility decreases for the grease-protected specimens ranged from 11 to 24% while the grout-protected specimens exhibited a 4% decrease. Corresponding strength and ductility decreases for unprotected specimens were 8 and 60%, respectively. Study conclusions were that prestressing materials should be continuously protected from time of manufacture; exclusion of sulfide, nitrite, and chloride environments is required to prevent reduction in mechanical properties of prestressing; and when properly applied, both Portland cement and organic corrosion inhibitors provide positive exclusion of corrosive environments from prestressing materials.

3.4.6.4 Acoustic emission evaluation

Acoustic emissions are small-amplitude elastic stress waves generated during material deformation resulting from a mechanical or thermal stimulus. The stress waves are detected by transducers as small displacements on the specimen surface. The emissions are classified as being either continuous or burst. Continuous acoustic emissions are low-level, high-signal-density emissions such as might be observed during tension testing of unflawed specimens. Burst acoustic emissions are generated when a plastic zone or microcracks form at a crack tip, or when crack extension occurs. Characterization of the stress wave emissions provides an insight into the type of inelastic deformation that is occurring: amplitude of the stress wave emission indicates the magnitude of flaw extension, rate of stress wave emission indicates the rate of flaw propagation, and the total acoustic emission energy generated is proportional to the loss of structural integrity. Flaws may be located by use of data from an array of three or more coupled transducers (two or more for one-dimensional source location). In order to demonstrate the feasibility of acoustic emission for monitoring concrete and simple concrete models two series of tests were conducted: (1) plain concrete compression cylinders and (2) grouted tendon beam structural models [21].

Three sets of four concrete cylinders 0.15 m diameter by 0.54 m long and three flexure prisms 0.15 by 0.15 by 0.91 m were fabricated to obtain acoustic emission data on concrete under compressive and tensile loadings. The variable between specimen sets was the water content, which was adjusted so that acoustic emission data could be obtained from low-, medium-, and high-strength concretes (19.5, 36.8, and 50.8 MPa, respectively). Prior to testing, each cylinder was instrumented with two 0.1-m gage-length wire-resistance strain gages placed at 180° intervals on the circumference, aligned in the direction of loading, and wired in series to minimize any bending effects. Two 50 kHz resonant-frequency transducers were attached to the specimen at a longitudinal spacing of 0.30 m, and two additional 50-kHz transducers were attached to the upper and lower loading platens to minimize noise from the platen-cylinder interface (Fig. 49). Three of the specimens in each set were tested to failure in compression with load-strain and acoustic emission data obtained. The fourth cylinder in each specimen set was loaded to failure in cycles, with each succeeding load cycle after an initial cycle to 20% of failure load being incremented by 10% of the average failure load for the first three cylinders tested. After completion of a load cycle, the load was reduced to 22.2 kN prior to initiation of a new cycle. Figure 50 presents acoustic emission-event histograms, cumulative acoustic emission-event counts, and normalized stress-strain as a function of percent failure stress for the medium-strength (36.8 MPa) concrete. Results indicate that, for the specimens loaded to failure in one cycle, there was good correlation between acoustic emission and stress-strain curves for low- and medium-strength concretes; that is, from 0 to 30% ultimate strength, the stress-strain curves were essentially linear and acoustic emission activity was small; from 30 to 70% ultimate strength, the stress-strain curves started to deviate from linearity due to an increase in bond cracks between the aggregate and matrix and the acoustic emission activity increased; and above 70% ultimate failure strength, there was a rapid deviation of the stress-strain curves from linearity due to a rapid increase in matrix cracking and there was an associated sharp increase in acoustic emission activity. The high-strength concrete specimens exhibited relatively uniform activity from initiation of loading until approximately 85 to 90% ultimate strength, when the activity increased sharply. Results for the specimens cyclically loaded to failure with each succeeding load cycle being to a higher load level indicated that the Kaiser effect (once a load has been applied to a member and the associated acoustic emission activity ceased, no more emission will occur until the load level is exceeded, even if the load is completely removed) apparently applies to concrete material systems when significant time between load cycles has not lapsed. Prior to testing, the flexure specimens were instrumented with a 0.1-m gage-length wire-resistance strain gage applied to the tensile face of the beam. Two 50-kHz resonant-frequency transducers were attached to the specimen at a spacing of 0.5 m on the same surface as the strain gage. After placing in the test fixture (Fig. 51), the specimens were loaded in flexure to failure with stress-strain and acoustic emission data obtained throughout loading. Stress-strain curves obtained for all the flexure specimens were essentially linear up to failure. As a result, acoustic emission activity was absent until just prior to failure, when a few (<10) events occurred.

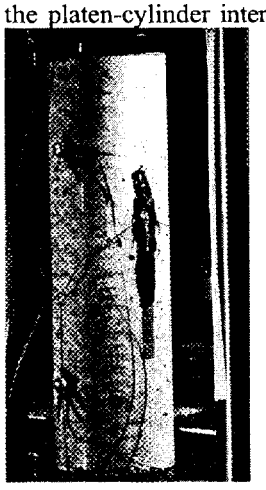

Figure 49. AE test setup: concrete cylinders.

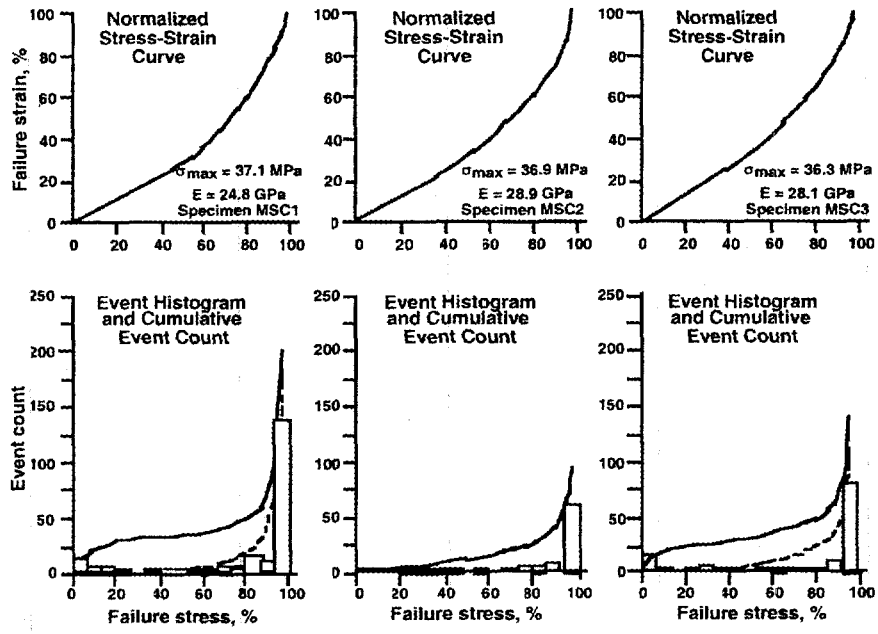

Figure 50. Acoustic emission test results: medium-strength concrete. (Dashed lines for cumulative event count are smoothed curves that have eliminated initial noise resulting from platen-cylinder interaction.)

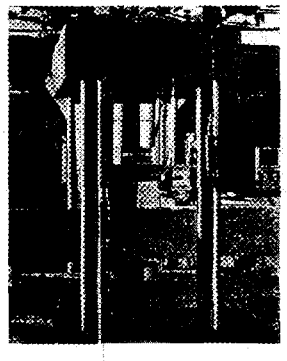

Figure 51. AE test setup: flexure.

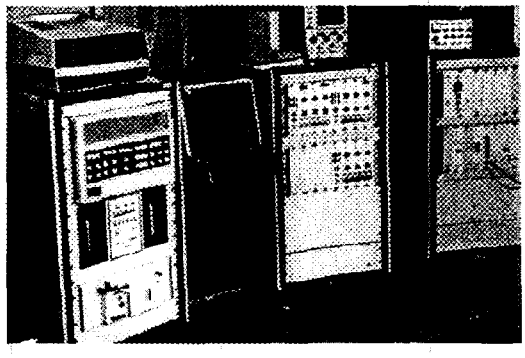

Figure 52. AE multi-channel source-location system.

Selected beams of the grouted-nongrouted tendon test series were also monitored by acoustic emission as they were tested to failure. Prior to testing, six 50-kHz acoustic emission transducers were attached to the bottom surface of the beam to be tested. Two were attached near the major span reaction points and used as "slave" transducers to lock out localized reaction noises. The remaining four transducers were spaced at 0.6-m incrementsto monitor the central 1.80 m of the beam and thus provide data on flexural crack locations. The acoustic emission system (Fig. 52) was programmed for one-dimensional source location and the beam loaded in flexure to failure with acoustic emission source location data obtained throughout the test. Figure 53 presents an example of load-centerline deflection data for a grouted-tendon beam (see Fig. 55) and the corresponding acoustic emission cumulative event count (S number) and cumulative event magnitude (Σ voltage). Acoustic emission results correlated well with beam inelastic behavior (i.e., micro and macrocracking). Figures 54 and 55 present typical acoustic emission data in the form of event activity as a function of location along the length of the beam for a nongrouted and grouted tendon beam, respectively. Superimposedabove the acoustic emission activity plots are photographs of the beams after testing so that the agreement between crack

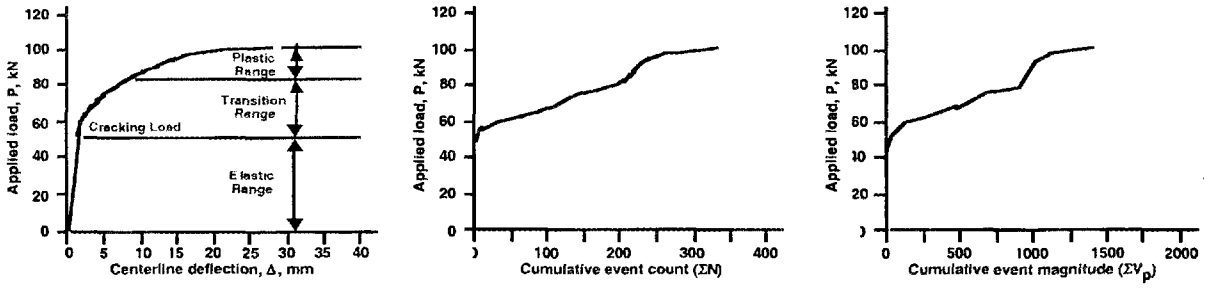

Figure 53. Beam load-deflection compared to AE results.

locations and acoustic emission active areas may be noted. Results indicate that, for nongrouted tendon beams where only one or two major cracks occurred during testing to failure, acoustic emission-determined crack locations and actual crack locations correlated very well. In grouted tendon beams tested to failure, four or more major cracks generally formed, and the correlation between acoustic-emission identified crack locations and actual crack locations was not as definite. Location of the first crack in the beam was accurate, but the accuracy decreased as more cracks formed. This "smearing" of acoustic emission active regions was related to development of several cracks so that a source-initiated stress wave had to travel around cracks to go from transducer to transducer, as required for source location, and, as noted in Fig. 55, the initial main cracks branched and propagated horizontally as the cracking increased.

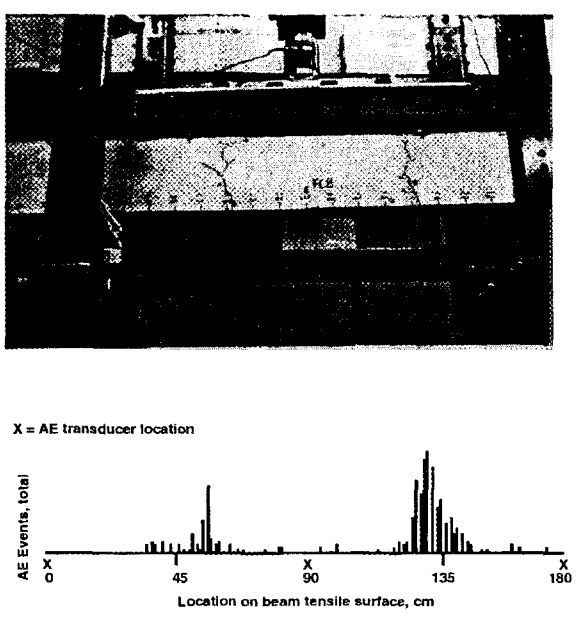

Figure 54. Nongrouted tendon AE result showing good correlation to crack locations.

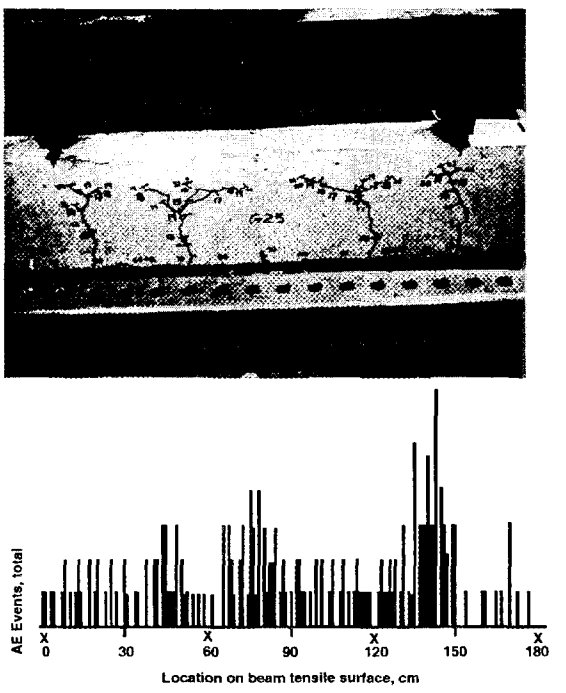

Figure 55. Grouted tendon AE results showing effect of increased cracking.

3.5 MATERIALS EVALUATION AND TESTING

Materials development and testing activities have addressed development of high-strength concrete and fibrous concrete materials, and evaluation of thermal barrier ceramic materials.

3.5.1 Development of High-Strength Concrete Materials and Model Testing Techniques

PCRV design optimization studies for a 2240 MW(t) HTGR Steam Cycle/Cogeneration plant (Fig. 56) indicated that significant size reductions (~ 1.3 m) could be effected through use of high-strength concrete (55 MPa) in conjunction

with large-capacity post-tensioning systems (13.3 MN). This translates to substantial cost savings [~$5.7 M (1980 dollars)] in both the PCRV and containment. Additional benefits associated with the use of high-strength concrete included reduced concrete creep (lower prestress losses), and lower temperature rise of fresh concrete and reduced potential for alkali-aggregate reactions due to incorporation of fly ash into the mixes as partial replacement for the cement. Furthermore, this newer generation PCRV included an asymmetric cavity arrangement that was not supported by existing model test data that met the intent of the American Society of Mechanical Engineers (ASME) Code for Reactor Vessels and Containments [22]. In support of the optimization study, high-strength concrete materials were developed and evaluated [23,24], and model testing techniques were developed and demonstrated through testing of two PCRV single-cavity models (i.e., high-strength concrete and fibrous concrete models) [25].

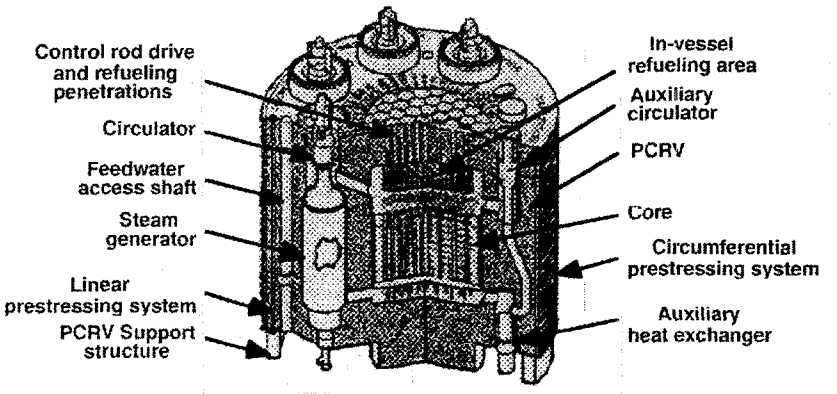

Figure 56. PCRV for HTGR steam cycle/cogeneration plant.

3.5.1.1 High-strength concrete materials

The objective of the high-strength concrete materials program was to develop concrete materials having compressive strength ≥ 63.4 MPa using aggregate materials from sources in close proximity to areas representing potential sites for an HTGR plant (i.e., Florida City, Florida; Port Arthur, Texas; Pennsylvania-Delaware border area; and Blythe, California). Reference [22] requires that an average compressive strength at least 8.3 MPa greater than the specified strength be produced in the laboratory. After conduct of tests to select the admixture exhibiting the best compatibility with the Type II Portland cement chosen for use throughout the investigation, optimum cement contents were determined using 9.5- and 38-mm maximum size Pennsylvania-Delaware border area aggregates. Optimum cement contents were determined because there is an optimum cement factor for concrete mixes of equal workability and the same consistency that use a specific aggregate of a certain maximum size (beyond the optimum cement factor additional cement does not provide increased strength). Cementitious materials contents (90% cement plus 10% Type C fly ash, by weight) ranged from 7 to 12 sacks/cu.yd. In the mixes the coarse aggregate content was held constant, the water content was adjusted to maintain the slump at 89 ±13mm, and the fine aggregate content was adjusted to account for the changing cement and water contents. Figures 57 and 58 present compressive strength as a function of age and cementitious materials content for the 9.5- and 38–mm maximum size aggregate mixes, respectively. Based on these

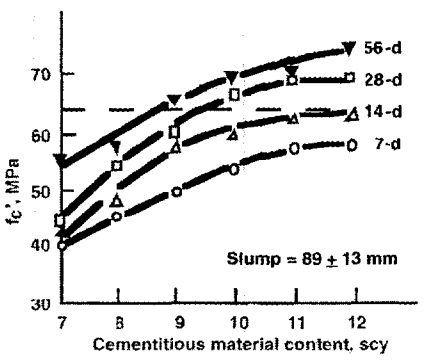

Figure 57. Optimum cementitious materials test results: 9.5-mm maximum size aggregate.

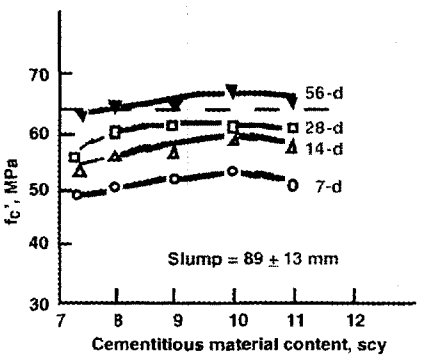

Figure 58. Optimum cementitious materials test results: 38-mm maximum size aggregate.

results optimum cement contents selected for the 9.5- and 38-mm maximum size aggregate mixes were 530 and 586 kg/m^3, respectively. The final series of tests evaluated the aggregate sources as well as the effect of the use of fly ash as a partial replacement for cement. Utilizing aggregate materials from each of the four sources, specimens were prepared in which from 0 to 40%, by weight, of the cement had been replaced by fly ash. Each of these mixes was

designed for equal workability by adjusting the water content to maintain the slump at 89 ± 13mm. Fine aggregate contents were adjusted to account for the changing volume from mix-to-mix of the cement, fly ash, and water. Compressive strength, modulus of elasticity, and Poisson's ratio results were obtained at concrete ages to 182 days using both sealed and moist-cured specimens cast from each mix. Figures 59 and 60 present compressive strength test results for 9.5- and 38-mm maximum size Pennsylvania-Delawareborder area aggregates,respectively. These test results indicate that the desired compressive strength of 63.4 MPa at 91 days was easily achievable.

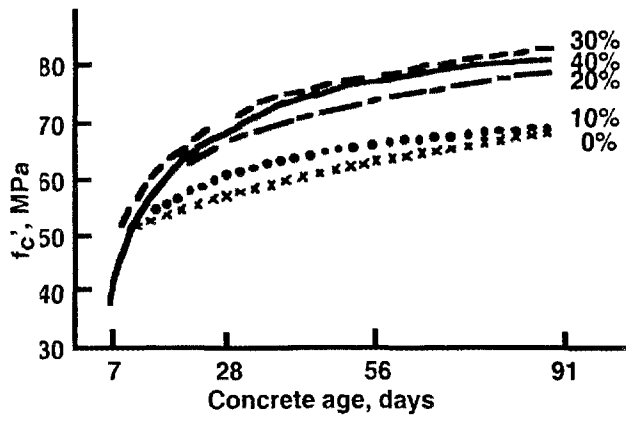

Figure 59. Effect of partial cement replacement with fly ash: 9.5-mm maximum size aggregate.

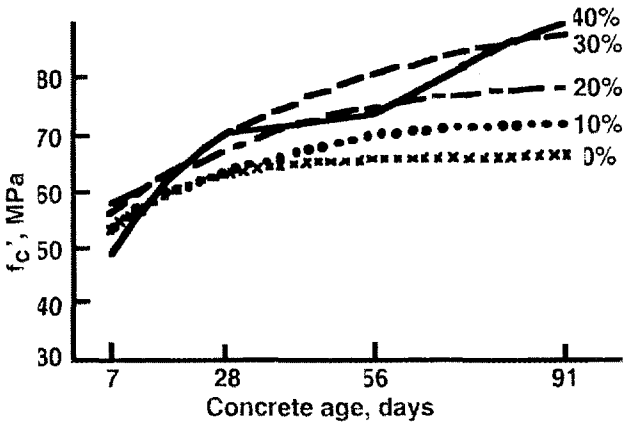

Figure 60. Effect of partial cement replacement with fly ash: 38-mm maximum size aggregate.

Similar results were obtained with the other three aggregate sources. Other benefits attributed to the incorporation of fly ash into the mixes include increased workability,reduced bleeding and reduced temperature rise of the fresh concrete. When evaluating the Blythe, California aggregate materials sufficient test specimens were cast so that the compressive strength could be monitored over a five-year period. Figures 61 and 62 presents compressive strength and modulus of elasticity results, respectively, for specimens that were either moist cured in lime-saturated water or sealed with plastic until testing. At the relatively low water-to-cement ratios used in this investigation (0.26<w/c<0.28), optimum compressive strength results were achieved at a fly ash content of 30% for the moist-cured specimens and 20% for the sealed specimens.

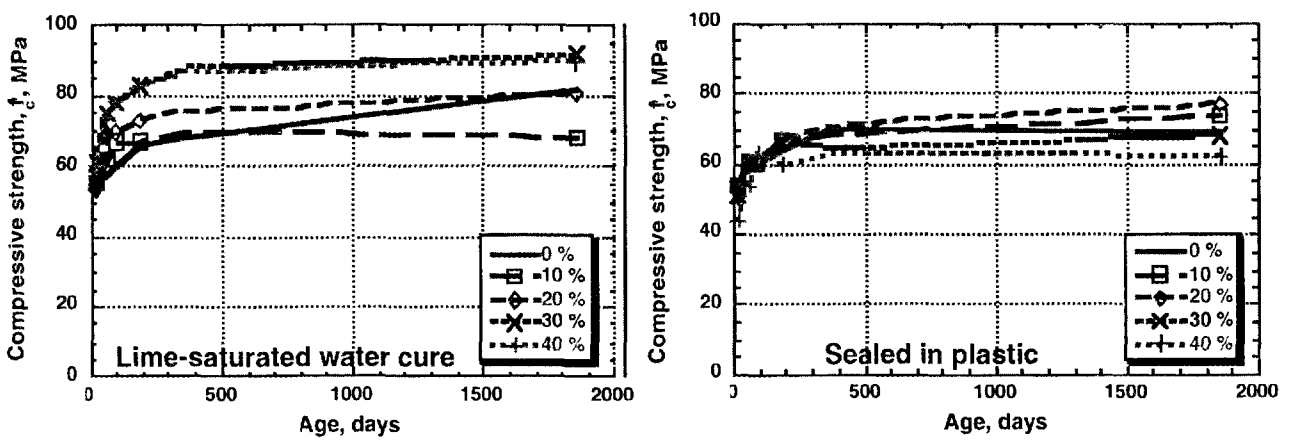

Figure 61. Effect of age and fly ash content on compressive strength.

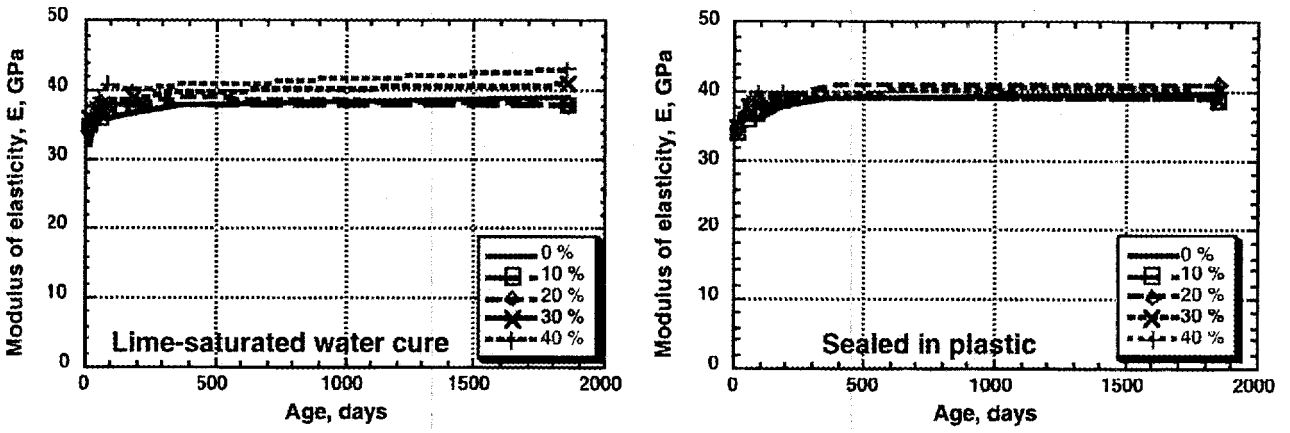

Figure 62. Effect of age and fly ash content on modulus of elasticity.

3.5.1.2 Model testing techniques

Section III, Division 2 of the ASME Code [22] requires a model test whenever a model of a prototype with characteristics similar to those of the current design has not been constructed and tested in accordance with Code provisions, or if analytical procedures to predict ultimate strength and behavior in the range approaching failure are not established. Because the newer generationPCRV design (Fig. 56) included an asymmetric cavity arrangement and offset core, existing model test data that were developed for single-cavity and axisymmetric multicavity PCRV designs may not meet the intent of the above requirements.

Using results of a review of PCRV-relatedmodel tests [26], it was established that two model testing areas may require some development: circumferential prestressing and leak-tight liner systems. A test program was therefore undertaken to establish satisfactory methods for circumferentially prestressing PCRV models ranging in size from 1:30- to 1:10-scale, and for lining the models so that they would not leak prematurely to terminate a test [25]. Activities related to circumferentially prestressing the models were merely to identify a prestressed concrete pipe manufacturer who could apply prestress at a prescribed force level to models ranging in size from about 1- to 4–meters in diameter. Relative to the liner system, a design was developed that incorporated the use of a 2.67-mm thick AISI 1008 drawing quality steel in conjunction with a flanged head. The flanged head eliminated the corner joint which had been a problem area in prior model tests.

To demonstrate the validity of the above concepts, two ~1:30-scale single-cavity PCRV models were fabricated: one using a high-strength concrete mix design and one to provide an indication of the merit of fibrous concrete (50-mm long hooked and collated fibers, 1.1% by volume) for PCRV applications. The two PCRV models were identical in geometry to those tested to investigate the shear strength of end slabs of PCRVs (see Fig. 23), except that the concrete mix designs and liner were developed specifically for these two tests, and circumferential prestressing was applied by a prestressed concrete pipe manufacturer. After filling with water, each model was hydraulically pressurized to failure. The plain concrete model failed abruptly in the head region by shear of the concrete at a pressure of 24 MPa. The mode of failure for the plain concrete models appeared to be influenced by the concrete strength with the failure tending to be more of a "punching-shear" type than the cryptodome formation observed in earlier models fabricated from lower strength concretes. Comparing results from this test with those obtained from models having identical geometries and tested under a previous program [13,14] indicates that the concrete compressive strength directly influences the internal failure pressure. The fibrous concrete model failed by rupturing twenty-three wraps of the circumferential prestress wire at a pressure of 28 MPa. The head of the fibrous concrete model remained intact and the few cracks that developed were relatively small and closed on depressurization. Figures 63 and 64 present the models after testing. Compressive strengths of the plain and fibrous concrete at the time of testing were 79 and 69 MPa, respectively. Results demonstrated that the circumferential prestressing and liner systems performed satisfactorily. It was also demonstrated that the shear strength of the fibrous concrete was at least 15% greater than that of the plain concrete at comparable strength levels.

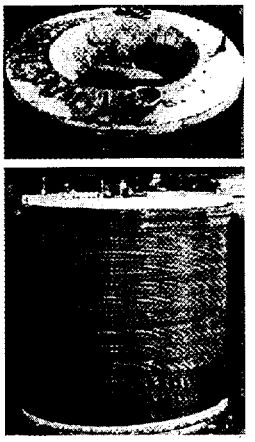

Figure 63. PCRV plain concrete model post-test.

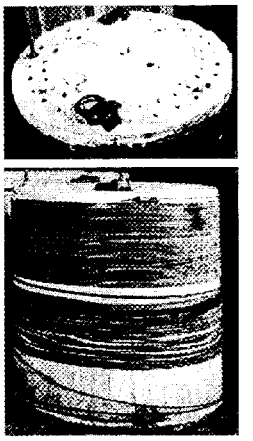

Figure 64. PCRV fibrous concrete model post-test.

3.5.2 Testing of Thermal Barrier Hard Ceramic Pad Materials

The function of the HTGR thermal barrier is to protect the PCRV liner and adjacent concrete from overheating due to high temperature helium. This protection is provided by a system of fibrous insulation blankets plus cover plates and seals, and hard structural ceramics. In the bottom head region of the core outlet plenum the thermal barrier also functions as a dissipater of hot gas streaks and provides structural support for the reactor core. A testing program was conducted to determine the ability of typical ceramic pad configurations to withstand mechanical loading conditions. The mechanical loading conditions were intended to provide a parametric representation of what would be induced into the ceramic pads due to thermal gradients. Conical platens were used to induce mechanical loadings into the pads.

Structural response tests were conducted on pads fabricated from Grade 85 and 995 alumina, and fused silica hard ceramic materials [27,28]. The pads were in the form of right circular discs having an outside diameter of 216 mm, an inside diameter of 76 mm, and a thickness of either 38, 51, or 76 mm. Either two or four layers of woven silica fabric having a thickness of 1.37 mm was used as the interface material between the pads and conical platens to provide more uniform loading and to permit more pad rotational freedom. The ceramic pads were loaded to a maximum load of 890 kN using the test fixture presented in Fig 65. A breakdown of the components of the test fixture is shown schematically in Fig. 66. Platen-to-platen displacements, pad strains and rotations, and acoustic emission activity were monitored throughout loading. Flat platen loading did not produce failures of any of the materials. Specimens that failed exhibited only one apparent mode of failure – failure in three or less cracked sections with the cracks not extending completely through the specimen thickness over its entire diameter (i.e., specimen remained intact). Acoustic emission

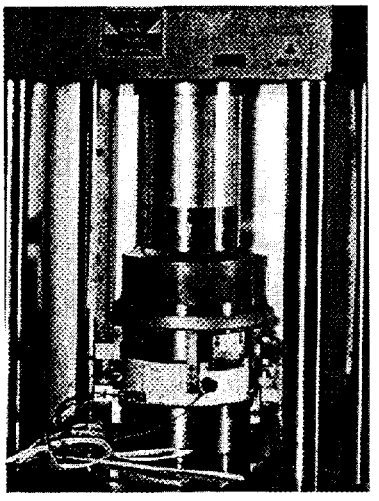

Figure 65. Ceramic pad test setup.

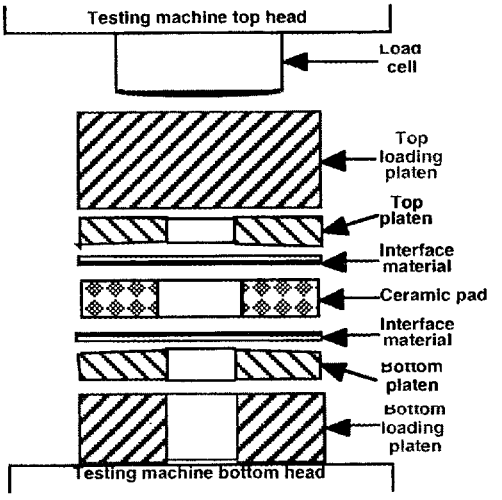

Figure 66. Schematic of test fixture.

activity for the fused silica material was much more intense than for the alumina material. As the number of interface layers between the pad and platens increased the acoustic emission activity decreased and the load at which cracking occurred increased. Also the acoustic emission results correlated well with sudden changes in strain versus load curves. Although results were very limited, there was some indication that acoustic emission might be able to be used as a potential nondestructive evaluation method to identify defective pads.

3.6 STATE-OF-THE-ART STUDIES AND TECHNOLOGY ASSESSMENTS

State-of-the-art studies and technology assessments have addressed evaluations of major PCRV components, concrete embedment instrumentation systems, development of an optimized PCRV, studies as part of an evaluation of pebble bed versus prismatic fueled HTGRs, and pressure vessel concepts for application to HTGR modular reactor systems.

3.6.1 Major PCRV Components:

Functions of a prestressed concrete reactor vessel are to: (1) resist the internal pressure of the coolant; (2) provide radiation shielding for the reactor core; (3) contain radioactive products; and (4) contain the entire primary cooling system-reactor, heat exchangers and pumps. The PCRV consists of three major component groupings: (1) concrete; (2) conventional mild steel reinforcement and post-tensioning system; and (3) liner, insulation, and cooling system. The concrete provides radiation shielding, temperature shielding for the steel, a reaction medium for the post-tensioning, and contributes to the overall strength of the vessel. Conventional steel reinforcement controls cracking and the crack widths in the concrete, helps carry tensile forces where concrete has cracked, and can be used to carry excessive compressive stress. The post-tensioning system inhibits concrete cracking and carries tensile forces associated with internal pressurization. The liner produces a leak-tight barrier for the vessel coolant and forms a barrier against the release of radioactive fission products into the concrete. The cooling and insulation systems prevent excessive temperatures in the concrete and steel. State-of-the-art assessments have been conducted for each of these major PCRV components.

3.6.1.1 Concrete properties in a nuclear environment

Two reviews of concrete properties in a nuclear environment have been conducted [29,30].

The first report presents results of a literature review to ascertain current knowledge regarding plain concrete properties under conditions imposed by a mass concrete structure such as a PCRV. The effects of high temperature on such properties as strength, elasticity and creep are discussed, as well as changes in thermal properties, multiaxial behavior, and the mechanisms thought to be responsible for the observed behavior. In addition, the effects of radiation and moisture migration were addressed. It was concluded that sustained exposure of normal concretes to current PCRV operating conditions will not result in any significant loss of properties. However, lack of knowledge regarding effects of temperatures exceeding 100 C, moisture migration, and multiaxial behavior precludes a statement advocating operations beyond current design limits. Also included in the report are recommendations for future research on concretes for PCRVs.

In the second report concrete material systems were reviewed with respect to constituents, mix design, placing, curing, and strength evaluations, and typical concrete property data are described. Specialty concrete material systems (high strength, fibrous, polymer, lightweight, and refractory) were reviewed. Conclusions derived from the review were that: (1) portland cement concrete property data for normal operating conditions are adequate (some additional multiaxial property data are desirable); (2) portland cement concrete property data for elevated temperature conditions require development, especially with respect to basalt and serpentine aggregate concretes; (3) multiaxial concrete property data, especially at elevated temperatures, are required for development of improved constitutive relations for concrete; (4) additional data on effects of irradiation on concrete properties are required; (5) high-strength concretes (>41.4 MPa) have application to PCRVs, but they need to be investigated to define their mechanical behavior more clearly, develop fracture criteria, and assess current American Concrete Institute code applicability; (6) fibrous concrete exhibits significant potential to effect improved PCRV performance at reduced costs as a result of property enhancements provided by the fiber reinforcement; (7) polymer concrete and lightweight concrete material systems apparently have limited application to PCRVs because of high costs and poor hot strengths of the former and low strengths of the later; and (8) refractory concretes offer potential as thermal barrier materials for PCRVs, Examples of data identified in the literature on the effects of elevated temperature and radiation are presented in Figs. 67 and 68, respectively.

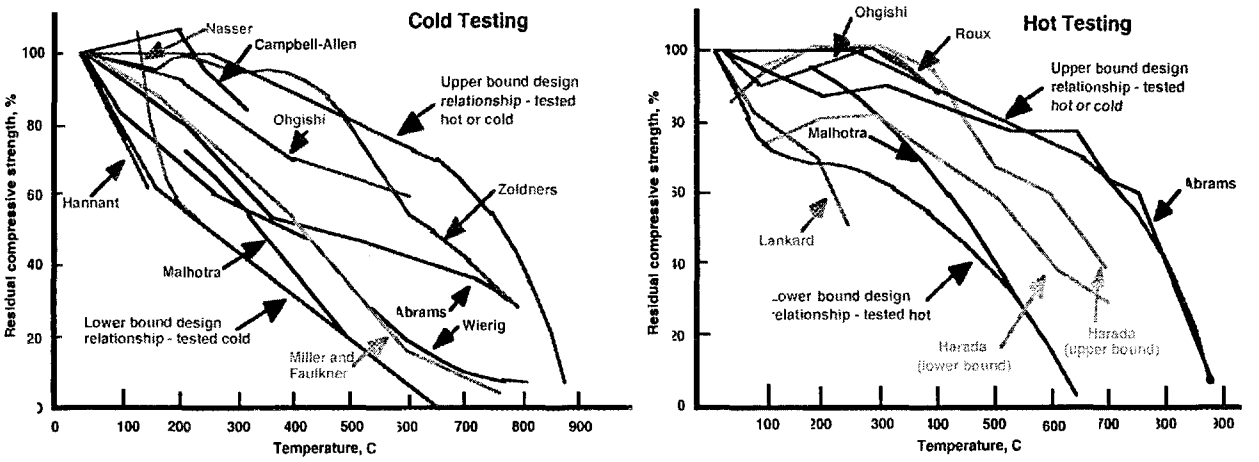

Figure 67. Data reported in the literature on the effects of elevated temperature on concrete compressive strength for specimens tested either after returning to room temperature (cold) or tested at temperature (hot).

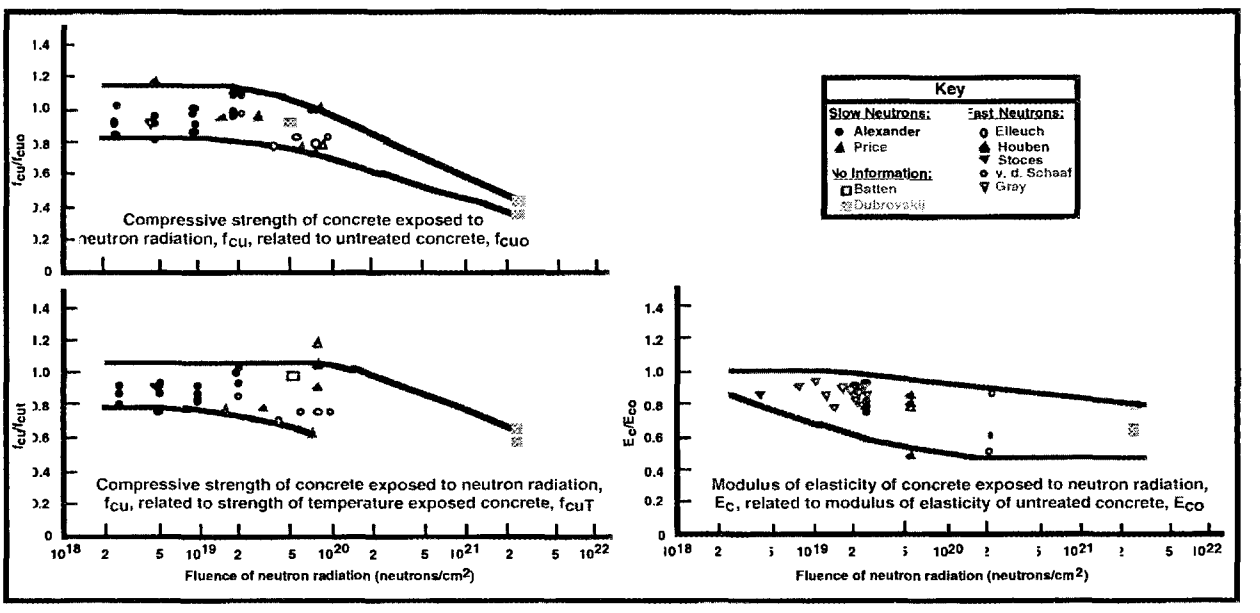

Figure 68. Data reported in literature on effects of radiation on concrete compressive strength and modulus.

3.6.1.2 Steel reinforcement and post-tensioning systems

The design of prestressed concrete reactor vessels for HTGR systems is based on the integral concept; that is, the entire pressurized gas circuit composed of reactor core, primary coolant system, and portions of the secondary coolant system are contained within a single vessel. The PCRV is, in essence, a spaced steel structure since its strength is derived from a multitude of steel elements made up of deformed reinforcing bars and prestressing that are present in sufficient quantities to carry tension loads imposed on the vessel. Bonded reinforcement (deformed bars) is provided in PCRVs to: control the extent and width of cracks at operating temperatures, resist tensile stresses and computed compressive stresses for elastic design, and provide structural reinforcement where required by limit condition design procedures. Prestressing is applied to concrete members to eliminate or materially reduce tensile stresses in concrete (i.e., the prestress forces inhibit concrete cracking, thus enabling the entire concrete cross section to share in the stiffness of the

vessel over a wide range of elastic behavior). Figure 69 presents an example of a multistrand post-tensioning system. The steel reinforcement and prestressing in PCRVs thus plays a vital role in assuring their structural integrity.

PCRV Code requirements in the United States, United Kingdom, Germany and France have been reviewed with respect to the bonded steel and prestressing systems [31]. Materials and fabrication procedures for production of prestressing wire, strand, rope, strip, and bar tendons are described. Material properties and the effect of elevated temperature and irradiation on these properties are presented. Available linear and circumferential post-tensioning systems applicable to PCRVs are described (i.e., BBRV wire, VSL strand, and Stresssteel wire and strand). Incidences of tendon corrosion and corrosion-protection techniques used in conjunction with prestressing steels in PCRVs are identified as well as the various Code requirements. Also, Code requirements for PCRV structural integrity testing and in-service surveillance are discussed.

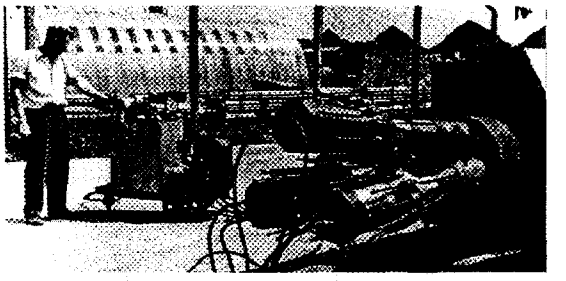

Figure 69. Simultaneous stressing of multistrand post-tensioning systems.

3.6.1.3 Liner, insulation, and cooling systems

Liner, insulation, and cooling systems for application to PCRVs have been reviewed [32].

The liner serves a number of separate functions: (1) part of the system of forms used in placing the concrete during construction, (2) the barrier preventing the escape of primary coolant gas and gaseous fission products, (3) an essential part of the system protecting the concrete from excessive temperature, and (4) aid in transferring the loads on the penetration closures into the PCRV structure through shear anchors embedded in the concrete. The liner must also be of sufficient thickness to withstand external pressure during partial evacuation of the vessel without the necessity of extensive stiffeningribs and ties to prevent its collapse; however, for cylindrical vessels it should be as thin as possible in order to keep the loads on corner details and keying system to a minimum. Although other methods of lining a vessel to accomplish the above functions have been considered (e.g., coating of the concrete with an impermeable membrane), most of the concepts were rejected since they either transferred concrete cracking through the liner material, they could not withstand the irradiation effects without deterioration, or they could not perform the liner secondary functions. Although all operating PCRVs have been designed with an insulated liner that has welded cooling tubes attached to the concrete side of the liner (cold liner), the Germans, Austrians, and French have conducted investigations related to use of a hot liner for application to PCRVs. Advantages cited for the use of hot liner systems include: (1) possibility of leak location, (2) earlier detection of leaks, (3) small contaminated volume, (4) accessible outer surface of vessel, (5) clear separation of thermal barrier from the prestressed concrete (no pressurized flaws), and (6) no uncontrolled moisture migration between the high (insulating) and low temperature concretes. In addition, a hot liner by not having a thermal barrier between the liner and coolant gas should be easier to repair if a leak develops. For a hot liner system to operate effectively, however, there are a number of requirements that must be met: (1) liner material should have good ductility and weldability, and preferably remain elastic (stresses in the liner can be controlled through the concrete temperature, designs can be developed that permit plastic flow); (2) the liner must be designed to withstand between 800 and 1400 load cycles; (3) anchorage of the liner to the concrete must be designed to prevent liner buckling (anchorage requirements are a function of liner thickness, liner material yield point, design life); (4) insulating material between liner and structural concrete must be strong enough to withstand imposed mechanical and thermal stresses and also be of low thermal conductivity; (5) cooling system must be designed to dissipate considerable heat (anchorages transfer heat into the structural concrete); (6) since the liner is directly exposed to the coolant fluid, corrosion may be an important consideration; and (7) potential cooling problems exist at closures. Problems related to research requirements for development of the hot liner concept and potential licensing difficulties have resulted in assessment studies generally recommending that a cold liner concept be utilized for application to PCRVs. Hot liners may, however, have application to PCPVs for non-nuclear applications such as coal gasification vessels where codification requirements may not be as stringent as for nuclear pressure vessels. Figure 70 presents a comparison of hot- and cold-liner concepts.

Basic requirements of insulation for PCRVs are as follows: (1) low coefficient of conductivity to minimize thickness; (2) good stability under nuclear radiation so that the insulation will not affect the operation of the reactor by emission of either water or dust; (3) ability to withstand the normal operating conditions and the greatly varying transient service

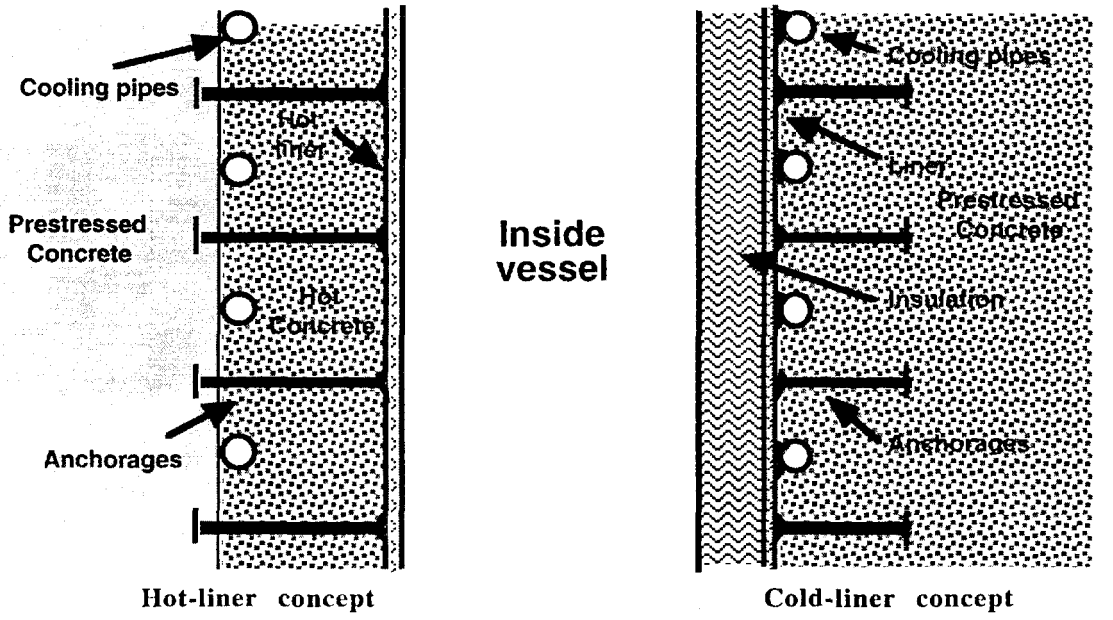

Figure 70. Schematics of hot- and cold-liner concepts.

conditions, ranging from operation under vacuum to rapid variations in both temperature and pressure, and durability and strength to sustain years of service without maintenance or repair; (4) ease of mounting and adaptation to the configuration of the reactor; and (5) low cost. Pumice concrete has been used by the French in their EDF 3, St. Laurent 1 and 2, and Vandellos reactors. Advantages claimed for pumice concrete are that: (1) it is not subject to internal natural convection, provided it is properly grouted to the liner; (2) it has isotropic properties and is easier to adapt to any geometric shape; and (3) it suffers less from partial deterioration due to radiation damage, friction, decompression, or thermal cycling. Disadvantages of the system are its relatively high price, the thickness required (50 cm, or more), and the complex castings required, especially under high-temperature conditions. Metallic reflective insulation has been used in Bugey 1 (France), Schmehhausen (Germany), and the United Kingdom reactors at Oldbury, Wylfa, Dungeness B, Hartlepool, and Heysham. The initial stainless steel foils investigated were formed from alternating layers of corrugated and plain foil, but were later changed to layers of ribbed foils of approximately 0.33 mm thickness. Difficulties with this insulation system relative to pressure dependence of thermal conductivity, not being able to deform the foil on a small radius that would guarantee complete line contact between corrugations and adjacent foil, and presence of convection paths at vertical joints between foils forming a layer led to development of an improved system that has been used in the United Kingdom, an insulation system made of alternating layers of 0.1 mm thick foils separated by 1.3 mm thick wire mesh. The system is fixed to the liner by studs with a cover plate on the gas side and with internal bellows-type seals. The basic philosophy of the system is to trap the primary coolant in cells within the insulation, and hence achieve a thermal conductivity approaching that of stagnant gas. The design is susceptible to flow bypass through the insulation caused by pressure gradients in the primary circuit. Internal natural convection may also occur if the internal seals are not well fitted. In addition, it is difficult to ensure that the insulation conforms to the liner surface. Problems have also been experienced in several vessels during startup, and design of the insulation system to withstand fatigue is difficult because of high noise levels (> 160 dB) experienced in the CO_2 reactors. Fibrous ceramic insulation has been used at Hunterston B, Hinkley B, and Fort St. Vrain. It has advantages of low conductivity, ability to conform to liner surfaces, resistance to permeating hot gas flow, compatibility and stability in high temperature gas, ease of installation, and its relatively low cost. Figure 71 presents a fibrous ceramic insulation system for a steam cycle high-temperature gas-cooled reactor. It consists of insulation blankets compressed uniformly against the liner by cover plates, seal sheets, and multiple attachment devices. The fibrous ceramic material, which is generally an alumina-silica mixture or a relatively pure silica felt, ranges in thickness from 50 to 150 mm. The metallic components are designed to suit the temperature; that is, carbon steel may be used to 425 C and Hastelloy X materials to 800 C. Disadvantages of fibrous ceramic insulation are: (1) ensuring of compatibility of materials with the primary circuit, (2) limiting particulate or dust release to the primary circuit, and (3) maintaining resiliency of the insulation pack to conform to the liner surface thereby maintaining permeation resistance over the design life.

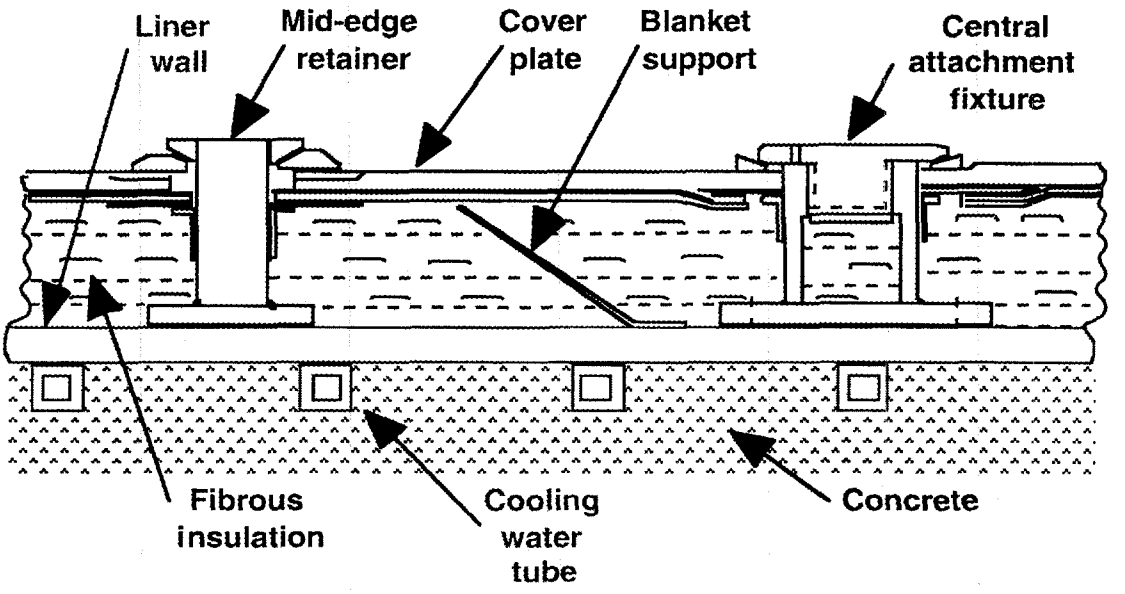

Figure 71. Liner, insulation, and cooling system for HTGR-SC plant.

The concrete in PCRVs is heated in two ways: (1) heat transfer from the hot reactor gas, and (2) heat generated by the neutron and gamma energy. Neither of these heat sources can be completely eliminated, but each can be reduced to an acceptable level through material selection; that is, the heat flux from reactor coolant is reduced by insulation and the nuclear heating by radiation shields. Since it is not economically feasible to prevent all heat from reaching the liner, the liner must be cooled so that temperature gradients across the concrete wall do not lead to unduly high thermal stresses. Heat that passes through the insulation is conducted along and through cooling tubes attached to the outer surface of the liner and embedded in the concrete such as illustrated in Fig. 71.

3.6.2 Concrete Embedment Instrumentation Systems

Measurement of structural response (e.g., stress, strain, deflections) in concrete structures is more difficult than what might appear superficially. Concrete is a heterogeneous material composed of a hydrated portland cement paste matrix that may contain unhydrated cement, voids, water, and fine and coarse aggregate particles. Behavior of the concrete material system is a function of the relative quantities of its constituents and their response to loading and environmental influences. Characteristics of concrete include a nonlinear stress-strain response, elastic modulus and strength variation with age, time- and temperature-dependent deformations, and differences in tensile and compressive behavior. To further complicate measurement, the concrete is usually under a complex state of stress, and any attempt to measure one quantity tends to disturb the structure and can influence the results of another quantity.

Ideally, a device for embedment in concrete to indicate structural response should bond perfectly and should precisely match concrete elastic and viscoelastic properties, coefficients of thermal expansion, and material volume stability. Also, the device should be unaffected by changes in environmental conditions, resistant to corrosion, easily handled, able to survive placement, and relatively inexpensive. Monitoring capabilities should include high resolution, long-term stability and reliability, and adaptability to automatic data acquisition. The capability of monitoring dynamic response is also desirable. However, complete compatibility of an embedded instrument with the concrete it replaces cannot in reality be achieved. As a result, instruments are designed to minimize errors introduced by physical property mismatch or to ensure that differences can be represented using a well-defined relationship.

Various instrumentation systems for embedment in concrete are available commercially to indicate strain, stress, and moisture. Temperature measurement capability often is included in the stress or strain instrumentation, or readings may be readily obtained using thermocouples or thermistors. PCRVs are designed so that concrete remains in compression, but in the event the stress becomes tensile, surface cracks that develop may be easily detected by visual, gage, or acoustic methods, and internal cracks could possibly be detected using acoustic, holography, or other methods.

In order to evaluate the capability of various types of concrete embedment instrumentation for monitoring PCRVs for projected operating periods of 20 to 30 years, or more, an experimental investigation was conducted in which selected commercially-available embedment strain instrumentation were evaluated [33,34]. Figure 72 presents examples of vibrating-wire strain meters evaluated in the study. Included in the study were seven types of vibrating-wire strain gages, three types of unbonded wire gages, one polyester encapsulated gage type, and one single-wire gage type. The strain gages were evaluated with respect to general gage performance, performance in a simulated PCRV environment, and performance under extreme operating conditions.

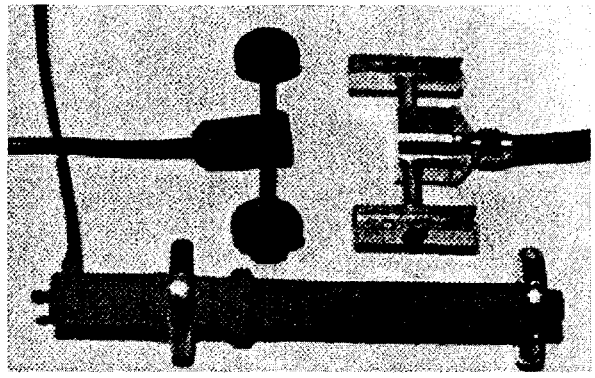

Figure 72. Vibrating-wire strain gages.

3.6.2.1 General gage performance

Each type of gage was evaluated with respect to sensitivity, accuracy, stability, response, data acquisition requirements, adequacy of calibration, and durability (e.g., whether or not it is necessary for protection purposes to precast the gages in briquettes). With the exception of calibration and stability, the evaluations were based on manufacturers' data, the results of which are summarized in Table 1. Studies were also conducted to determine a satisfactory calibration specimen. Prior to conduct of the test series to evaluate the gage calibration data a limited laboratory study was conducted to select a test specimen. Three sets of specimens were cast using the same mix (gravel/cement ratio = 2.64, sand/cement ratio = 2.04) except for the water/cement ratio (0.575, 0.500, 0.425) that was varied to produce different strength concretes. Each set of specimens consisted of cylinders having diameters of 0.05, 0.08, 0.10 and 0.15 m and constant length-to-diameterratios of 3.54. One unbounded wire Type A strain gage, aligned with the longitudinal axis, was embedded in each specimen. After curing in a laboratory environment, two 0.1-m surface strain gages were applied to each specimen at 180° intervals and connected in series to eliminate bending effects. The specimens were loaded in compression to failure with surface and embedded strain gage readings obtained at specific intervals. Results indicated that surface strains were always less than embedded strains at the same stress level and that as the specimen diameter increased there was a trend toward better agreement between experimentally determined and manufacturer's calibration factors. For example, the differences in calibration factors for 0.08 and 0.15-m diameter cylinders were 45 and 8%, respectively. Based on these results a 0.15 m diameter by 0.54 m long test specimen was selected to evaluate gage calibration factors. No apparent strength affect was noted from these preliminary tests.

Table 1 General embedment strain meter performance characteristics.

Type Gage	Gage length (cm)	Strain range (μm/m)	Temperature range (C)	Sensitivity (μm/m)	Gage factor	Readout req'ts	Comments
Electrical Resistance							
Unbonded wire Type A	10 to 15	1,050 to 2,100	65	±5		Bridge circuit	Proven reliability
Unbonded wire Type B	10 to 25	+500 to -1,000	-30 to +70	±6		Bridge circuit	Proven reliability
Unbonded wire Type C	5 to 10	±5,000	-20 to +100	5 to 10	-2.5	Strain indicator	Temperature compensated
Polyester encapsulated	1 to 13	-20,000 to +15,000	-20 to +60	10	2.11	Strain indicator	Stability in moist environment questionable, volume change of plastic
Single wire	5 to 15	±20,000	-200 to >600	5 to 10	2	Strain indicator	High-temperature use, small cross section requires careful placement
Acoustic							
Vibrating wire Type A	7 to 14	>1,000	80	0.5	0.96 x E-3	Period or frequency meter	Used extensively, additional sealing recommended
Vibrating wire Type B	14	>1,000	80	0.5	3.00 x E-3	Period or frequency meter	Used extensively, additional sealing recommended
Vibrating wire Type C	12.7	4,000	-40 to +66	1.0	(from table)	Period or frequency meter	Wire tension easily adjusted, temperature measurement
Vibrating wire Type D	13	3,000		0.5	2.60 x E-3	Period or frequency meter	Temperature measurement, stability poor in moist environment
Vibrating wire Type E	10	3,000	-40 to +80	0.1	2.01 x E-3	Period or frequency meter	Temperature measurement
Vibrating wire Type F	8.8	1,000	-10 to +70	1	1.20 x E-3	Period or frequency meter	Temperature measurement
Vibrating wire Type G	13.3	2,000	-10 to +70 (or +200)	1	3.00 x E-3	Period or frequency meter	Temperature measurement

Calibration factors were determined for the strain gages noted in Table 1. One embedment strain gage was cast in each cylindrical test specimen with the gages aligned with the cylinder axis. The concrete mix design consisted of Type II Portland cement, 0.02-m maximum size crushed limestone aggregate, a gravel/cement ratio of 1.85, a sand/cement

ratio of 2.84, and a water/cement ratio of 0.56. After specimen curing, three sets of 0.20-m-gage length mechanical gage points were attached at 120° intervals and two 0.10-m electrical resistance strain gages were attached at 180° intervals on each specimen's circumference. Figure 73 presents a calibration test specimen prior to testing. The test procedure consisted of: taking zero readings; loading the specimen compressively in 22.2 kN increments to approximately 50% of ultimate load with mechanical, surface, and embedded readings taken at each increment; unloading in 22.2 kN increments with readings taken at each increment; and reloading the specimen in compression to specimen failure with surface and embedded strain readings taken at the same load increments. Average percentage differences between manufacturer's supplied calibration factor and the factor calculated using surface strain output ranged from +5.7% (polyester encapsulated) to –25.7% (vibrating wire Types A and G).

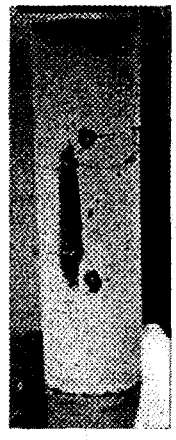

Figure 73. Calibration test specimen.

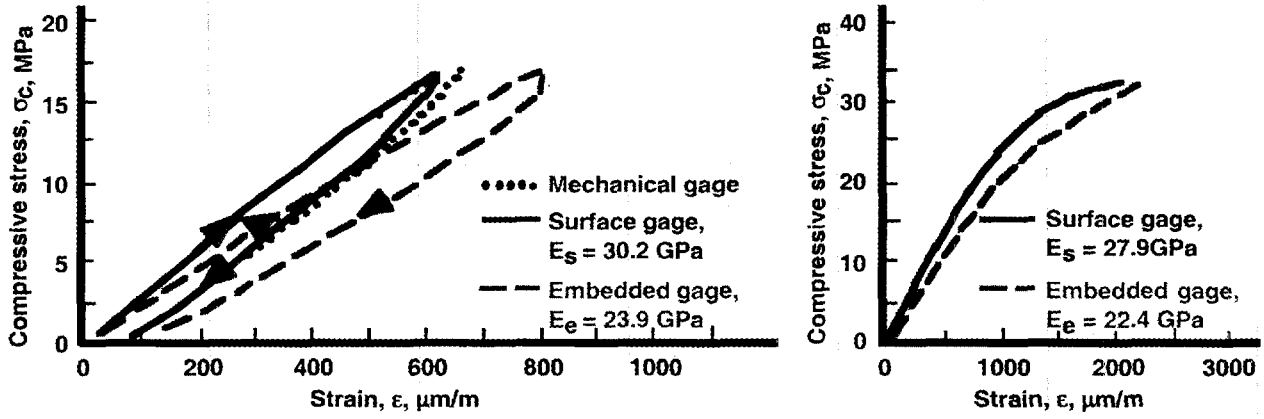

Figure 74. Calibration results: VWSG Type G, specimen 1.

Figure 74 presents an example of results obtained for one of the vibrating wire strain gages. Results indicated that gage calibration factors should always be determined using representative samples from the particular batch of gages. Also, calibration test specimens should be of sufficient size to provide reliable results and should be fabricated using a representative concrete mix.

The stability of embedded strain gages was evaluated by using a copper-sealed cylindrical concrete test specimen 0.41-m diameter by 1.02-m long. The specimen was cast using a 0.02-m maximum aggregate size concrete mix that had a gravel/cement ratio of 2.60, sand/cement ratio of 2.02, and water/cement ratio of 0.48. Contained within the cylinder were 18 embedment strain gages consisting of three unbonded wire Type A, one unbonded wire Type B, two unbonded wire Type C, two polyester encapsulated, three single wire, two vibrating wire Type A, one vibrating wire Type B, two vibrating wire Type F, and two vibrating wire Type G. Figure 75 presents the reinforcement cage and strain gage locations prior to placing in the copper-lined cardboard mold for casting the concrete. Figure 76 presents the test specimen after casting concrete and soldering the copper lid in place. Mechanical gage points were attached to the cylinder at 120° intervals and three weldable strain gages had been attached at 120° intervals to the steel reinforcement cage used to maintain gage alignment during fabrication. Strain and temperature readings were monitored periodically while the cylinder was maintained in a laboratory environment. Results of the stability test for the unbonded wire resistance strain meters are presented in Fig.77. At conclusion of the test series, 4 of the 18 embedded strain meters had failed, with failure defined as being either excessive strain (arbitrarily selected as a strain drift rate in excess of 1 με/3 days) or the inability to obtain a reading. Meter failures included two plastic encapsulated Type A (excessive strain), one single wire (excessive strain), and one vibrating wire Type F (no reading). Two additional meters, an unbonded wire Type C and a single wire, exhibited excessive strains for approximately 100 days in the first half of the test series, but thereafter their readings returned within acceptable limits. Results from this phase of the study tend to

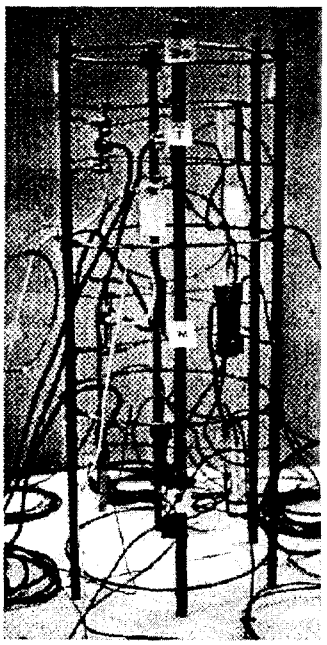

Figure 75. Reinforcement cage used to maintain gage alignment during specimen fabrication.

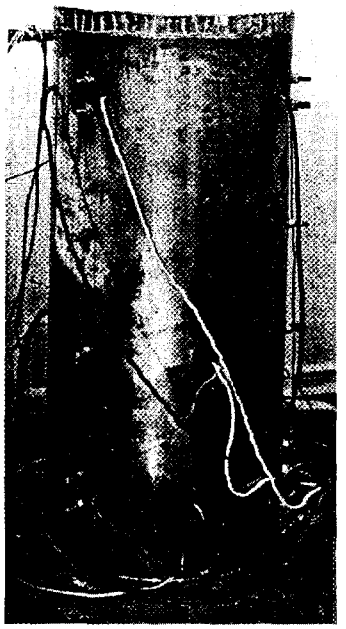

Figure 76. Gage stability test specimen.

indicate that the stability of the strain meters under controlled conditions (i.e., loaded neither by application of external forces nor by temperature) was generally good. The one notable exception was the plastic encapsulated gage that had a tendency to absorb moisture and thus exhibited excessively large systematic drift errors. However, results obtained from the calibration test series indicate that for short-term tests, these meters provide very good results, and are among the least expensive of the embedment meter types.

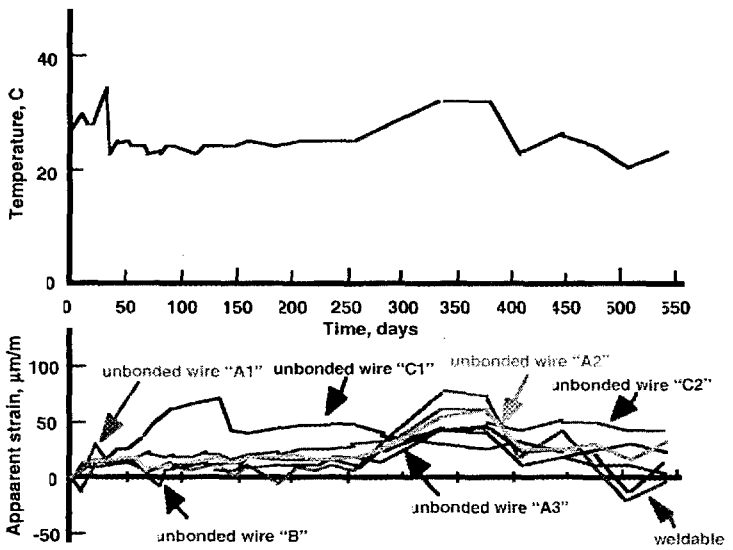

Figure 77. Gage stability test results: unbonded wire resistance meters.

3.6.2.2 Gage performance in "simulated" PCRV environment

A second 0.41-m diameter by 1.02 m cylinder was fabricated to evaluate gage performance in a "simulated" PCRV environment in which specimens were subjected to both uniaxial compression and thermal loading. In an actual PCRV loading would be multiaxial. Contained in the cylinder were 12 embedment strain gages consisting of one unbonded

wire Type A, one unbonded wire Type B, one unbonded wire Type C, one polyester encapsulated, one single wire, one vibrating wire Type A, one vibrating wire Type B, one vibrating wire Type D, one vibrating wire Type E, two vibrating wire Type F, and one vibrating wire Type G. Also included were three weldable strain gages attached to the steel reinforcement cage at 120° intervals, one stress meter, and three thermocouples. At a test age of 29 days, the cylinder was heated by means of an insulated heating blanket until it reached the desired test temperature of 65°C ± 5°C where it was maintained. Axial compressive loading of the cylinder was initiated 196 days into the test series. The specimen was loaded in increments of approximately 2.42 MPa with each loading increment maintained for two to three weeks. Temperature and strain readings were obtained just prior to, one hour after, and during each loading increment, and periodically throughout the 377-day duration of this test series. Figure 78 presents the insulated test specimen positioned in the testing frame and Fig. 79 presents results for the wire resistance, single wire, and plastic encapsulated gages. At conclusion of the test series, 5 of 12 embedment strain meters were considered to have failed. These meters included: a plastic encapsulated Type A (excessive strains), an unbonded wire Type B (no resistance ratio reading obtainable), and vibrating wire Types A, D, and E (no reading obtainable). In addition, the single-wire and unbonded-wire Type C gages were exhibiting significantly less compressive strains than the other functioning embedded meters. The results for this phase of the investigation indicate that the majority of the meters performed adequately; however, the 377-day duration of this test was considerably shorter that the desired operating life for a PCRV of 30 years. Several of the embedment strain meters could benefit from improved sealing techniques, especially if they are being relied upon to help assure the safety and reliability of PCRV-type structures.

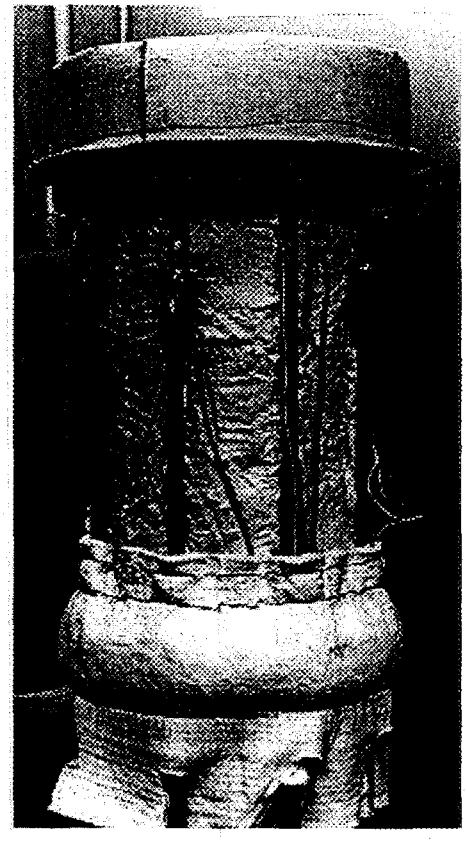

Figure 78. Insulated test specimen: "simulated" PCRV environment.

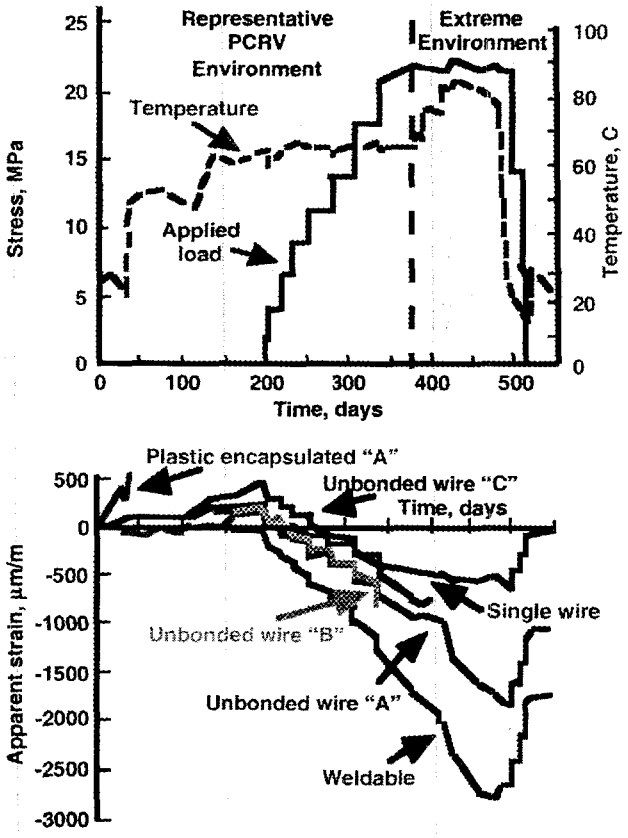

Figure 79. Example of results for "simulated" PCRV environment.

3.6.2.3 Gage performance under extreme operating conditions

The stability of strain meters subjected to environmental conditions more severe than would be encountered during normal operation was evaluated in this test series. Test environments included room-temperature alkaline-water immersion, elevated-temperature alkaline-water immersion, and elevated temperature. Since these environments are

relatively severe, they should provide an accelerated indication of the long-term performance of the meters with respect to moisture penetration and elevated-temperature effects.

The effectiveness of the techniques used to prevent the ingress of moisture into concrete embedment strain meters, where it either produces a breakdown of meter resistance to ground or causes corrosion, was investigated in this test series. Each of the 12 types of meters presented in Table 1 was investigated. The test setup, including pertinent meter readout instrumentation, is presented in Fig. 80. The procedure followed for this phase of the test series included: (1) adding a small amount of unhydrated cement to the water bath to increase the pH of the solution; (2) placing samples of each type of meter into the solution; (3) connecting the wire resistance meters (plastic encapsulated Types A and B, unbonded wire Type C, and single wire) and their dummy meters (to compensate for temperature fluctuations) to a switching and balancing box; (4) connecting unbonded wire meters (Types A and B) and vibrating wire meters (Types A through G) to a switching box; (5) zeroing resistance meter readings and obtaining reference (zero) readings for the unbonded wire and vibrating wire meters; and (6) periodically monitoring strain output from each of the meters until either a meter failed or the test series was completed. After a meter failed, with failure defined as the meter indicating excessive strain output (> 3 μm/m/day) or the inability to obtain a reading, it was generally replaced with a meter of the same type. The total duration of the room-temperature [26 ± 5 C] alkaline-water immersion test was 590 days. During this time span, a total of 39 meters were evaluated. Table 2 presents a summary of the number of meters of each type tested and the number and type of failures experienced, if any.

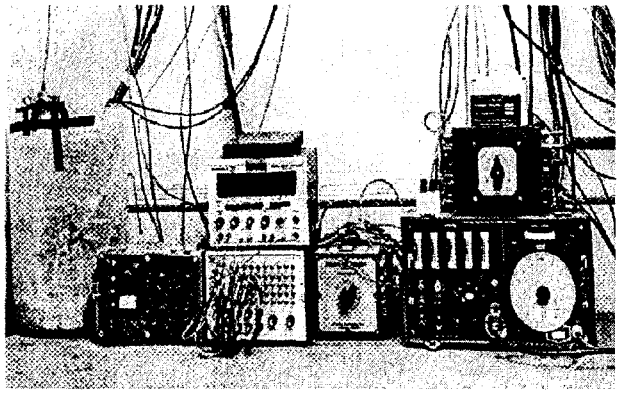

Figure 80. Alkaline-water immersion test setup.

Table 2 Results of alkaline-water immersion test.

Type Gage	Room-temperature water bath		Elevated-temperature water bath	
	Number tested	Number failed (type failure)*	Number tested	Number failed (type failure)*
Electrical Resistance				
Unbonded wire Type A	4	0(0)	8	2(a), 1(b)
Unbonded wire Type B	2	0(0)	2	0(0)
Unbonded wire Type C	1	0(0)	1	0(0)
Polyester encapsulated	3	3(a)	6	6(a)
Single wire	9	4(a)	15	7(a)
Acoustic				
Vibrating wire Type A	3	1(b)	3	1(b)
Vibrating wire Type B	1	1(b)	0	0(b)
Vibrating wire Type C	2	0(0)	2	0(0)^
Vibrating wire Type D	2	2(b)	1	1(b)
Vibrating wire Type E	1	1(a)	1	1(b)
Vibrating wire Type F	3	0(0)	4	1(b)
Vibrating wire Type G	2	0(0)	3	2(b)

*Type failure, a = excessive strain drift, b = no reading obtainable.
^Erratic readings at temperatures greater than manufacturer's stated upper limit.

The effectiveness of meter sealing techniques was evaluated in a more severe test using an elevated-temperature water bath. The procedure followed for this test series was the same as the one employed for the room-temperature alkaline-water immersion test except that the temperature of the alkaline-water bath was maintained at approximately 66°C using an immersion heater. The total duration of the test series was 440 days. During this time span, a total of 46 meters were tested. Seventy-seven days prior to conclusion of this phase of the test series, the temperature of the water bath was permitted to return to room temperature, and twenty-four days later the water was removed from the bath, and the meters still under evaluation were permitted to air dry for an additional 53 days. The meters were periodically monitored throughout this drying phase. The number of meters of each type tested and the number and type of failure experienced, if any, are summarized in Table 2.

The elevated-temperature (T > 66 C) test series was conducted merely as an extension of the test series that evaluated the performance of strain meters subjected to a "simulated" PCRV environment (Fig. 78). The meters evaluated were those that were still operating at the conclusion of the initial series: one single wire, one unbonded wire Type A, one unbonded wire Type C, one vibrating wire Type B, two vibrating wire Type F, and one vibrating wire Type G. The testing procedure consisted of maintaining the uniaxial compressive stress of 21.7 MPa on the 0.41-m-diam by 1.02-m-long cylinder while incrementally increasing the cylinder temperature above its 66 C value. Temperature increments were to nominal temperatures of 70, 75, and 80 C, with the cylinder temperature held at these values for periods of 10, 21, and 70 days, respectively. At the conclusion of the 101-day elevated-temperature test series (478 days total testing for this specimen), the cylinder temperature was permitted to return to room temperature over a 12-day interval. Uniaxial compressive loading of the cylinder was then incrementally reduced, with loads held for several days at each increment. The reduced loading levels were nominally 14, 7, and 0 MPa, with loads held at each increment for periods of 7, 8, and 26 days, respectively. Readings were obtained periodically throughout the elevated-temperature phase of the test series. Temperature and strain histories are presented in Fig. 79 for selected strain meters. During the 101-day duration of the elevated-temperature test series, three additional strain meters failed and one was registering excessively low strains.

Thus, by the conclusion of the test, only three meters were functioning in addition to the weldable strain gages contained on the reinforcement cage. Judging from the performance of the meters examined, it appears that the majority of these meters could not provide reliable data throughout an anticipated 20- to 30-year operating lifetime of a PCRV; selection of a strain meter should be based on its application, that is, a meter may provide excellent results in short-duration tests, but may exhibit unacceptable systematic drift in extended-time tests; and improved corrosion-resistant materials and sealing techniques require development if the strain meters are to survive in PCRV environments, particularly if temperature excursions are involved.

3.6.3 Optimized PCRV for HTGR/SC Plant

In conjunction with representatives of Gas-Cooled Reactor Associates and Stone and Webster Engineering Corporation, a plan was developed for an optimized PCRV for the HTGR steam-cycle reference plant [35]. The purpose of the study was to identify desirable construction innovations and cost-effective changes in configuration, materials, and design criteria, in order to provide the basis for the evolution of more economical plants. Modularization, prefabrication, and precasting sufficiently early in the design process to permit incorporation of essential features and to appropriately influence the configuration and arrangement of components were recommended. The potential cost savings realized through a shortened construction interval is thought to be substantially greater than the potential for reducing direct costs of labor and materials in HTGR-SC plants. Prior studies have indicated that, on a preliminary basis, the HTGR nuclear island configuration should result in a construction duration advantage of approximately six months. The concept of modularization has proved that LWR construction times can be reduced significantly; however, LWRs have been limited with respect to construction optimization due to the lead time of the steel reactor pressure vessel and its restraint on the construction schedule. The PCRV used with the HTGR does not necessarily present the same optimization constraints because of the field-intensive nature of this type of vessel. Also, since the PCRV is the critical path item during a substantial portion of the construction of an HTGR, it is feasible and therefore a goal of this study to reduce the HTGR construction period by as much as one year. The cost savings associated with any reduction in the construction period are substantial. Estimates at the time of this study indicated savings in the order of $4 to 5 million per month due to the effects of allowance for funds used during construction (AFUDC) and escalation. Thus, a one-year savings in construction time for an HTGR power plant could produce a total savings of $60 million. Figure 81 presents the PCRV and containment structure for a gas-reheat HTGR-SC plant.

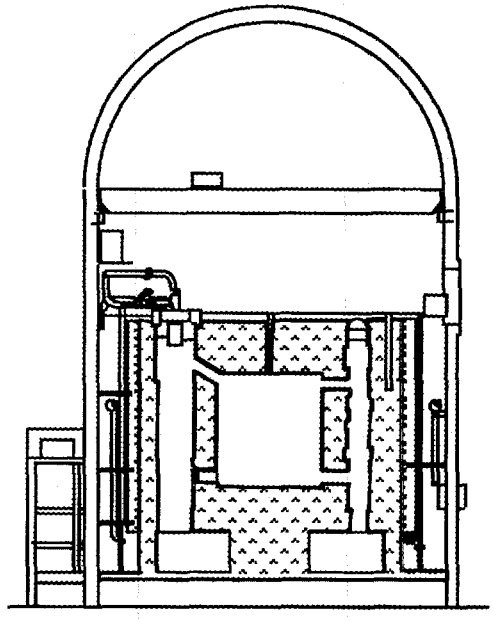

Figure 81. Elevation view of PCRV and containment structure for gas-reheat HTGR-SC plant.

3.6.4 Pebble-Bed-Fueled vs Prismatic-Fueled HTGRs

An assessment of PCRV and containment building capital costs was conducted as part of an overall comparison of pebble-bed (PBR)- and prismatic (PR)-fueled HTGR's [36]. Because the PBR has a lower power density than the PR (5.5 W/cm^3 vs. 7.1 W/cm^3), it will have a larger core diameter for the same power rating, and thus will require a larger core cavity than the PR. This will mean increased capital costs for the PCRV and containment building of a PBR. The purpose of this phase of an overall assessment of the two HTGR types was to determine the significance of these increased costs for both 1000 MW(t) and 3000 MW(t) power reference systems, considering a coolant outlet temperature of 850 C. At the time of this study, results indicated that for the 1000 MW(t) plant, costs for the PBR would exceed those for the PR by 7.2 to 9.0% and for the 3000 MW(t) plant, PBR costs would be greater by 10.6 to 12.6%. While these results are for gas turbine designs, the PCRVs and containment structures associated with the other reactor applications, namely, steam cycle and process heat cases, should have relative cost differentials about the same as those provided above.

3.6.5 Pressure Vessel Concepts for HTGR Modular Reactor Systems

Small modular reactor systems offer potential advantages relative to the larger HTGR-SC systems. Some of these advantages include potential for complete replacement of individual units, an assured path of shutdown cooling, high availability, reduced technical risks, and competitive capital costs and economics. As a part of an overall assessment of modular reactor systems at ORNL, an evaluation of pressure vessel concepts for application to these systems was conducted [37]. In comparing the various pressure vessel concepts several study parameters were utilized. They included modular reactor systems with each module having a core thermal power of about 250 MW, core inlet temperature of 425 C, core outlet temperature of 950 C, core geometry of 6.34 m high by 3.5 m diameter, and a design pressure of 4.8 MPa. The primary system of each module is based on the design of the in-line reactor reformer arrangement and consists of a core, steam reformer, steam generator, and helium circulator. The entire primary coolant system is enclosed in a pressure vessel. It is with respect to vessel concepts for the in-line design that this study was concerned.

Three pressure vessel concepts were considered: prestressed concrete, prestressed cast iron, and steel. Each of these concepts was reviewed with respect to: (1) general description; (2) materials and fabrication; (3) design and analysis; (4) experience; (5) advantages and limitations; (6) requirements for quality assurance, structural integrity testing, and in-service inspection; and (7) failure modes and repair considerations. Based on this review, a qualitative comparison of the vessel concepts was made and a rating assigned. Capital cost estimates were prepared for each of the vessel concepts and results obtained at the time of this study indicated that approximate costs for the prestressed concrete, prestressed cast iron, and steel vessels would be $7.5 M, $7.8 M and $4.4 M, respectively. Results of this evaluation indicate that, at present, the steel vessel appears to be the most favorable concept for the modular reactor system. This is based on the steel vessel's lower estimated capital costs and its established technology. Prestressed concrete reactor vessels offer advantages with respect to safety, but the small size of the modular reactor system does not enable them to be cost effective relative to the steel vessels. Prestressed cast iron vessels offer promise, but they also can not compete economically with the steel vessels for small modular reactor systems and they suffer from a lack of developed technology and experience, especially in the United States.

3.7 U. S. NUCLEAR REGULATORY COMMISSION-RELATED ACTIVITIES

Recent research sponsored by the U. S. Nuclear Regulatory Commission is directed at assessments of safety-related nuclear power plant concrete structures and addresses regulatory guide-related evaluations (i.e., inspections of post-tensioning tendons and containment leak-rate testing requirements) and aging management of safety-related concrete structures and containment pressure boundary components.

3.7.1 In-Service Inspections of Greased Tendons in Prestressed Concrete Containments

Thirty-eight of the operating nuclear power plant stations in the United States use a prestressed concrete containment structure. Virtually all of these structures make use of post-tensioned unbonded prestressing tendons coated with some type of corrosion inhibitor. The principal functions of these structures are to (1) provide the reactor coolant system with protection for such potentially disastrous events as aircraft impact, wind-generated missiles, and earthquakes, and (2) prevent the release of radioactivity in the event of a loss-of-coolant accident. Because these functions are safety related, the *Code of Federal Regulations* [38] requires in part that the containment be designed to permit a periodic inspection of all important areas and that an appropriate surveillance program be developed. The U.S. Nuclear Regulatory Commission (NRC) published Regulatory Guide 1.35, "Inservice Surveillance of Ungrouted Tendons in Prestressed Concrete Containment Structures" with the intent that the Guide was to provide utilities with a basis for developing surveillance programs that would be acceptable to the NRC and to provide reasonable assurance, when properly implemented, that the structural integrity of the containment was being maintained. Because a variety of factors such as tendon corrosion, anchorage failure, and material defects can weaken structural integrity, the guide sought to examine all sources of potential problem areas before they became critical. A random sample of tendons is selected from the total accessible tendon population. Anchorage components for each tendon in the sample are visually inspected for defects or other abnormalities. Prestressing force for each sample tendon is measured (with corresponding elongation measurements), a grease sample is obtained for laboratory analysis of impurities, and a wire sample is removed for material property determinations. The prestressing forces, elongation, grease impurities, and material properties are compared with allowable limits. In the case of the prestressing forces, these limits vary with time and must be calculated for the time of the surveillance, Fig. 82.

As experience with the surveillances mounted, the Guide has been revised to keep pace with technological advances in containment design, to reflect the knowledge obtained through experience, and to eliminate points of confusion concerning interpretation and implementation of the Guide. Three revisions have been made, with the latest revision concerned primarily with changes in sample size, changes in the number of wires to be removed for material property determinations, and expanded applicability of the Guide to include newer designs.

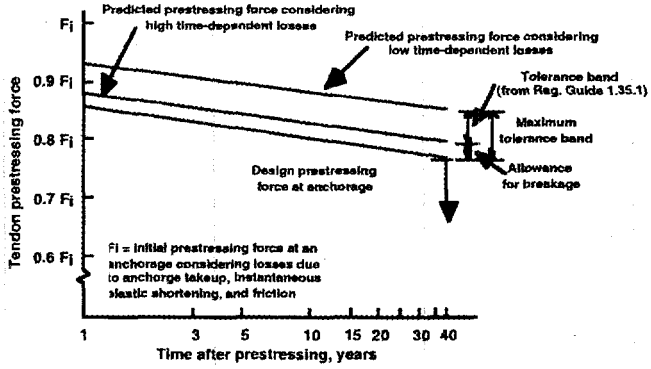

Figure 82. Example of tolerance band for prestress.

ORNL conducted an assessment of the proposed Guide revisions [39].In the study an analysis of the available utility surveillance data and an evaluation of current proposed guidelines was conducted. Comments from utility and industry personnel were factored into the analysis. The results indicated that the majority of the few incidences of problems or abnormalities that occurred with the post-tensioning systems were minor in nature and did not threaten the structural integrity of the containment. All of the available surveillance reports concluded that the respective containments were in good condition. However, the surveillance reports did reveal discrepancies between utilities in the interpretation of the results. Evaluation of the proposed guidelines also revealed areas that could be modified to provide improved results; that is, some consideration should be given to modifying the sample size, the tendon force levels should be evaluated both as a group and individually, and the acceptable levels of impurities in the grease should be reexamined as more data become available. Additional research on the long-term effects of the impurity levels on the effectiveness of the grease also seemed justified. Furthermore, because only a limited amount of data were available during this study, perhaps the most important suggestion was that more surveillance data should be examined before firm conclusions are drawn. Also, there should be a continuing effort to utilize the information gained through containment inspection experience.

This activity was followed by a review of all the changes in Rev. 3 (Draft 2) of the Guide and conduct of a regulatory analysis for all positions in the guide to determine if it was cost-effective to backfit the Guide to containments of existing plants [40]. Revision 3 (Draft 2) of the Guide provided industry with clarification of certain issues not fully addressed in Rev. 2. Application of the revision to operating plants was intended to provide consistency in review and a uniform standard for assessing the in-service condition of the ungrouted tendons in prestressed concrete containments. Although Rev. 3 would effect increased costs to industry in certain areas (e.g., visual inspection of grease caps of all vertical tendons, requirements for lift-off tests on second containment where two essentially identical containments exist at a site), a reassessment of requirements in other areas (e.g., tendon sample size, tendon detensioning) would produce a net cost savings. Under the comparative regulatory analysis major decision factors affected by the proposed changes in Rev. 3 were identified and differential risk and cost factors were addressed in relation to the current version of the Guide that was in effect (Rev. 2). The backfit analysis was conducted in accordance with the requirements of the "Backfitting" Rule, §50.109 (*Code of Federal Regulations*) for each of the revised or added positions contained in Rev. 3 (Draft 2). Results obtained indicated that even though changes in the Guide were determined to produce an unquantifiable change in public risk, it was concluded that a reduction in number of tendons to be detensioned and the increased requirements for visual inspections, grease impurity levels, and prestress monitoring of the second containment at a site will have a positive impact on safety and thus lower the risk. Containment availability also should be enhanced. Backfitting of the revised guide was determined to be possible for most plants licensed since 1974; however, backfitting of the Guide to plants licensed prior to 1974 (pre-guide plants) would have to be on a case-by-case basis.

Current basic requirements for inspection of ungrouted tendons in nuclear power plant containments are provided in Section XI, Subsection IWL, "Requirements for Class CC Concrete Components of Light-Water Cooled Plants," of the ASME Code [41].

3.7.2 Evaluation of Containment Leak-Rate Testing Criteria

Containment leaktightness is verified periodically through pressure tests and the measurement of the subsequent leakage. The verification process is composed of three types of test: Type A tests of the entire containment system; Type B tests of all containment penetrations, except isolation valves; and Type C tests of isolation valves. These tests are conducted in accordance with Appendix J of the *Code of Federal Regulations* [38] with guidance provided by an industry standard, ANSI/ANS-56.8 [42]. To assist in a revision of Appendix J, a review of the existing and proposed guidelines in light

of utility test data and experience was conducted [43].

A review of 49 Type A test reports and 46 Type B and C test reports was accomplished. Exemption requests found in 25 reports and 100 Licensee Event Reports (LERs) were also reviewed. Two major findings of the data analysis were that Type A test durations of less than 24 h are practical and that almost all Type A test failures and delays were caused by excessive leakage through Type B- and C-tested components. Excessive valve leakage represented 38% of the LERs and highlighted the need for improved maintenance, repair, and testing of these components. Excessive airlock leakage was generally the result of worn, damaged, misaligned, or dirty door seals. It was concluded that Appendix J appears to be very responsive to the results of test experience and technological changes. One major change is the requirement that as-found leakages must be reported as well as as-left leakages. This will help eliminate the poor performance of local leak testing programs. The clarification and rewording of several areas should help reduce the number of exemptions requested. The introduction of a regulatory guide provides a vehicle for the Nuclear Regulatory Commission to specify any exceptions to the relevant industry standards and to resolve areas of conflict.

Appendix J was amended on September 26, 1995 to provide a performance-based option (Option B). Under this option, licensees with good integrated leakage-rate test results can reduce their Type A testing frequency from three times in a ten-year interval (Option A) to one time, and Type B and C testing frequency also can be reduced based on operating experience. However, if Option B is selected, the licensee must still perform a general visual examination of accessible interior and exterior containment surfaces prior to the Type A test and during two other refueling outages prior to the next test.

3.7.3 Aging Management of Safety-Related Concrete Structures

Nuclear power provides in excess of 20 percent of the net electricity generation in the United States. Currently (2002) about 25% of the 104 nuclear power plants that have been licensed for commercial operation are less than 20 years old, with over one-third of the plants being over 30 years old. Starting in 2006, the first of these plants will reach the end of its initial 40-year operating license period. By 2010 ten percent of the plants will reach the end of their initial operating license period with this number rising to forty percent by 2015, Fig. 83. Faced with the prospect of having to replace the lost generating capacity from other sources and the potential for substantial shutdown and decommissioning costs, many utilities are expected to seek extensions to their initial plant operating licenses. In fact this is what is happening. As of July 2002, 24 plants have either been through the license renewal process or submitted an application to renew their operating license for an additional 20 years, and 23 additional plants have announced that they intend to do so.

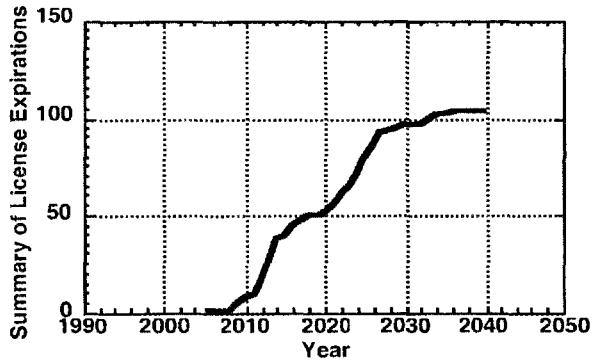

Figure 83. Nuclear power plant initial operating license expiration.

The importance of nuclear power and the necessity for ensuring continued satisfactory operation is thus clearly established. One of the primary factors that could affect the continued operation and development of nuclear power relates to aging of the plants and its potential impact on performance. Nuclear power plants are designed, built, and operated to standards that aim to reduce the releases of radioactive materials to levels as low as reasonably achievable. Nuclear power plants, however, involve complex engineering structures and components operating in demanding environments that potentially can challenge the high level of safety (i.e., safety margins) required throughout the operating life of the plant. It is necessary that safety issues related to plant aging and continuing the service of the nuclear plants be resolved through development of sound scientific and engineering understanding. One specific area that has been noted is the aging behavior of structural materials – particularly those in pressure-retaining structures. Although major mechanical and electrical equipment items in a plant could be replaced, if necessary, replacement of many of the safety-related structural components would be economically unfeasible. Approval for a continuation of service must be supported by evidence that these structures will continue to be capable of withstanding potential future extreme events.

All commercial nuclear power plants contain concrete structures whose performance and function are necessary for protection of the safety of plant operating personnel and the general public, and the environment. Typical safety-related functions that the concrete structures provide include foundation, support, biological shielding, containment, and protection against internal and external hazards. Each boiling-water reactor (BWR) or pressurized-water reactor (PWR) unit in the U.S. is housed within a much larger metal or concrete containment. Concrete containments for PWRs are fabricated from reinforced concrete, that in some cases may be post-tensioned. They all enclose the primary circuit that includes the reactor pressure vessel, steam generators, etc. Three general categories of PWR containments exist: large dry, ice condenser, and subatmospheric. The large dry containment is designed to have a capacity to contain the energy of the entire volume of primary coolant fluid in the unlikely event of a loss-of-coolant-accident (LOCA). The ice condenser containments channel the steam resulting from a LOCA through ice beds to reduce the pressure buildup and thus the containment volume and pressure requirements. The subatmospheric containments are designed so that a slightly negative pressure is maintained in the containment to reduce the volume requirements. Although the majority of BWR plants utilize a steel containment vessel, a number of units utilize either a post-tensioned-or reinforced-concrete containment. With only one exception, all BWR plants in the United States that utilize a steel containment have reinforced concrete structures that serve as secondary containments or reactor buildings and provide support and shielding functions for the primary containment. The containments are divided into two main compartments — wetwell and drywell. After a LOCA, the air and steam in the drywell are forced through a number of downcombers to a pool in the wetwell, where the steam condenses. Water spray systems are provided and the auxiliary systems are generally housed in the secondary containment. A myriad of other concrete-based structures are also contained as part of a light-water reactor (LWR) plant (e.g., reactor pedestal/support, intake structures, and primary shield wall).

Nuclear safety-related concrete structures are composed of several constituents that, in concert, perform multiple functions (e.g., load-carrying capacity, radiation shielding, and leaktightness). These constituents include concrete, conventional steel reinforcement, post-tensioning steel, and steel liner materials. The concretes typically consist of a moderate heat of hydration cement, fine aggregates (sand), water, various admixtures for improving properties or performance of the concrete, and either normal-weight or heavyweight coarse aggregate. Both the water and aggregate materials are normally obtained from local sources and are subjected to material characterization prior to use. Mild steel reinforcement is used primarily to provide tensile and shear load resistance/transfer and consists of plain carbon steel bar stock with deformations (lugs or protrusions) on the surface. Minimum tensile yield strengths generally range from 270 to 415 MPa. The post-tensioning system consists of post-tensioning tendons that are installed, tensioned, and then anchored to the hardened concrete forming the structure. The post-tensioning tendons provide primary resistance to tensile loadings and also improve resistance to shear forces that might develop during earthquake loadings. Three major categories of post-tensioning system exist depending on the type of tendon utilized — wire, bar, or strand. Minimum ultimate strengths of post-tensioning tendons generally range from 2,000 to 10,000 kN. The tendons are installed within pre-placed ducts in the containment structure and are post-tensioned from one or both ends after the concrete has achieved sufficient strength. After tensioning, the tendons are anchored by buttonheads, nuts, or wedges, depending on the tendon type. With the exception of two plants (Robinson 2 and Three Mile Island 2), corrosion protection is provided by filling the ducts with wax or corrosion-inhibiting grease. Metallic liners are provided on the inside surface of the containments to provide a barrier against leakage. A typical liner is composed of steel plate stock less than 13–mm-thick, joined by welding, and anchored to the concrete by studs, structural steel shapes, or other steel products. The PWR containments and drywell portions of BWR containments are typically lined with carbon steel plate. The liner of the wetwell of BWR containments, as well as the LWR fuel pool structures, typically consists of stainless steel plates. Certain LWR facilities have used carbon steel plates clad with stainless steel for the liner. Although the liner's primary function is to provide a leak-tight barrier, it also can act as part of the formwork during concrete placement. Figure 84 shows a concrete containment under construction illustrating some of the key components (e.g., liner, steel reinforcing, and concrete.

Reinforced concrete structures at nuclear power plants historically have been designed in accordance with national consensus codes and standards in force at the time (e.g., American Concrete Institute 318, "Building Code Requirements for Structural Concrete"). The rules in these documents were developed over the years by experienced people and are based on the knowledge that was acquired in testing laboratories and supplemented by field experience. Design principles have been dominated by analytical determinations based on strength principles. Durability considerations require that the time element be factored into the design of reinforced concrete structures. Associated with the design specifications developed for concrete structures in conformance with these calculations was a certain level of durability (e.g., minimum concrete cover requirements to protect embedded steel reinforcement under different anticipated environmental conditions). Although the vast majority of reinforced concrete structures, and particularly those associated with nuclear power plants, have met and continue to meet their functional and performance requirements, several instances can be cited where these structures have exhibited degradation. Primary mechanisms or factors that can

produce premature deterioration of concrete structures include those that impact either the concrete or reinforcing steel materials. Degradation of concrete can be caused by adverse performance of either its cement-paste matrix or aggregate materials under chemical or physical attack. Chemical attack may occur in several forms: efflorescence or leaching, sulfate attack, attack by acids and bases, salt crystallization, and alkali-aggregate reactions. Physical attack mechanisms for concrete include freeze/thaw cycling, thermal exposure/thermal cycling, abrasion/erosion/cavitation, irradiation, and fatigue or vibration. Degradation of mild steel reinforcing materials can occur as a result of corrosion, irradiation, elevated temperature, or fatigue effects. Post-tensioning materials are susceptible to the same degradation mechanisms as mild steel reinforcement, plus loss of post-tensioning force, primarily due to tendon relaxation and concrete creep and shrinkage.

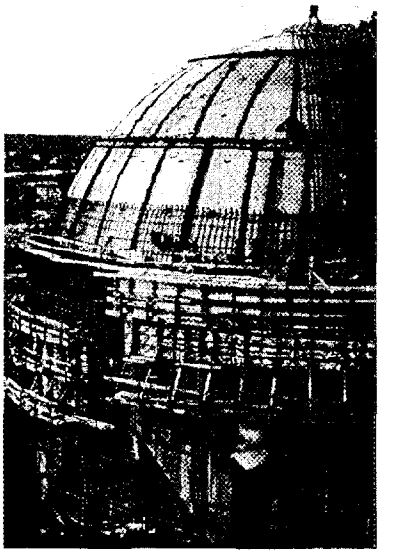

Figure 84. Concrete containment under construction.

Overall the performance of nuclear power plants concrete structures has been very good. Long-term performance evaluations of these structures indicate that they can continue to meet their functional and performance requirements over a period significantly longer than their initial design life. However, there have been several isolated instances that if not remedied could challenge the capacity of the concrete containment and other safety-related concrete structures to meet future functional and performance requirements. In general, many of the reported degradation instances associated with nuclear power plant concrete structures occurred early in the life of the structures and primarily have been attributed to construction/design deficiencies, improper material selection, or environmental effects. Although the vast majority of these structures will continue to meet their functional and performance requirements during their service period, it is reasonable to assume that there will be isolated incidents where the structures may not exhibit the desired durability without some form of intervention. Some general observations derived from condition surveys of concrete structures in several nuclear power plants in both the U.S. and Europe were that virtually all nuclear power plants have experienced cracking of the concrete structures that exceeded typical acceptance criteria for width and length, numerous plants had groundwater intrusion occurring through the power block or other subsurface structures, few plants had a comprehensive program for conducting periodic inspections of the concrete structures (at the time the survey was taken), and aging concerns exist for subsurface concrete structures as their physical condition cannot be easily verified [44].

Figure 85 presents examples of environmental stressor-related degradation that has occurred. Additional degradation has included corrosion of post-tensioning tendon wires, low prestressing forces, freeze/thaw damage, and corrosion of

Water Intake Structure
Rebar Corrosion

Leaching in
Tendon Gallery

Concrete Cracking
with Grease Leakage

Figure 85. Examples of environmental stressor-related degradation.

containment metallic liners [45]. As the nuclear power plant structures age, incidences of degradation, particularly those related to environmental factors, are expected to increase. Some of the aging concerns that have been identified to date include inaccessibility of reinforced concrete basemats for inspection to detect potential degradation resulting from mechanisms such as leaching or sulfate attack, corrosion of steel in water-intake structures, and corrosion of embedded portions of the steel pressure boundary (liner) due to a breakdown of the seal at the floor-to-liner interface. Incidences of structural degradation related to the concrete components in nuclear power plants indicate a potential need for improved surveillance, inspection/testing, and maintenance to enhance the technical bases for assuring continued safe operation. Two NRC programs have been conducted for this purpose: concrete component aging and structural aging.

3.7.3.1 Concrete component aging program

Information provided in a report prepared for the Electric Power Research Institute (EPRI) indicated that concrete durability (aging) under the influence of either material interactions, aggressive environments (freeze-thaw, wetting-drying, or chemical), or exposure to extreme environments (elevated temperature, irradiation, or seismic) is one of the key issues in continuing the service of nuclear power plants [46]. Although operating plants have reported little difficulty with concrete materials, an evaluation of the long-term effects of the environmental challenges to which these structures are subjected had not been adequately addressed. As a result, NRC implemented a study under their Nuclear Plant Aging Research (NPAR) Program to expand on the prior EPRI study relative to longevity and life extension considerations of safety-related concrete components in light-water reactor (LWR) facilities and to provide background that would logically lead to subsequent development of a methodology for assessing and predicting the effects of aging on the performance of concrete-based materials and components [47]. The approach followed was in accordance with the NPAR strategy to evaluate the long-term environmental challenges of LWR concrete facilities and thus provide the background material to meet the previously stated objectives and consisted of: (1) description of primary safety-related concrete components in LWRs; (2) review of the performance of concrete components in both nuclear and non-nuclear applications; (3) identification and discussion of potential environmental stressors and aging factors to which concrete safety-related components may be subjected in an LWR environment; (4) review of the current state-of-the-art for in-service inspection, surveillance, and detection of concrete aging phenomena and assessment of structural adequacy; (5) discussion of remedial measures for the repair or replacement of degraded concrete components; and (6) remarks concerning correlations between damage assessment and life extension considerations.

Applications of safety-related concrete components to LWR technology were identified, and pertinent components (containment buildings, containment base mats, biological shield walls and buildings, and auxiliary buildings), as well as the materials of which they are constructed (concrete, mild steel reinforcement, post-tensioning systems, embedments, and anchorages) were described. Historical performance of concrete components was established through information presented on concrete longevity, component behavior in both LWR and high-temperature gas-cooled reactor applications, and a review of problems with concrete components in both general civil engineering and nuclear power plant applications. The majority of the problems identified with nuclear power applications were minor and involved either concrete cracking, concrete voids, or low concrete strengths at early ages. Five incidences involving LWR concrete containments considered significant were described in detail from occurrence and detection through remedial measures used to restore structural integrity or continuity. These incidences were related either to design, construction, or human error (not aging) and involved two dome delaminations, voids under tendon-bearing plates, anchor head failures, and a breakdown in quality control and construction management. Figure 86 summarizes results of a survey according to problem type. An annotated problem listing is provided in Appendix B of the final report for this activity [47].

Potential environmental stressors and aging factors to which LWR safety-related components could be subjected were identified and discussed in terms of durability factors related to the materials used to fabricate the components (e.g., concrete, mild steel reinforcement, post-tensioning systems, and embedments). The current technology for detection of concrete aging phenomena was also presented in terms of methods applicable to the particular material system that could experience deteriorating effects.

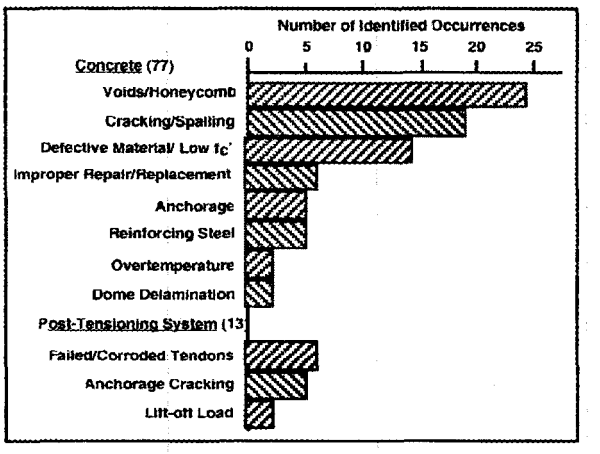

Figure 86. LWR concrete component problem areas.

Remedial measures for the repair or replacement of degraded concrete components were discussed, and examples of pre-repair and post-repair structural performance presented to indicate the effectiveness of these measures. Finally, considerations relative to development of a damage methodology for assessment of durability factor deterioration rates and prediction of structural reliability are discussed. Conclusions and recommendations of the report note the need for (1) obtaining aging data from decommissioned plants, (2) using in-service inspection programs to provide aging trends, (3) developing a methodology to quantitatively and uniformly assess structural reliability as affected by aging or degradation of structural materials, and (4) performing research in support of all these needs.

3.7.3.2 Structural aging program

The Structural Aging (SAG) Program had the overall objective of preparing documentation that provides NRC license reviewers with (1) identification and evaluation of the potential structural degradation processes; (2) issues to be addressed under nuclear power plant continued service reviews, as well as criteria, and their bases, for resolution of these issues; (3) identification and evaluation of relevant in-service inspection, structural assessment or remedial measures programs; and (4) methodologies to perform current assessments and reliability-based life predictions of safety-related concrete structures . To meet this objective, SAG Program activities were conducted under three task areas: (1) materials property data base, (2) structural component assessment/repair technologies, and (3) quantitative methodology for continued service determinations [48].

Materials property data base. The materials property database task has developed a reference source that contains data and information on the time variation of material properties under the influence of pertinent environmental stressors and aging factors. This source can be used to assist in the prediction of potential long-term deterioration of critical structural components in nuclear power plants and to establish limits on hostile environmental exposure for these structures. Primary activities under this task included development of the Structural Materials Information Center, assemblage of materials property data, and material behavior modeling (i.e., review and evaluation of service life models and performance of post-tensioning systems). Initial development of the *Structural Materials Information Center* (SMIC) has been completed [49]. Contained in this reference are detailed descriptions of the *Structural Materials Handbook* and *Structural Materials Electronic Data Base* that comprise the SMIC, Fig. 87. The *Structural Materials Handbook* is an expandable, hard-copy reference document containing complete sets of data and information for each material. The *Structural Materials Electronic Data Base is* an electronically-accessible version of the handbook that provides an efficient means for searching the data base files.

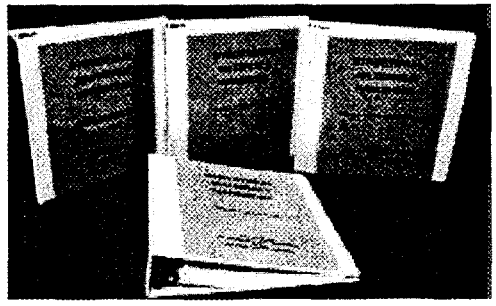

Structural Materials Handbook

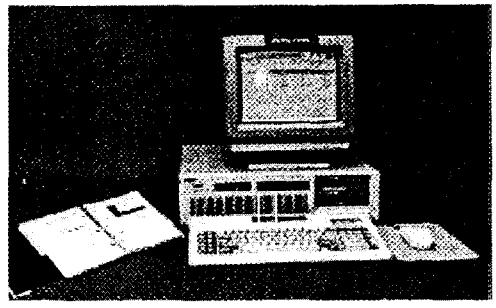

Electronic Data Base

Figure 87. Structural materials information center.

In parallel with efforts to develop the SMIC, activities were conducted to establish materials property data for input into the SMIC. Two primary approaches were utilized — open-literature information and testing of prototypical samples. To date, 144 material data bases have been developed (i.e., 128 concrete, 12 metallic reinforcement, 1 prestressing tendon, 2 structural steel, and 1 rubber). Several of these data bases relate to testing of samples associated with nuclear power plant facilities. Summary descriptions of the material property data base files contained in SMIC are available [50]. Figure 88 presents long-term concrete compressive strength results for data obtained from the literature as well as from testing specimens obtained from nuclear power plants. Compressive strength data have been normalized to their

28-day strength values.

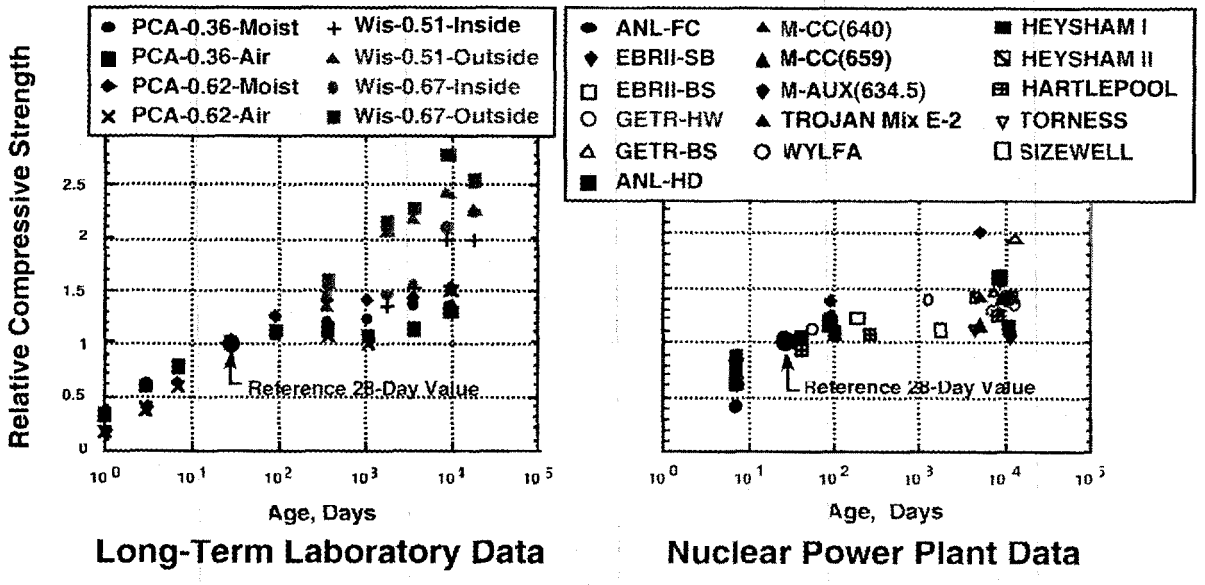

Figure 88. Long-term concrete compressive strength results

A review and evaluation of accelerated aging techniques and tests that can either provide data for service life models or can be used by themselves to predict service life or performance of reinforced concrete was completed [51]. Models were identified and evaluated for each of the degradation processes that can potentially impact the performance of nuclear power plant concrete structures. The most promising approach for predicting the remaining service life of concrete utilizes models of the degradation processes. Figure 89 identifies techniques for estimating the service life of concrete structures and the primary recommendation of this study.

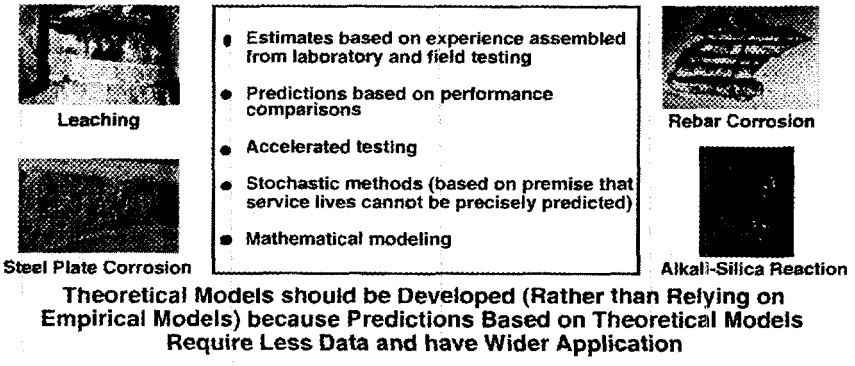

Figure 89. Summary of the study reviewing and assessing service life models

Two studies have addressed aging of post-tensioning systems in nuclear power plants: factors affecting aging of post-tensioning systems and an investigation of tendon corrosion inhibitor migration into concrete. Primary degradation mechanisms considered under the first study were corrosion, loss of prestressing force, and (potential) loss of strength and ductility of the post-tensioning elements [52]. Results indicate that deterioration of the system hardware has not been significant. Wire (or strand) strength and ductility do not appear to lessen with time. Water has occasionally been found in the anchorage end caps but has been of no consequence or produced only minor surface staining of load-bearing elements. Tendon end-anchorage data tends to be quite scattered, but forces generally were above the required limits although some of the older plants have experienced tendon forces below these limits. As a consequence, it was recommended that additional studies be undertaken so that the tendon force can be determined in a manner that ensures the average force (along the tendon length) can be computed with reasonable accuracy. Leakage of corrosion-inhibiting grease has occurred at the tendon end caps due to overfilling or presence of defective gaskets. Grease has also been observed on exterior concrete surfaces, apparently migrating through duct seams and concrete cracks to the surface, Fig. 90. In an effort to determine if leakage of grease through a containment wall interacts with the concrete to affect its strength or bond to conventional steel reinforcement, a limited study was conducted [53]. Concrete core samples were obtained in four areas of grease leakage at the Trojan Nuclear Plant that was being decommissioned, Fig. 91.

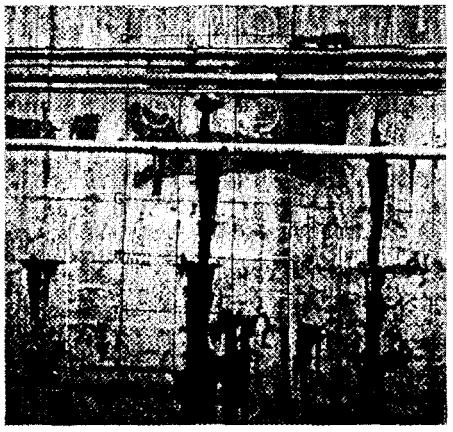

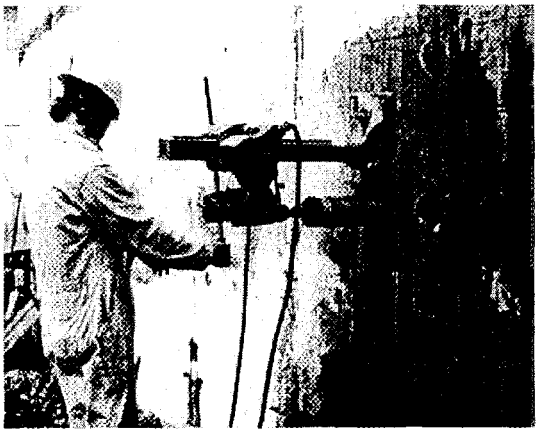

Figure 90. Grease leakage at Trojan Plant. Figure 91. Coring to obtain grease migration samples.

Leakage of grease from the tendon conduits probably initiated at this plant when there was a breakdown in the seal (taped joint) between adjacent tendon sheaths due to build-up of excessive pressure. The grease then migrated through cracks that had formed over the vertical tendons and appeared on the containment surface. Examination and testing of the core samples indicated that migration of the grease was confined to the cracks and there was no perceptible movement into the concrete. Also, there were no visible indications of chemical interactions between the grease and the concrete (i.e., absence of concrete spalling and pattern cracking). For this one plant, except for the loss of corrosion inhibitor from the tendon conduit, the problem appears to be primarily related to aesthetics or maintenance, and not a potential structural problem.

Structural component assessment/repair technologies. New structures can be designed for improved durability based on operating experience (e.g., use of high performance concrete materials). Existing structures, however, have already been designed and constructed, so apart from possibly the addition of barrier materials and sealants to accessible surfaces to prevent ingress of hostile environments, the most prudent approach to maintaining adequate structural margins is through an aging management program that involves application of in-service inspection and maintenance strategies.

The objectives of this task were to develop a systematic methodology that can be used to make quantitative assessments of the presence, magnitude, and significance of any environmental stressors or aging factors that can adversely impact the durability of safety-related concrete structures in nuclear power plants; and provide recommended in-service inspection or sampling procedures that can be utilized to develop the data required both for evaluating the current condition of concrete structures and for trending the performance of these components. Associated activities included an assessment of techniques for repair of concrete, and identification and evaluation of methods for mitigation of any environmental stressors or aging factors that may act on critical concrete components.

A methodology was developed that provides a logical basis for identifying the critical concrete structural elements in a nuclear power plant and the degradation factors that can potentially impact their performance [54]. Numerical ranking systems were established to indicate the relative importance of a structure's subelements, the safety significance of each structure, and the potential influence of the particular environment to which it is exposed. Results of this activity can be utilized as part of an aging management program to prioritize in-service inspection activities. Figure 92 presents a flow diagram of the degradation assessment methodology that can be used to provide a ranked ordering of concrete structures and their subelements based on their aging significance.

Nondestructive test methods are used to determine hardened concrete properties and to evaluate the condition of concrete in structures. Application of these methods for detection of degradation in reinforced concrete structures involves either a direct or indirect approach. The direct approach generally involves a visual inspection of the structure, removal/testing/analysis of material, or a combination of the above. Indirect approaches measure some property of concrete (e.g., rebound number or ultrasonic pulse velocity) and relate it to strength, elastic behavior, or extent of degradation through correlations that have been established previously. Many of the nondestructive test methods are based on the indirect approach, in which a small number of destructive and nondestructive tests are conducted in tandem at noncritical locations in a structure to develop the required correlation curve(s). However, destructive tests may not be possible in many areas of a nuclear power plant structure to develop the required curves so assessment of in-place strength must be based on published relations. Capabilities, accuracies, and limitations of candidate techniques were

established (e.g., audio, electrical, infrared thermography, magnetic, stress wave reflection/refraction, radioactive/nuclear, rebound hammer, and ultrasonic) [55]. Information was assembled on destructive (e.g., coring, probe penetration, and pull-out) and emerging (e.g., leakage flux, nuclear magnetic resonance, and capacitance-based) techniques. Recommendations were developed on application of testing methods to identify and assess damage resulting from typical factors that can degrade reinforced concrete. Also, statistical data were established for nondestructive testing techniques commonly used to indicate concrete compressive strength (i.e., break-off, pull-out, rebound hammer, ultrasonic pulse velocity, and probe penetration) [56]. This information is required where destructive and nondestructive tests cannot be conducted in tandem at noncritical locations to develop a regression relation between the parameter measured and the concrete compressive strength. The methods developed can be used to estimate variance in strength or to yield information about distribution of strength population that is required to calculate the characteristic strength for use in structural integrity assessments. Environment-specific methods are used where surfaces of structures are not accessible for direct inspection due to the presence of soils, protective coatings, or portions of adjacent structures. These methods provide an indirect assessment of the physical condition of the structure (i.e., potential for degradation) by quantifying the aggressiveness of the environment adjacent to the structure (e.g., air, soil, and groundwater). If results of these tests indicate that the environment adjacent to the structure is not aggressive, one might conclude that the structure is not deteriorating. However, when conditions indicate that the environment is potentially conducive to degradation, additional assessments are required that may include exposure of the structure for visual or limited testing. In general with respect to inspection of nuclear power plant concrete structures the nondestructive evaluation methods are good at indicating the relative concrete quality or identifying cracking, voids, and delaminations; however with respect to determining concrete strength the methods tend to be more qualitative for reasons cited above. Figure 93 presents an application of nondestructive testing to determine steel reinforcement characteristics.

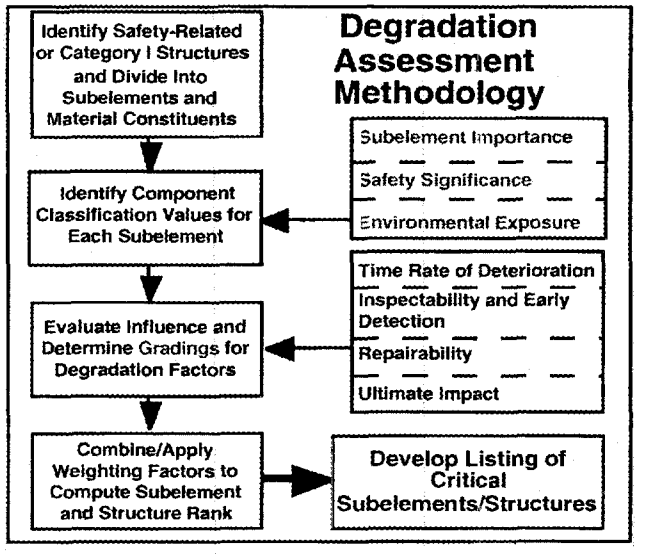

Figure 92. Degradation assessment methodology.

Figure 93. Location of steel reinforcement.

Damage repair practices commonly used for reinforced concrete structures in Europe and North America were reviewed [57,58]. In Europe, activities have concentrated on repair of damage resulting from corrosion of steel reinforcement. Basic repair solutions include: (1) realkalization by either direct replacement of contaminated concrete with new concrete, use of a cementitious material overlay, or application of electrochemical means to accelerate diffusion of alkalis into carbonated concrete; (2) limiting the corrosion rate by changing the environment (e.g., drying) to reduce the electrolytic conductivity; (3) steel reinforcement coating (e.g., epoxy); (4) chloride extraction by passing an electric current (DC) from an anode attached to the concrete surface through the concrete to the reinforcement (chloride ions migrate to anode); and (5) cathodic protection. Repair strategies and procedures were developed in the form of flow diagrams. Information specifically addressing inspection, degradation, and repair of concrete structures in LWR plants was assembled through a questionnaire sent to U.S. utilities. Responses provided by 29 sites representing 41 units indicated that the majority of the plants perform inspections of concrete structures only in compliance with integrated-leakage-rate test requirements (visual inspections), and surveillances of the post-tensioning systems of prestressed concrete containments. The most common deterioration causes were drying shrinkage, acid/chemical attack, thermal movement, freeze-thaw cycles, and seawater exposure. Most of the repair activities were associated with problems during initial construction (cracks, spalls, and delaminations), with the repairs performed on an as-needed basis. When

the performance of a repair was evaluated, visual inspection was used. Detailed information on repair materials and techniques is presented elsewhere [58].

Assessing the ability of nuclear power plant concrete components to continue to meet their functional and performance requirements is an essential part of an aging management program. Given the complex nature of the various environmental stressors and aging factors that potentially can exert deteriorating influences on the concrete components, a systems approach is probably best. Such an approach would encompass the development of: (1) a classification scheme for structures and elements, and deterioration causes and effects; (2) a methodology for conducting a quantitative assessment of the presence of active deteriorating influences; and (3) remedial measure considerations to reestablish the capability of degraded structures or components to meet potential future requirements, such as a loss-of-coolant accident (LOCA). As items (1) and (3) have been addressed previously in this section, only pertinent aspects of item (2) are addressed below (i.e., condition assessments, inspection methods, acceptance criteria, and scheduling). An example illustrating development and application of an inspection program to a PWR with large-dry post-tensioned concrete containment is provided elsewhere [59].

Determining the existing performance characteristics and extent and causes of any observed distress is accomplished through a condition assessment. Common in the condition assessment approaches is the conduct of a field survey, involving visual examination and application of nondestructive and destructive testing techniques, followed by laboratory and office studies. Guidelines and direction on conducting surveys of existing general civil engineering buildings are available [60,61].

Inspection and testing methods generally fall into three categories: (1) visual inspection, (2) nondestructive and destructive testing, and (3) analytical assessments. Visual inspections are one of the most valuable of the condition survey methods because many of the manifestations of concrete deterioration appear as visible indications or discontinuities on exposed concrete surfaces. Visual inspections encompass a variety of techniques (e.g., direct and indirect inspection of exposed surfaces, crack and discontinuity mapping, physical dimensioning, environmental surveying, and protective coatings review). To be most effective, the visual inspection should include <u>all</u> exposed surfaces of the structure; joints and joint materials; interfacing structures and materials (e.g., abutting soil); embedments; and attached components (e.g., base plates and anchor bolts). Degraded areas of significance are measured. The condition of the surrounding structures should also be examined to detect occurrence of differential settlement or note aggressiveness of the local operating environment. Results obtained should be documented and photographs or video images taken of any discontinuities and pertinent findings. Nondestructive testing techniques employ specialized equipment to obtain specific data about the structure in question, and in certain instances (e.g., inaccessible surfaces) its surrounding environment (i.e., structure-specific or environment-specific). Destructive testing involves a direct examination of the material sample removed and, as such, it provides information of significant value for use in aging management programs. Both the presence and impact of deterioration can be determined quantitatively. Also, supplemental testing can be done using these samples to indicate future performance (e.g., durability evaluations through accelerated testing techniques, and to determine the potential for alkali-aggregate reactions). Analytical methods involve the use of supplemental calculations or analytical procedures to re-evaluate the behavior and resistance of the structure (e.g., structural margins determinations). This re-evaluation may be required due to either a change in performance requirements (e.g., plant modification) or the identification of deterioration. Finite-element and ultimate strength design methods provide two techniques for re-analysis.

An approach has been developed for assistance in the classification and treatment of conditions or findings that might emanate from in-service inspections of nuclear power plant reinforced concrete structures. This approach is based primarily on the results of visual inspections since these inspections provide the cornerstone of any condition assessment program for concrete structures. Also, with the exception of some guidance on half-cell potential and ultrasonic pulse velocity measurements, few standards have been published presenting acceptance criteria for results obtained from nondestructive evaluation tests. The information below is provided only as a basis for development of acceptance criteria as each structure is unique due to its application, geometry, materials of construction and environmental exposure.

The visual-based approach uses a "three-tiered" hierarchy [59]. Through use of different levels of acceptance, minor discontinuities can be accepted and more significant degradation in the form of defects can be evaluated in more detail. The three acceptance levels include acceptance without further evaluation, acceptance after review, and additional evaluation required. In the event that the conditions provided below are exceeded, or observed conditions are determined to be deserving further evaluation, a more detailed review is required. Structures that are partially or totally inaccessible for visual inspections may require supplemental evaluations as environments may be present that are conducive to

degradation. Provided below are guidance criteria for unlined concrete surfaces. Additional criteria for concrete surfaces lined by metal or plastic; areas around embedments in concrete; joints, coatings, and non-structural components; and post-tensioning systems are provided elsewhere [59].

Unlined concrete surfaces that are exposed for inspection are generally acceptable without further evaluation if the following criteria are met:

a. Absence of leaching and chemical attack;
b. Absence of abrasion, erosion, and cavitation;
c. Absence of drummy areas (poorly consolidated with paste deficiencies);
d. Popouts and voids less than 20 mm in diameter or equivalent surface area;
e. Scaling less than 5 mm in depth;
f. Spalling less than 10 mm in depth and 100 mm in any dimension;
g. Absence of any signs of corrosion in reinforcing steel system or anchorage components (including concrete staining or spalling);
h. Passive cracks less than 0.4 mm in maximum width ("passive cracks" are defined as those having an absence of recent growth and absence of other degradation mechanisms such as leaching at the crack);
i. Absence of excessive deflections, differential settlements, or other physical movements that may affect structural performance; and
j. Absence of cement-aggregate reactions, chemical attack, fire damage, or other active degradation mechanism.

Findings listed below require review and interpretation in order to evaluate acceptability. Such a review involves determining the likely source of degradation, its activity level, and its net effect on the component. Based on results of the review and evaluation, possible approaches include acceptance as-is, further evaluation using enhanced visual inspection (e.g., magnification), scheduling follow-up inspections at a later date, or use of nondestructive or destructive testing techniques. An analytical assessment of the necessity for repair may also be required. The analytical assessment should examine the impact of existing degradation on the performance characteristics of the structure. Accessibility of the components in question also will enter into the decision process relative to the action to be taken.

Unlined concrete surfaces exhibiting the following surface conditions shall be reviewed to determine if they are either acceptable, require further evaluation, or require repair. Discontinuities exceeding the quantitative limits below require additional evaluation.

a. Appearance of leaching or chemical attack;
b. Areas of abrasion, erosion, and cavitation degradation;
c. Drummy areas that may exceed the cover concrete thickness in depth;
d. Popouts and voids greater than 20 mm but less than 50 mm in diameter or equivalent surface area;
e. Scaling greater than 5 mm but less than 20 mm in depth;
f. Spalling greater than 10 mm but less than 20 mm in depth, and less than 200 mm in any planar dimension;
g. Corrosion staining on concrete surfaces;
h. Passive cracks greater than 0.4 mm but less than 1 mm in maximum width; and
i. Passive settlements or deflections exceeding the original design limits or expected value.

Conditions outside the criteria provided in the previous two sections must be evaluated to determine the appropriate course of action. This generally will involve extensive application of both nondestructive and destructive testing methods. Detailed analytical evaluations frequently will be required to better characterize the current condition of the structure and provide the basis for formulation of a repair strategy (if needed). Even if the analysis results indicate that the component is acceptable at present, additional assessments should be conducted to demonstrate that the component will continue to meet its functional and performance requirements during the desired service life (i.e., take into account the current structural condition and use service life models to estimate the future impact of pertinent degradation factors on performance). If the structure's desired service life is short, and its loss of function due to degradation is occurring at a rate such that sufficient structural margins will be maintained during this period, no action may be required. However, when the opposite is true and loss of function due to degradation is occurring at a rate such that structural margins will not be adequately maintained during the desired service life period, analytical and test results should be utilized to develop an in-service inspection/repair strategy that maintain structural margins over the desired service life.

In-service inspection programs for nuclear power plants have traditionally focused on the concrete containment vessel. Schedules for the containment-related inspections are considered to be "outage based" in that most or all of these inspections are performed during planned plant outages (e.g., refueling) to provide improved plant access. The plant owner does have the option of electing to perform certain inspections (e.g., tendon surveillances) at other times as long as the Code-mandated frequencies and schedules are met. Information on recommended frequencies and schedules for conducting inspections of safety-related concrete structures other than containments has been developed [59]. These schedules take into account the relative aggressiveness of environmental conditions and physical exposures of these structures, and help assure that any age-related degradation is detected at an early stage of development so appropriate mitigative actions can be taken. Ten-year inspection intervals are recommended for structures located below-grade or in a controlled interior environment. Five-year inspection intervals are recommended for other structures. These frequencies may be modified to smaller intervals if plant environments are particularly severe or degradation has been observed to occur. When the observed degradation exceeds criteria provided previously, increased visual inspections should be supplemented by nondestructive, and possibly destructive testing. Reliability-based methods also can be used to schedule inspections of safety-related concrete structures. These methods assess the reliability of the nuclear power plant reinforced concrete structures in terms of damage state and rate of degradation, inspection method detectability functions, remedial actions, and frequency of inspection. Optimized strategies for inspection and maintenance can be developed that minimize future costs associated with inspection, repair, and loss of service, while maintaining the component probability of failure at or below a target value over the service life of the structures [62-64].

Quantitative methodology for continued service determinations. The overall objective of this task was to develop a methodology to facilitate quantitative assessments of current and future structural reliability and performance of concrete structures in nuclear plants. Specific objectives associated with accomplishing this goal include (1) identification of models to evaluate changes in strength of concrete structures over time and (2) formulation of a methodology to predict structural reliability of existing concrete structures during future operating periods.

Structural loads, variations in engineering material properties, and strength degradation mechanisms are random in nature. Time-dependent reliability analysis methods provide a framework for performing condition assessments of existing structures and for determining whether in-service inspection and maintenance are required to maintain reliability and performance at the desired regulatory level.

The strength, R(t), of the component and the applied loads, S(t), both are functions of time. At any time, t, the margin of safety, M(t), is

$$M(t) = R(t) - S(t). \tag{1}$$

Making the customary assumption that R and S are statistically independent random variables, the (instantaneous) probability of failure is,

$$P_f(t) = P[M(t) < 0] = \int_0^\infty F_R(x)\, f_S(x)\, dx. \tag{2}$$

in which $F_R(x)$ and $f_S(x)$ are the probability distribution function of R and density function of S. Equation 2 provides one quantitative measure of structural reliability and performance, provided that P_f can be estimated and validated.

For service life prediction and reliability assessment, one is more interested in the probability of satisfactory performance over some period of time, say (0,t), rather than the snapshot of the reliability of the structure at a particular time provided by Eqn. 2. Indeed, it is difficult to use reliability analysis for engineering decisions without having some time period (say, an in-service inspection or maintenance interval) in mind. The probability that a structure survives during interval of time (0,t) is defined by a reliability function, L(0,t). If, for example, n discrete loads $S_1, S_2, \ldots, S_n$ occur at times $t_1, t_2, \ldots, t_n$ during (0,t), the reliability function becomes,

$$L(0,t) = P[R(t_1) > S_1 \ldots, R(t_n) > S_n]. \tag{3}$$

If the load process is continuous rather than discrete, there is an analogous but more complex expression. The conditional probability of failure within time interval (t,t+dt), given that the component has survived during (0,t), is defined by the hazard function:

$$h(t) = -d(\ln L(0,t))/dt. \tag{4}$$

Solving for L(0,t) yields,

$$L(0,t) = \exp\left[-\int_0^t h(x)dx\right]. \tag{5}$$

The hazard function is especially useful in analyzing structural failures due to aging or deterioration. For example, the probability that time to structural failure, T_f, occurs prior to a future maintenance operation scheduled at $t+\Delta t$, given that the structure has survived to t, can be evaluated as,

$$P[T_f \le t + \Delta t \mid T_f > t] = 1 - \exp\left[-\int_t^{t+\Delta t} h(x)dx\right]. \tag{6}$$

The hazard function for pure chance failures (case 1 in next section) is constant. When structural aging occurs and strength deteriorates, h(t) characteristically increases with time. In-service inspection and maintenance impact the hazard function, causing it to change discontinuously at the time an inspection is performed. The main difference between time-dependent reliability of undegrading and degrading structural components can be characterized by their hazard functions.

Significant structural loads often can be modeled as a sequence of load pulses, the occurrence of which is described by a Poisson process with mean rate of occurrence λ, duration τ, and random intensity S_j (see Fig. 94). Such a simple load process has been shown to be an effective model for extreme loads on structures, since normal service loads challenge the structure to only a small fraction of its strength. With this assumption, the reliability function becomes [62]

$$L(0,t) = \int_0^\infty \exp\left(-\lambda t\left[1 - t^{-1}\int_0^t F_S(rg)\,dt\right]\right) f_R(r)\,dr, \tag{7}$$

in which $f_R(r)$ is the probability density function of initial strength, R(0), and g(t) equals the mean of R(t)/R(0), a function describing the degradation of strength in time (see Fig. 94). The limit state probability, or probability of failure during (0,t), can be determined as F(t) = 1 - L(0,t); it should be noted that F(t) is not the same as $P_f(t)$ in Eqn. 2.

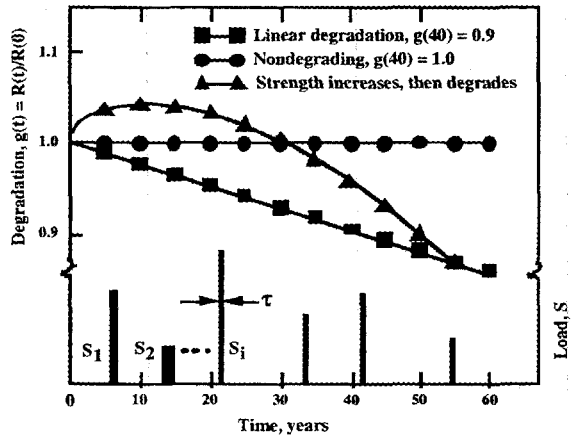

Figure 94. Mean degradation functions of one-way slab.

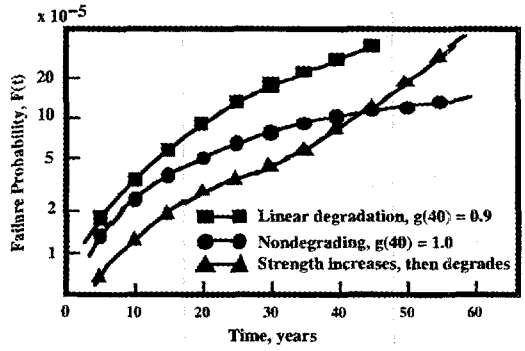

Figure 95. Failure probability of one-way slab.

Time-dependent reliability concepts are illustrated with a simple example of a concrete slab [62,63] that was designed using the requirements for flexure strength found in ACI Standards [65,66]:

$$0.9\ R_n = 1.4\ D_n + 1.7\ L_n, \tag{8}$$

in which R_n is the nominal or code resistance, and D_n and L_n are the code-specified dead and live loads, respectively. The strength of the slab changes in time, initially increasing as the concrete matures and then decreasing due to (unspecified) environmental attack, this situation is illustrated conceptually in Fig. 94. In the absence of in-service data, the behavior of the resistance over time must be forecast from mathematical models describing the degradation mechanism(s) present. In that sense, the reliability estimates are "a priori" in nature. Additional data would cause these estimates to be revised, as described later.

Figure 95 presents a comparison of limit state probabilities for intervals (0,t) for t ranging up to 60 years. Three cases are presented (see Fig. 94): (1) no degradation in strength (i.e., R(t) = R(0), a random variable); (2) R(t) initially increasing with concrete maturity and then decreasing; and (3) R(t) decreasing linearly over time to 90% of its initial strength at 40 years. The statistics used in the illustrations that follow are summarized in Table 3 [67]. Neglecting strength degradation entirely in a time-dependent reliability assessment can be quite unconservative.

Table 3. Statistical properties of strength and load.*

Parameter	Rate of Occurrence	Duration	Main	Coef. of Var.	Pdf
Flexure Strength	—	—	1.12 Mn	0.14	Lognormal
Shear Strength	—	—	$1.7V_n$	0.18	Lognormal
Dead Load	—	—	1.0 D_n	0.07	Normal
Live Load	0.5/yr	3 mo.	0.4 L_n	0.50	Type I
Earthquake Load	0.05/yr	30 sec.	0.08 E_{sse}	0.85	Type II

* Nominal values M_n, V_n, and P_n are the capacities that would be computed according to Code requirements [65,66].

In the probability-based method described above to estimate the strength degradation of a component and to evaluate the effect of periodic maintenance from a reliability point of view [62,62] it was assumed that strength degradation at any section is caused by one randomly occurring defect of random intensity. Such a model is reasonable when the degradation is such that at most one defect or zone of damage is likely to occur within a given cross section. However, there are cases where several defects or zones of damage may contribute in reducing strength. The evaluation of the (random) residual strength of a large wall requires that the cumulative effect of defects in a cross section be considered. Recent research has provided a method whereby the impact of randomly occurring multiple defects on structural capacity can be considered [68].

A low-rise shear wall with a height-to-width ratio equal to one is considered. It is subjected to vertical load, D, that is uniformly distributed on the top of the wall, and in-plane lateral load, V, that is concentrated at the top of the wall. The shear strength of concrete walls can be estimated from empirical models [65,69]. These models are not sufficient to analyze the strength of deteriorating low-rise shear walls. Although finite-element analysis is versatile and able to provide detailed information on the shear resistance mechanisms, it requires lengthy computational effort, especially when adapted to reliability analysis. A recent theoretical approach for evaluating shear strength of reinforced concrete components determines the ultimate shear strength as the sum of the forces sustained by truss, V_t, and arch, V_a, mechanisms [70-72]. It is assumed that the wall fails if all the reinforcing bars yield in tension and the concrete arch crushes in compression. According to the lower bound theorem of plasticity [73], this approach provides a conservative estimate of the shear strength. These models were modified for the reliability analysis of a degrading low-rise shear wall [68]. Figure 96 shows that the strength predicted by this method compares well to experimental tests of low-rise shear walls [74,75].

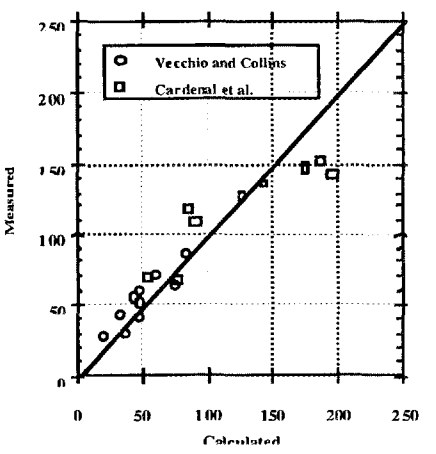

Figure 96. Comparison of measured and calculated shear strength.

A wall subjected to expansive aggregate reaction or chemical attack suffers a loss of concrete section. If the wall is not heavily reinforced in the transverse direction, the contribution of the truss mechanism is small. Thus, it can be assumed

that only the strength of the arch mechanism decreases due to the loss of concrete section while the strength attributed to the truss mechanism is independent of the degradation. If the wall is reinforced in the longitudinal direction, the vertical reaction is sustained by the longitudinal reinforcement, and degradation of concrete outside the concrete strut in the arch mechanism can be neglected. Assuming that the stress in the concrete strut is uniform, the degradation function of the shear wall can be given by:

$$G(t) = \frac{V_t + V_a(t)}{V_{u0}} = \frac{V_t + G_a(t) \cdot V_a(0)}{V_{u0}} \tag{9}$$

in which V_{u0} is the initial shear strength of the wall, $V_a(t)$ is the shear strength of the arch mechanism at time t, and $G_a(t)$ is the degradation function of the shear strength of the arch mechanism.

For illustration, assume that:

- The wall is subjected to time-invariant dead load, D, that is uniformly distributed, and intermittent lateral load V, that is concentrated at the top of the wall and may act either in-plane or out-of-plane.
- The wall is designed for in-plane shear due to the safe-shutdown earthquake based on the current design requirements of ACI 349 [66],

  $$0.9R_n = E_{SS} \tag{10}$$

  in which R_n is the nominal shear strength and E_{SS} is the structural action due to safe-shutdown earthquake. The statistical characteristics of the shear strength and the earthquake load are shown in Table 3. The basis for the statistics used in the illustration is presented elsewhere [63]. It is assumed that E_{SS} = 3D = 3.21 MN.
- The mean initiation rate of local damage per unit surface area due to expansive aggregate reaction is time invariant and is $0.1/m^2$/year.
- The defect intensity is modeled as,

  $$Y(t) = C(t - T_I)^2 \tag{11}$$

  in which C is a time-invariant random variable described by a lognormal distribution with mean value, m_c, of 2.22×10^{-6}/year and coefficient of variation, V_C, of 0.5. This value results in an average defect size large enough after several years following its initiation to be found by visual inspection.
- The 28-day specified compressive strength of concrete equals 27.6 MPa. The corresponding mean compressive strength at 28 days is 28.7 MPa [76]. The specified yield strength of the reinforcement is 414 MPa and the mean is 465 MPa.
- Compressive strength of the concrete increases during the first 10 years, but does not change thereafter. Using published information on concrete strength gain [77] and assuming the concrete and curing conditions are similar to this study, the mean compressive strength (in units of MPa) at time t is evaluated by

  $$E[f_C(t)] = \begin{cases} 15.51 + 3.95\ln t, & t < 10 \text{ years} \\ 47.91, & t \geq 10 \text{ years} \end{cases} \tag{12}$$

  in which t is in days. The concrete section area decreases with time as damage accumulates. Other engineering properties of the wall are assumed to be time-invariant.

The mean degradation in shear strength of the wall in which expansive aggregate reactions occur is illustrated in Fig. 97. Also illustrated in the figure is the mean degradation in wall shear strength evaluated when the cumulative effect of

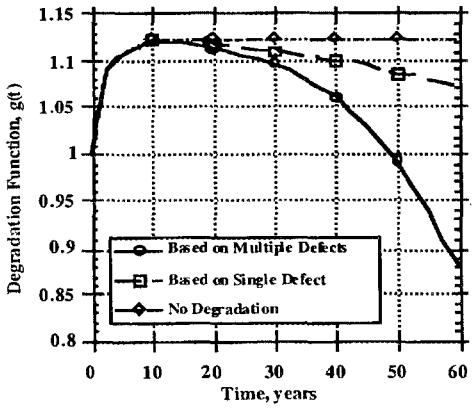

Figure 97. Mean degradation function of wall in shear without repair.

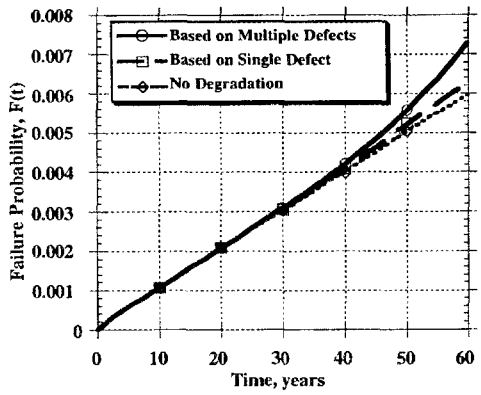

Figure 98. Failure probability of wall in shear without repair.

multiple defects in a section is ignored. The gain in shear strength due to the continuous hydration of concrete more than compensates for the strength degradation due to the loss of section area up to about 50 years. Ignoring the cumulative effect of defects provides an overly optimistic estimate of degradation.

The failure probabilities and the hazard functions associated with the strength degradation illustrated in Fig. 97 are presented in Figs. 98 and 99, respectively. The increase in failure probability due to the strength degradation is small because of the large variability in earthquake load intensity [68]. However, the hazard function increases rapidly after about 50 years when the cumulative effect of defects is considered. Forecasts of reliability of the type illustrated in Figs. 95 and 98 enable the analyst to determine the time period beyond which the desired reliability of the structure cannot be ensured. At such a time the structure should be inspected. Intervals of inspection and maintenance that may be required as a condition for continued operation can be determined from the time-dependent reliability analysis. In-service inspection and maintenance are a routine part of managing aging and deterioration in many engineered facilities; work has been conducted to develop policies for offshore platforms and aircraft [78,79]. When a structure is inspected and/or repaired, something is learned about its in-service condition that enables the probability distribution of strength to be updated. The density function of strength, based on prior knowledge of the materials in the structure, construction, and standard methods of analysis, is indicated by $f_R(r)$. Scheduled inspection, maintenance, and repair cause the characteristics of strength to change; this is denoted by the (conditional) density $f_R(r|B)$, in which B is an event dependent on in-service inspection. Information gained from the inspection usually involves several structural variables including dimensions, defects, and perhaps an indirect measure of the strength or stiffness. If these variables can be related through event B, then the updated density of R following in-service inspection is,

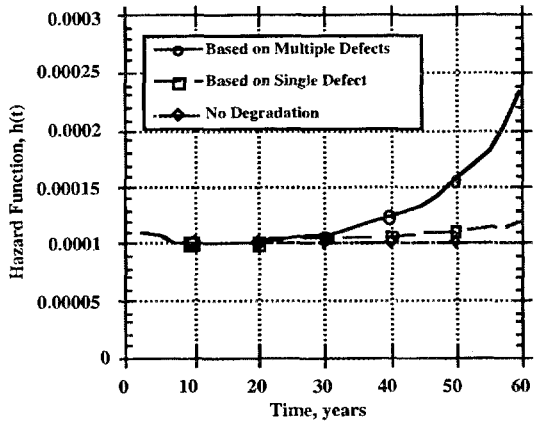

Figure 99. Hazard function of wall in shear without repair.

$$f_R(r|B) = P[r < R \le r + dr, B]/P[B] = c\, K(r)\, f_R(r), \tag{13}$$

in which $f_R(r)$ is termed the prior density of strength, K(r) is denoted the likelihood function, and c is a normalizing constant. The time-dependent reliability analysis then is re-initialized following in-service inspection/repair using the updated $f_R(r|B)$ in place of $f_R(r)$. The updating causes the hazard function (e.g., Fig. 99) to be discontinuous.

Uncertainties in methods of in-service inspection/repair affect the density $f_R(r|B)$. Using a combination of methods usually is more effective from a reliability point of view than using one method. When there are limited resources, it often is most effective to select a few critical safety elements and concentrate on them [54,67]. Optimal intervals of inspection and repair for maintaining a desired level of reliability can be determined based on minimum life cycle expected cost considerations. Preliminary investigations of such policies have found that they are sensitive to relative costs of inspection, maintenance, and failure [63]. If the cost of failure is an order (or more) of magnitude larger than inspection and maintenance costs, the optimal policy is to inspect at nearly uniform intervals of time. However, additional research is required before such policies can be finalized as part of an aging management plan.

3.7.3.3 Concrete aging conclusions

Summarized below are major conclusions that can be derived from the concrete aging activities:

- The performance of the concrete structures in nuclear power plants has been good. The majority of the identified problems initiated during construction and were corrected at that time. However, as these structures age, incidences of degradation due to environmental stressor effects may threaten their durability. Items of note would be corrosion of steel reinforcement following carbonation of the concrete or ingress of chloride ions, excessive loss of post-tensioning force, leaching of concrete, and leakage of post-tensioning system corrosion inhibitor through cracks in the concrete.
- Techniques for detecting the effects of environmental stressors are sufficiently developed to provide qualitative data. Areas of concern include massive members that contain large quantities of steel reinforcement (e.g., the basemat) and members that are inaccessible (e.g., portions of the steel pressure boundary that are embedded in concrete). Despite the limitations associated with many of the techniques, their proper use and application provides vital input for assessing the structural condition of reinforced concrete members. Frequently, increased confidence in results can be provided by using a combination of methods.
- Methods for use in conducting condition assessments of reinforced concrete structures are fairly well established and generally start with a visual examination of the structure's surfaces. Condition assessments provide an effective aging management tool in that when a discontinuity is detected, a maintenance activity can be implemented to prevent the discontinuity from becoming a defect that requires a major repair. To be of most use, the condition assessments should be conducted at regular intervals. Established condition assessment methods, however, have been application-specific (e.g., parking structure decks). Few standards or criteria are available for interpreting the results obtained from the condition assessments. Due to the importance of condition assessments in effectively managing aging of structures and the likelihood for incidences of degradation to increase as the nuclear power plant structures age, it seems prudent that condition assessments of these structures should be conducted periodically. Structures identified to be of high safety significance and potentially at risk should receive the most detailed and frequent inspections. The inspection interval for future inspections could be increased based on a proven performance history. Evaluation of structures having limited accessibility for visual examinations or conduct of other nondestructive evaluations could start with an indirect approach such as monitoring the structure's ambient environment to determine if it is potentially aggressive. More detailed examinations would be required if the environment is found to be potentially aggressive.
- Techniques for repair of concrete structures are well established and when properly selected and applied are effective. Specific criteria that may be used to determine when a repair action should be implemented generally are not available (i.e., parameters that relate damage state such as crack width to environmental exposure). Data on the long-term effectiveness or durability of remedial measures is required. Effective implementation of a repair strategy requires knowledge of the degradation mechanisms and the environment of the structure at the macro and micro level, proper preconditioning of the structure to be repaired, correct choice of repair technique and material, and workmanship of good quality.
- A reliability-based methodology has been developed that can be used to facilitate quantitative assessments of current and future structural reliability and performance of concrete structures in nuclear power plants. The methodology is able to take into account the nature of past and future loads, and randomness in strength and in degradation resulting from environmental factors. The methodology can be used as a basis for selecting appropriate periods for continued service and/or determining optimum intervals and extent of inspection and repair activities. Inspection/repair strategies can be developed to minimize expected future cost while keeping the failure probability of the structure at or below an established target failure probability during its anticipated service period. Implementation and extension of the method to realistic condition assessments is difficult due to a lack of supporting quantitative data on strength degradation models, including initiation and rate of damage growth, the mean occurrence rate of loads, and cumulative density function of the intensity of time-varying loads. Despite the large uncertainties, the state of the art has now advanced to the point where

estimated risks can be evaluated in a relative sense, and perspectives on alternate risk management strategies can be developed. Additional validation of these reliability models through application to laboratory or prototypical structures would further enhance their usefulness.

3.7.4 Aging Management of Containment Pressure Boundary Components

Each boiling-waterreactor (BWR) or pressurized-water reactor (PWR) unit in the United States is locatedwithin a much larger metal or concrete containment that also houses or supports the primary coolant system components. Although the shapes and configurations of the containment can vary significantly from plant-to-plant depending on the nuclear steam supply system vendor, architect-engineeringfirm, and owner preference, leak-tightnessis assured by a continuous pressure boundary consisting of nonmetallic seals and gaskets, and metallic components that are either welded or bolted together. Nonmetallic components are used to prevent leakage from pumps, pipes, valves, personnel airlocks, equipment hatches, manways, and mechanical and electrical penetration assemblies. The remaining pressure boundary consists primarily of steel components such as metal containmentshells, concrete containment liners, penetrationliners, heads, nozzles, structural and nonstructural attachments, embedment anchors, pipes, tubes, fittings, fastenings, and bolting items that are used to join other pressure-retaining components. Each containment type includes numerous access and process penetrations that complete the pressure boundary (e.g., large opening penetrations, control rod drive removal hatch, purge and vent system isolation valves, piping penetrations, and electrical penetration assemblies). Ensuring that the capacity of these components has not deteriorated unacceptably due to either aging or environmental stressor effects is essential to reliable continued service evaluations and informed aging management decisions.

Metal containments are free-standing, welded steel structures that are enclosed in a reinforced concrete reactor or shield building. The reactor or shield buildings are not part of the pressure boundary and their primary function is to provide protection for the containment from external missiles and natural phenomena (e.g., earthquakes, tornadoes, or site-specific environmental events). Thirty-nine of the nuclear power plants presently licensed for commercial operation in the U.S. employ a metal containment. These containmentsfall into six general categories: (1) BWR Mark I, (2) BWR Mark II, (3) BWR III, (4) BWR and PWR spherical, (5) PWR cylindrical with hemispherical top and ellipsoidal base, and (6) PWR cylindrical with hemispherical dome and flat base. Figure 100 presents a cross-section of a BWR MK I steel containment. Leak-tightness of reinforced or post-tensionedconcrete containments is provided by steel liner plate. A typical liner plate is composed of steel plate stock less than 13 mm thick, joined by welding, and anchored to the concrete by studs (Nelson studs or similar), structural steel shapes, or other steel products.

The ASME Code [22] only permits the use of certain materials for fabrication of containment pressure boundary components. These materials must conform to ASME or American Society for Testing and Materials (ASTM) specifications. Section II, Parts A and D of the ASME Code provide specifications and property values for ferrous materials that are acceptable for use. The ASME Code also specifies which grade, class, or type of steel is permitted for a particular application. Tables 2.1 and 2.3 presented in the Ref. [80] provide a listing of material specifications permitted for construction of metal containments and concrete containment liners. Although the list of acceptable materials provided in this reference is fairly extensive, metal containments have primarily been fabricated of ASME SA 516 (Gr. 60 or Gr. 70), ASTM A 212 (Gr. B), and ASME SA-537 (Gr. B) materials. Mark III free-standing steel containments primarily utilize ASME SA-516 (Gr. 70) material for construction, with the shell plate in the suppression pool clad with ASME SA-240 (Type 304) stainless steel to avoid contact of the carbon steel plate with water. The steel liner plate that acts as a leak-tight barrier for the reinforced concrete containments has been fabricated primarily from ASME SA-36, ASME SA-285 (Gr. A or Gr. C), ASME SA-442 (Gr. 60), or

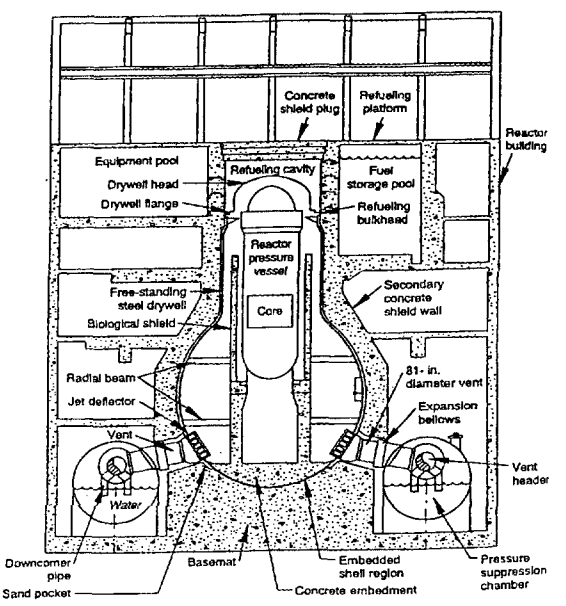

Figure 100. Cross-section of BWR MK I steel containment.

ASME SA-516 (Gr. 60 or Gr. 70) materials. Stainless steel [ASTM SA-240 (Type 304)] also has been used as liner material in some of the reinforced concrete containments.

If undetected, service-related degradation can affect the ability of the containment pressure boundary to perform satisfactorily in the unlikely event of a severe accident by reducing its structural capacity or jeopardizing its leak-tight integrity. Degradation is considered to be any phenomenon that decreases the load-carrying capacity of a pressure-retaining component, limits its ability to contain a fluid medium, or reduces its service life. The root cause for component degradation can generally be linked to a design or construction problem, inappropriate material application, a base-metal or weld-metal flaw, maintenance or inspection activities, or an excessively severe service condition. Component degradation can be classified as either material or physical damage [80]. Material damage occurs when the microstructure of a metal is modified causing changes in its mechanical properties. Degradation mechanisms that can potentially cause material damage to containment steels include (1) low-temperature exposure, (2) high-temperature exposure, (3) intergranular corrosion, (4) dealloying corrosion, (5) hydrogen embrittlement, and (6) neutron irradiation. Material damage to the containment pressure boundary from any of these sources is not considered likely, however. Physical damage occurs when the geometry of a component is altered by the formation of cracks, fissures, or voids, or its dimensions change due to overload, buckling, corrosion, erosion, or formation of other types of surface flaws. Changes in component geometry, such as wall thinning or pitting caused by corrosion, can affect structural capacity by reducing the net section available to resist applied loads. In addition, pits that completely penetrate the component can compromise the leak-tight integrity of the component. Primary degradation mechanisms that potentially can cause physical damage to containment pressure boundary components include (1) general corrosion (atmospheric, aqueous, galvanic, stray-electrical current, and general biological); (2) localized corrosion (filiform, crevice, pitting, and localized biological); (3) mechanically-assisted degradation (erosion, fretting, cavitation, corrosion fatigue, surface flaws, arc strikes, and overload conditions); (4) environmentally-induced cracking (stress-corrosion and hydrogen-induced); and (5) fatigue. Material degradation due to either general or pitting corrosion represent the greatest potential threat to the containment pressure boundary.

Although performance of the containment pressure boundary has been good, as plants age, degradation incidences (e.g., corrosion) are starting to emerge. To date, there have been over 30 reported occurrences of corrosion of steel containments or liners of reinforced concrete containments. In two cases, thickness measurements of the walls of steel containments revealed areas that were below the minimum design thickness. Two instances have been reported where corrosion has completely penetrated the liner of reinforced concrete containments. Examples of specific problems identified include corrosion of the steel containment shell in the drywell sand cushion region (Oyster Creek), shell corrosion in ice condenser plants (Catawba and McGuire), corrosion of the torus of the steel containment shell (Fitzpatrick, Cooper, and Nine Mile Point Unit 1), and concrete containment liner corrosion (Brunswick, Beaver Valley, North Anna 2, Brunswick 2, and Salem). Transgranular stress corrosion cracking in bellows has also occurred (Quad Cities 1 and 2, and Dresden 3). As the nuclear plant containments age, degradation incidences are starting to occur at an increasing rate. More detailed information on documented instances of containment pressure boundary degradation is available [81]. Figure 101 presents examples of containment pressure boundary degradation due to corrosion.

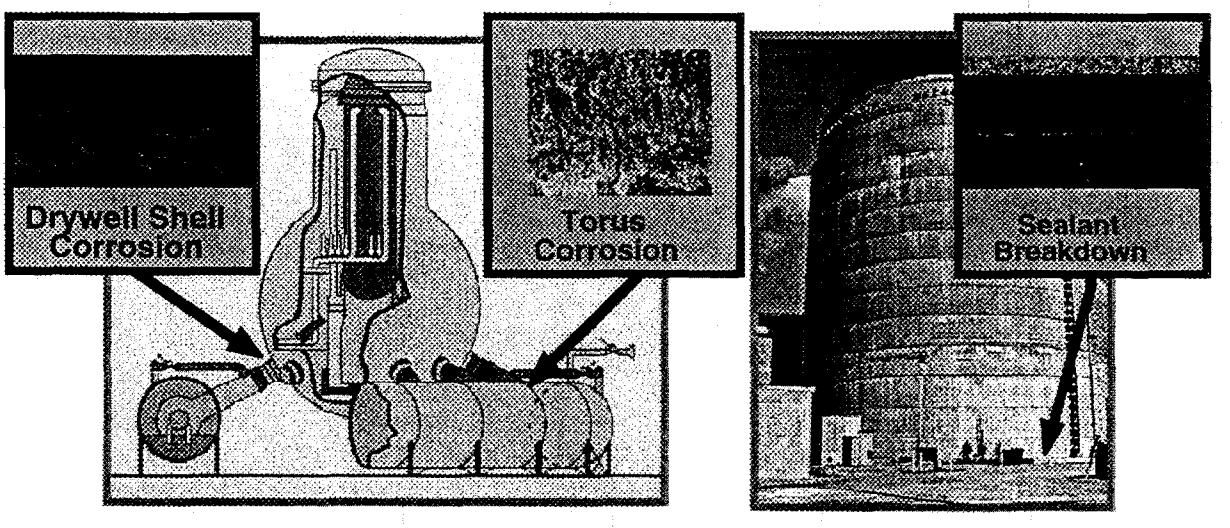

Figure 101. Containment pressure boundary corrosion examples.

Operating experience has demonstrated that periodic inspection, maintenance, and repair are essential elements of an overall program to maintain an acceptable level of reliability over the service life of a nuclear power plant containment, or in fact, of any structural system. Knowledge gained from conduct of an in-service condition assessment can serve as a baseline for evaluating the safety significance of any degradation that may be present, and defining subsequent in-service inspection programs, and maintenance strategies. Effective in-service condition assessment requires knowledge of the expected type of degradation, where it can be expected to occur, and application of appropriate methods for detecting and characterizing the degradation.

An essential element in the assessment of the integrity (or in the determination of available safety margins) of a containment pressure boundary is knowledge of the damage state of its materials of construction. Future condition assessments require not only knowledge of the current damage state, but knowledge of the change in damage state with time. In-service inspections and testing are performed to measure the current state of damage. Changes in damage state with time can be estimated through approaches such as physical models, correlation relations, or trending analyses. Many of the existing in-service inspection techniques have been developed primarily for the detection and assessment of fabrication-related flaws under controlled conditions. These techniques may not be adequate for use in helping to effectively manage the aging of the containment pressure boundary in nuclear power plants. In addition, accessibility of the containment pressure boundary may be restricted due to the presence of coatings, its location below water level or embedded in concrete, or certain areas may be accessible only from one surface. Because of the safety significance of the containment pressure boundary, the in-service inspections generally require a higher level of reliability and more quantitative definition of defects present then those associated with the general manufacturing sector. Basic approaches used to quantify the extent of damage present, or its change with time, include nondestructive examination, destructive testing, and in-service monitoring. Inaccessible areas of the containment metallic pressure boundary require special considerations.

As a part of the overall NRC research program to benchmark existing design criteria and evaluate containment performance under severe accident conditions, research is being conducted at ORNL related to condition assessment, in-service inspection, repair practices, and performance of degraded containments (i.e., corroded) during events at or beyond the design basis. This research is being conducted under The Inspection of Aged/Degraded Containments Program and has objectives of (1) understanding the significant factors relating corrosion occurrence, efficacy of inspection, and structural capacity reduction of steel containments and liners of concrete containments; (2) providing the NRC reviewers a means of establishing current structural capacity margins or estimating future residual structural capacity margins for steel containments and liners as limited by liner integrity; and (3) providing recommendations, as appropriate, on information to be requested of licensees for guidance that could be utilized by NRC reviewers in assessing the seriousness of reported incidences of containment degradation. In meeting these objectives, activities are conducted under two primary task areas: (1) steel containment/linerassessment and root-cause resolution practices and (2) reliability-based condition assessment.

3.7.4.1 Steel containment/liner assessment and root-cause resolution practices

The overall objectives of this task are to (1) identify procedures to quantitatively assess the presence, magnitude, and significance of any degradation factors that could impact structural capacity margins; and (2) provide data for use in current and future structural condition assessments. In addition, techniques will be established for (1) characterization of steel containment, steel liner, coating, and sealant materials; (2) mitigation of environmental stressor or aging factor effects; and (3) root-cause resolutions. Activities include characterization of containment pressure boundary materials, development of a degradation assessment methodology, evaluation of nondestructive and destructive examination techniques, inaccessible area considerations, in-service monitoring, and repair practices.

Characterization of containment pressure boundary materials. Characterization of containment pressure boundary materials has addressed the collection and presentation of data and information on these materials, and quantifying the effects (if any) of degradation factors such as corrosion on their properties. Desired data and information requirements for characterization of containment pressure boundary materials have been developed (i.e., general information covering a description of the material, processing information, and baseline data; material composition in terms of chemistry; and mechanical, physical, and other properties). Structural steels acceptable for use in the construction of the containment pressure boundary have been identified along with their corresponding ASME and ASTM specifications (e.g., carbon steel, ASME SA-36, and ASTM A 36). Potential nuclear power plant-related degradation factors for these materials have been identified, with corrosion being the most important. Two options were identified for presentation of the materials property data and information —incorporate additional chapters into the existing Structural Materials

Information Center [49], or use of object-oriented relational database software to develop a customized database. Recommendations to guide the collection and incorporation of data and information into a database on containment pressure boundary materials have been developed [82].

Degradation assessment methodology. A degradation assessment methodology intended for use in characterizing the in-service condition of metal and concrete containment pressure boundary components and quantifying the amount of damage present has been developed [83]. Because information required to characterize and quantify the condition of degraded components must be established on a case-by-case basis taking into consideration unique containment design features and plant operating constraints, the methodology does not include a step-by-step procedure, but has been developed in the form of general, non-prescriptive guidance.

Condition assessments are an essential element of both continued service evaluations and informed aging-management decisions. From an aging management perspective, metallic pressure boundary components that exhibit satisfactory long-term performance and do not experience in-service degradation can be considered acceptable for continued service. However, components found by in-service testing or examination to be deteriorated or damaged must be evaluated to determine whether continued service is appropriate or whether repairs, replacements, or retrofits are needed. More detailed acceptance standards and evaluation criteria for use in determining the acceptability of degraded components for continue service are provided in Section XI, Division 1, Subsection IWE of the ASME Code [84]. A diagram that illustrates the continued service evaluation process presented in Subsection IWE is shown in Fig. 102. Continued service evaluations are performed by qualified engineers and authorized personnel who determine the adequacy of components for their intended use [60]. The decision-making process begins with an understanding of the in-service condition of each containment component. Condition assessments that provide essential information for continued service evaluations involve detecting damage, classifying the types of damage that may be present, determining the root cause of the problem, and quantifying the extent of degradation that may have occurred. Knowledge gained from condition assessments can serve as a baseline for evaluating the safety significance of any damage that may be present and defining in-service inspection programs and maintenance strategies. Condition assessment results can also be used to estimate future performance and remaining service life. Four primary topics are associated with in-service condition assessment of metal and concrete containment pressure boundary components – damage detection, damage classification, root-cause determination, and damage measurement. Additional details on each of these topics and their interaction are provided elsewhere [83].

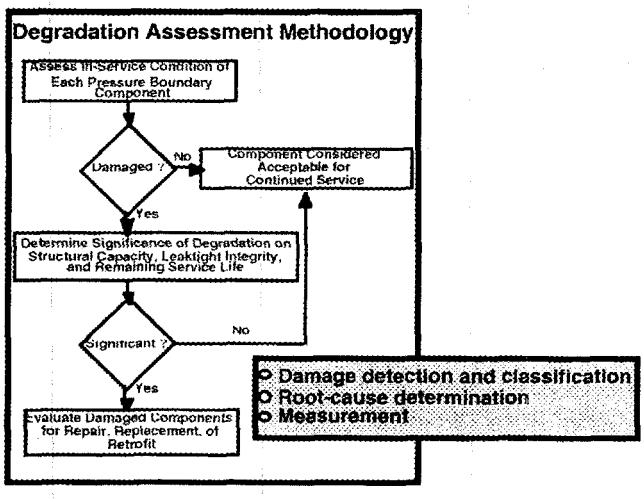

Figure 102. Degradation assessment methodology based on ASME Section XI, Subsection IWE.

Nondestructive examination techniques. Nondestructive examination is used to identify potential challenges to structural or leak-tight integrity in time to take remedial action. It also plays an important role in structural reliability assessment, especially when combined with failure analysis techniques such as fracture mechanics. Nondestructive examination methods for metallic materials (i.e., steel containments and liners of reinforced concrete containments) principally involve surface and volumetric inspections to detect the presence of degradation (i.e., coating deterioration, loss of section due to corrosion, or presence of cracking). The surface examination techniques primarily include the visual, liquid penetrant, and magnetic particle methods. Volumetric methods include ultrasonic, eddy current, and radiographic. Provisions are also included in the ASME Code for use of alternative examination methods provided results obtained are demonstrated to be equivalent or superior to those of the specified method. Acceptance standards are defined in Article IWE-3000 of the ASME Code. In order to obtain repeatable and reproducible nondestructive examination results using any of the methods described below, several factors must be understood and controlled: material evaluated, evaluation procedure utilized, environment, calibration/baseline reference, acceptance criteria, and human factors. Figure 103 presents several of the nondestructive examination methods discussed below. The most common nondestructive examination techniques in civil structures are visual inspection, liquid penetrant, magnetic

particle, ultrasonic, eddy current, and radiography [85].

Visual inspection is one of the most common and least expensive methods for evaluating the condition of a weld or component (e.g., presence of surface flaws, discontinuities, or corrosion). It is generally the first inspection that is performed as part of an evaluation process. It is beneficial for performing gross defect detection and in identifying areas for more detailed examination. It can identify where a failure is most likely to occur and when failure has commenced (e.g., rust staining or coating cracks). Once a suspect area is identified all surface debris and protective coatings are removed so that the area can be inspected in more detail. Visual examinations can be performed either with the unaided eye or optical magnifiers. Inspection mirrors, video cameras, and boroscopes can be used for inspection of areas with limited accessibility. Three classifications of visual examinations are specified in the ASME Code: (1) VT-1 (detect discontinuities and imperfections on the surfaces of components such as cracks and corrosion), (2) VT-2 (detect evidence of leakage from pressure-retaining components), and (3) VT-3 (determine general mechanical and structural condition of components and their supports). The effectiveness of a visual inspection is dependent on the experience and competence of the person performing the inspections. Also, without material or component removal, visual inspections are limited to accessible areas.

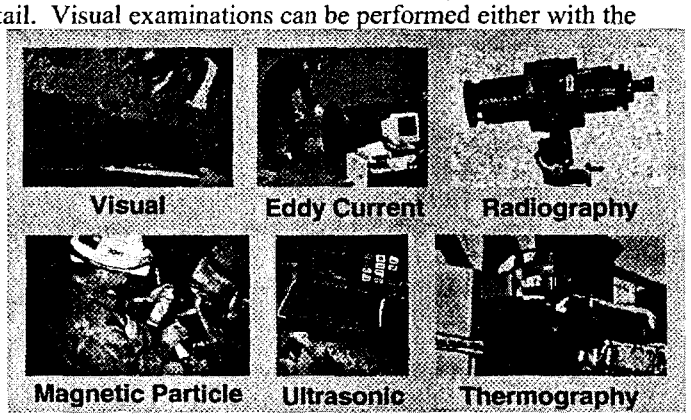

Figure 103. Examples of NDE methods.

Liquid penetrant testing can be used to detect, define and verify surface flaws in solid or essentially nonporus components (e.g., cracks, porosity, laminations or other types of discontinuities that have a capillary opening to the surface). Indications of a wide spectrum of flaw sizes can be found with little capital expenditure regardless of the configuration of the test article or the flaw orientation. The procedure consists of cleaning the surface to be examined followed by application of a liquid penetrant. Surface defects or cracks absorb the penetrant through capillary action. After a dwell period, excess penetrant is removed from the surface and a developer is applied that acts as a blotter to draw penetrant from the defects to reveal their presence. Colored or fluorescent penetrants may be utilized, with white light or black light, respectively, used for viewing. Effectiveness of the method is dependent on the properties of the penetrant and the developer. Limitations of the technique are that operator skill requirements are fairly high, only surface flaw defects can be detected, the area inspected must be clean as scale or paint film may hide flaws, results are affected by surface roughness and porosity, and no permanent record of inspection is provided.

Magnetic particle testing is used to detect surface and shallow subsurface discontinuities in ferromagnetic materials. A magnetic field is induced into the ferromagnetic material and the surface is dusted with iron particles that may be dry, suspended in a liquid, colored, or fluorescent. The magnetic lines of force (flux) will be disrupted locally by the presence of the flaw with its presence indicated by the iron particles that are attracted by leakage of the magnetic field at the discontinuity. The resulting magnetically-held collection of particles forms a pattern that indicates the size, shape, and location of the flaw. Effectiveness of the method quickly diminishes depending on flaw depth and type, and scratches and surface irregularities can give misleading results. Special equipment, procedures, and process controls are required to induce the required magnetic fields (e.g., use of proper voltage, amperage, and mode of induction). Also, linear discontinuities that are oriented parallel to the direction of the magnetic flux will not be detected.

Ultrasonic testing uses sound waves of short wavelength and high frequency to detect surface and subsurface flaws, and measure material thickness. The most commonly used technique is pulse echo in which sound is introduced into the test object and travels through the material examined with some attendant loss of energy. Reflections (echoes) are returned to the receiver from internal imperfections or the component's surfaces. The returning pulse is displayed on a screen that gives the amplitude of the pulse and the time taken to return to the transducer. Inclusions or other imperfections are detected by partial reflection or scattering of the ultrasonic waves, time of transit of the wave through the test object, and features of the spectral response for either a transmitted or reflected signal. Operator interpretation is made by pattern recognition, signal magnitude, timing, and probe positioning. Flaw size, distance, and reflectivity can be interpreted. The technique has good penetration capability, high sensitivity to permit detection of very small flaws, good accuracy relative to other nondestructive examination methods, only one surface has to be accessible, and rapid results are provided. For thickness measurements digital meters are commonly used. In the pulse-echo mode an

ultrasonic transducer transmits waves toward the metal surfaces, signals are reflected from the front and back surfaces, and the difference in arrival times of the two signals is used to indicate the thickness. Metal loss is then calculated by taking the difference between the as-built thickness and the thickness measured. Two types of systems are available commercially – ultrasonic thickness gage (digital display) and digital gage (A-scan, echo signals are displayed on an oscilloscope). Ultrasonic testing is commonly used in nuclear plants to monitor wall thinning of the containment vessel caused by corrosion. Rough surface conditions such as could be present on the surfaces of the metal components of BWR containment systems present problems relative to signal scattering. Because of its complexity, ultrasonic testing requires considerable technician training and skill. Also, good coupling between the transducer and component inspected is important, defects just below the surface may not be detected, and reference standards are required.

Eddy current inspection methods are based on electromagnetic induction and can be applied to electrically-conductive materials for detection of cracks, porosity, and inclusions, and to measure the thickness of nonconductive coatings on a conductive metal. In the flaw detection mode eddy current can detect surface connected or near surface anomalies. It is based on the principle that alternating current flow in a coil proximate to an electrical conductor will induce current flow in the conductor. The current flow (i.e., eddy current) creates a magnetic field that opposes the primary field created by the alternating current flow in the coil. The presence of a surface or near surface discontinuity in the conductor will alter the magnetic field (i.e., magnitude and phase) and can be sensed as a change in the flow of current in a secondary coil in the probe or change of inductance of the probe. The output signal from the detection circuit is fed to an output device, typically a meter, oscilloscope, or chart recorder. Flaw size is indicated by extent of response change as the probe is scanned along the test object. Eddy current techniques do not require direct contact with the test piece, and paint or coatings do not have to be removed prior to its application. For surface discontinuities of a given size, the sensitivity of eddy current decreases with distance below the surface. Best results are obtained when the magnetic field is in a direction that will intercept the principal plane of the discontinuity. Also, the technique requires calibration, is sensitive to geometry of the test piece, results may be affected by material variations, no permanent record is provided, and demagnification may be necessary following inspection.

Radiographic techniques involve the use of penetrating gamma or X-radiation and are based on differential absorption of the radiation. X-radiographic inspection is applied to the detection of surface connected and internal anomalies as well as the internal configuration of a test object. The source is placed close to the material to be inspected and the radiation passes through the material and is captured on film placed on the opposite side of the test article from the source. A two-dimensional projection of the area being inspected is displayed on the film (permanent record). The thickness, density, and absorption characteristics of the material affect the intensity of radiation passing through an object. Possible imperfections are indicated on the film as density changes (i.e., series of gray shades between black and white). The choice of type of source is dependent on the thickness of material to be tested. Gamma rays have the advantage of portability. Gamma radiometry systems consist of a source that emits gamma rays through the specimen and a radiation detector and counter. Direct transmission or backscattering modes can be used to make measurements. The count or count rate is used to measure the specimen dimensions or physical characteristics (e.g., density and composition). Primary limitations of radiography are that radiation protection has to be observed while applying the method, personnel must be licensed or certified, results are not immediately available, the structure must be accessible from both sides, and detection of crack-like anomalies is highly dependent on the exposure geometry and orientation of the crack with respect to incident irradiation.

Acoustic emission inspection is based on monitoring and interpretation of stress waves generated by a structure under load. Acoustic emissions are small amplitude stress waves resulting from release of kinetic energy as a material is strained beyond its elastic limit (e.g., crack growth and plastic deformation). Material stress can come from mechanical or thermal loading, as well as from a variety of other means. The stress waves propagate throughout the specimen and may be detected as small displacements by piezo-electric transducers positioned on the surface of the material. A typical system consists of a number of sensors, preamplifiers, signal filters, amplifier, and a recording system. Signal measurement parameters most commonly used to interpret results include ringdown counts (threshold-crossing pulses), energy counts (area under rectified signal envelope), duration (elapsed time for ringdown counts), amplitude (highest peak voltage), and rise time (time from first threshold crossing to signal peak). Primary applications of acoustic emission inspection include continuous monitoring or proof testing of critical structures, monitoring of production processes, and experimental research related to material behavior. Acoustic emission advantages are that it is extremely sensitive, the entire structure can be monitored, it is relatively unobtrusive, onset of failure can be identified, and triangulation can be used to identify source location. Certain aspects of the corrosion process are detectable by acoustic emission (e.g., stress-corrosion cracking, hydrogen cracking, and gas evolution) [86]. Disadvantages are that it requires considerable technical experience to conduct the test and interpret results, background noise can interfere with signals, and a material may not emit until the stress level exceeds a prior applied level (i.e., Kaiser effect).

Thermographic inspection methods are applied to measure a variety of material characteristics and conditions. In the flaw detection mode they are used for detection of interfaces and/or variation of properties of interfaces within layered systems. The test object must be thermally conductive and reasonably uniform in color and texture. The procedure involves inputting a pulse of thermal energy that is diffused within the test object according to thermal conductivity, thermal mass, inherent temperature differentials, and time of observation. The thermal state of the test object is monitored by a thermographic scanner camera that has infrared energy spectrum detection capability. Interpretation of results is done through visual monitoring of the relative surface temperature as a function of time and relating the time-dependent temperature differences to the internal condition of the test object. Results are recorded as a function of time and the process is relatively rapid. Specialized equipment is required and since the method is a volume inspection process, resolution is lost near the edges and at locations of nonuniform geometry change. Thermal inspection becomes less effective in the detection of subsurface flaws as the thickness of the object increases. Pulsed infrared techniques have been developed that can perform inspections through the thickness of test objects. The process basically entails providing heat through a thermal pulse or step heating, and dynamically collecting infrared images of the material surface. To be successful the heat applied at the top surface must penetrate to the bottom surface with a temperature differential of several degrees for good infrared contrast.

Electrochemical corrosion monitoring techniques are available to make measurements directly related to corrosion rate rather than indirectly in terms of the flaws produced by corrosion. Potential surveys, linear polarization, and AC impedance are techniques that have been utilized. Electrochemical potential measurements using a standard half-cell (e.g., copper-copper sulfate) can be used to locate anodic portions of a structure (i.e., potential gradients indicate possibility of corrosion). The linear polarization resistance method impresses DC current from a counter electrode onto the working electrode (e.g., steel structure). Current is passed through the counter electrode to change the measured potential difference by a known amount with the working electrode being polarized. An electronic meter measures the potential difference between the reference electrode and the working electrode. Measurements as a function of DC voltage applied across the cell provide an indirect measure of the corrosion current. The AC impedance-polarizing technique utilizes an alternating applied voltage with the data analyzed as a function of frequency. The AC technique provides polarization resistance as well as information on polarization mechanisms at the anode and cathode that is important for interpretation of the AC impedance data. The technique requires rather sophisticated equipment (e.g., AC frequency generator and analyzer system) and the Tafel slopes must be known to convert AC impedance data into corrosion rate information [87]. Each of these methods requires contact with the part of the structure monitored, and where corrosion rates are provided the rates are only since equipment installation and initiation of monitoring.

Destructive examination techniques. Tests that alter the shape, form, size, or structure of the material being tested are considered destructive tests. These tests may be performed to determine mechanical, physical, chemical, thermal, or other properties of the material, or to examine the material for microstructural imperfections, voids, or inclusions. Destructive tests are commonly used to determine mechanical properties of metallic materials and can involve tension, compression, ductility, shear, torsion, bend, creep, stress-relaxation, hardness, fatigue, or fracture testing. These tests are usually conducted in room-temperature air, but they can also be performed at higher or lower temperatures or under other environmental conditions. Test methods that require the removal and testing of representative portions of material from a component are also considered destructive tests when the affected component is rendered useless or unfit for future service. As part of a damage assessment process, tension, hardness, and metallographic testing may be conducted on material samples removed from containment pressure boundary components. Measurements obtained during tension testing can be used to develop stress-strain curves and to establish mechanical property values such as the modulus of elasticity, ultimate tensile elongation, ultimate tensile strength, yield strength, and reduction of area. Property values obtained from tension testing are generally used to determine conformance or nonconformance with material specifications. However, test results can also be used to compare the performance and properties of replicate specimens tested under a variety of exposure conditions or using different testing methods. Replicate specimen results can provide a basis for establishing limits on environmental exposure, working stresses, or operating temperatures. Hardness testing (e.g., Brinell or Rockwell), that uses small diamond points or hardened round steel balls to produce permanent indentations or deformations in the surface of the material being tested, is widely used for determining the relative quality of a metallic component and to establish the uniformity of its material properties. It is relatively easy to perform, requires very little material or surface preparation, and usually causes minimal surface damage to the material or component. Metallography is the branch of science that relates to the constitution and structure, and their relation to the properties of metals and alloys. Testing is usually performed in a laboratory where metallic specimens are prepared for microscopic examination. These examinations are conducted to reveal the constituents and structure of the material. Metallography is probably the most useful destructive testing method available for identifying differences in material microstructure caused by exposure to high temperatures or severe environments.

Inaccessible area considerations. Inspection of nuclear power plant structures can be difficult because there are a number of functionally different components in a variety of environments. In the previous section several techniques commonly used to assess civil structures were identified. Application of these techniques, however, generally requires that at least one surface of the component inspected be accessible and the techniques are most effective when an approach is utilized in which the structures have been prioritized with respect to such things as aging significance, environmental factors, and risk. Guidance on component selection is available [83,88]. Once the components have been selected for inspection, however, there are several locations in nuclear power plants where performing the inspections may not be straight forward. Inspection of inaccessible portions of metal pressure boundary components of containments (e.g., fully embedded or inaccessible containment shell or liner portions, the sand pocket region in Mark I and II drywells, and portions of the shell obscured by obstacles such as platforms or floors) represents one of these conditions.

Embedded metallic portions of the containment pressure boundary may be subjected to corrosion resulting from groundwater permeation through the concrete; a breakdown of the sealant at the concrete-containment shell interface that permits entry of corrosive fluids from spills, leakage, or condensation; or in areas adjacent to floors where the gap contains a filler material that can retain fluids. Although no completely suitable technique for inspection of inaccessible portions of the containment metallic pressure boundary have been demonstrated to date, preliminary investigations have been conducted using high-frequency acoustic imaging, magnetostrictive sensors, electromagnetic acoustic transducers, and multimode guided waves.

Exploratory analytical and experimental simulations have been conducted to investigate the feasibility of high frequency acoustic imaging techniques for the detection and localization of thickness reductions in the metallic pressure boundaries of nuclear power plant containments [89,90]. The analytical study used an elastic layered media code (OASES Code, Massachusetts Institute of Technology) to perform a series of numerical simulations to determine the fundamental two-dimensional propagation physics. The analytical simulation suggests that for the case of steel-lined concrete containments (Fig. 104), the thin steel liner and additional concrete backing contribute to give unacceptable loss of signal to the concrete. Approximately 100 dB of signal loss is incurred for small degradations near the concrete interface. Due to this loss, it appears unlikely that acoustic imaging technology can be applied to this scenario. For embedded steel containments, analytical simulation (Fig. 105) suggests that significant degradations (i.e., 2 mm) of containment thickness below the concrete/air interface provide reasonable backscatter signal levels of approximately

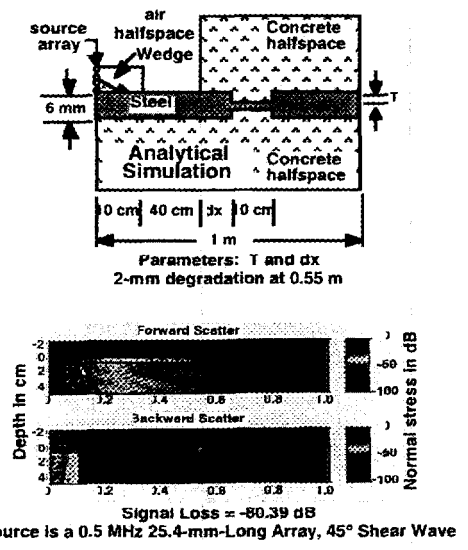

Figure 104. Simulation scenario for steel liner-reinforced concrete containment.

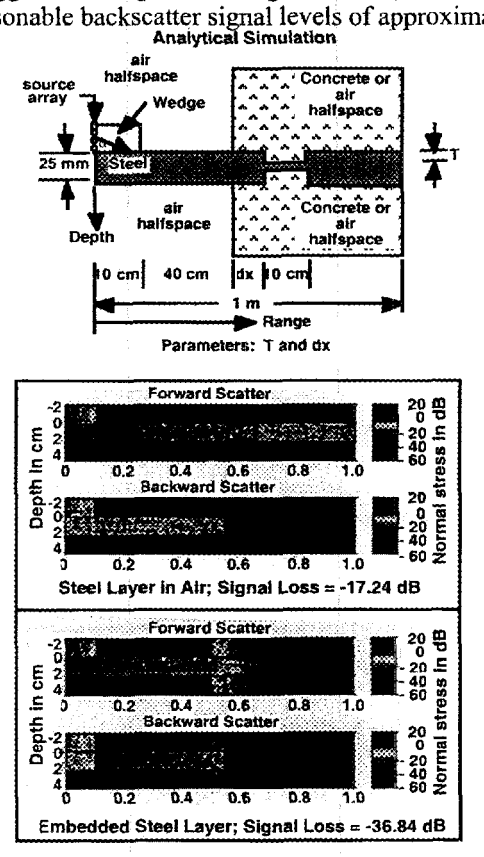

Figure 105. Simulation scenario for steel containment.

–15 dB. This yields signals that are 10-15 dB above the expected effective noise level due to surface imperfections. It was concluded from this that given enough sensor input power, acoustic imaging technology can be applied to this scenario. The study also concludedthat currently available sensors can not be used in array configurations to interrogate a large area (global inspection) due to their intrinsic narrow beam pattern, which does not allow steering. This limits these sensors to spot detection and mapping scenarios, where degradation is already suspected. For wide-area surveys, the use of scannable sensors appears to be applicable, but they will require development. The sensors would be manufactured by bonding many signal wires to a solid piezo-electric block on a substrateand then cutting the block into individual sensors, leaving a line array of sensors in the substrate. The competing signals from unfocused source transducers and wave guide signal distortion remain as two significant barriers for localizing and characterizing degradations.

The experimental study utilized a commercial ultrasonic testing system to carry out several full-scale tests. The experimental studies were designed to also effectively restrict case scenarios to two dimensions. Measurements of 0.5 MHz shear wave levels propagatedin 25-mm-thick steel plates embeddedin concrete showed 1.4 to 1.6 dB of signal loss for each centimeter of two-way travel in untreated plates (compared with prior numerical predictions of 3-4 dB) and 1.3 dB of signal loss per centimeter of two-way travel in steel plates embedded in concrete prior to concrete setting (i.e., plastic). Scattered signals from simulated degradations of different shape and size were investigated (Fig. 106). For a 70° wedge, the returns from the rectangular slot were, averaged over source location, around 5 dB higher than those from the rounded slot and 9 dB higher than for the "V" shaped slot of similar depth. Also shown in Fig. 106 is the effect of notch depth and wedge angle. For the 45° wedge pair, the returns from the 4-mm deep notch were, averaged over source location, about 3 dB lower than those from the 8-mm deep notch and about 6 dB lower that those from the 12-mm deep notch. For the 70° wedge pair the results were somewhat surprising and require interpreting using advanced scattering theories that were beyond the scope of this investigation. Negligible losses were measured in plates with a decoupling treatment applied between the steel and concrete to simulate unbonded portions of the pressure boundary (Fig. 107, lined plate). Also shown in the figure is the effect of test setup (i.e., mono-static versus bistatic measurements). By altering the test setup to bistatic measurements, the "self noise" (e.g., inner wedge reverberant field and through-thickness standing echoes) was eliminated. Overall, experimental results showed that the measurementsystem displayed a dynamic range of 125 dB and measurement variability less than 1-2 dB. Based on these results, a 4–mm-deep round-faced degradation embedded in 30 cm of concrete has expected returns of –73 dB relative to input and should be detectable. Analytical and experimental results indicate that this approach has merit, but needs to be demonstrated in the field.

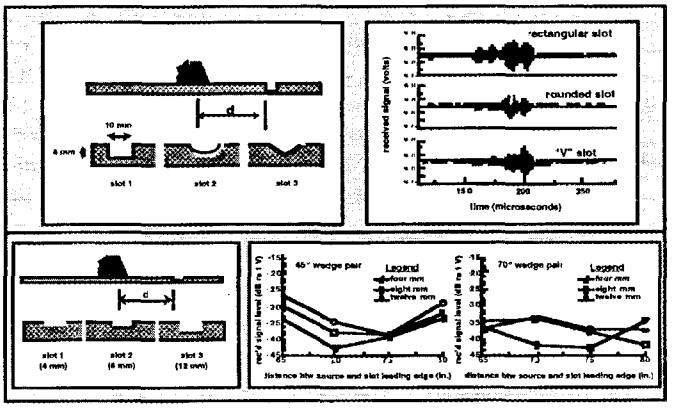

Figure 106. Experimental results evaluating defect geometry and wedge angle.

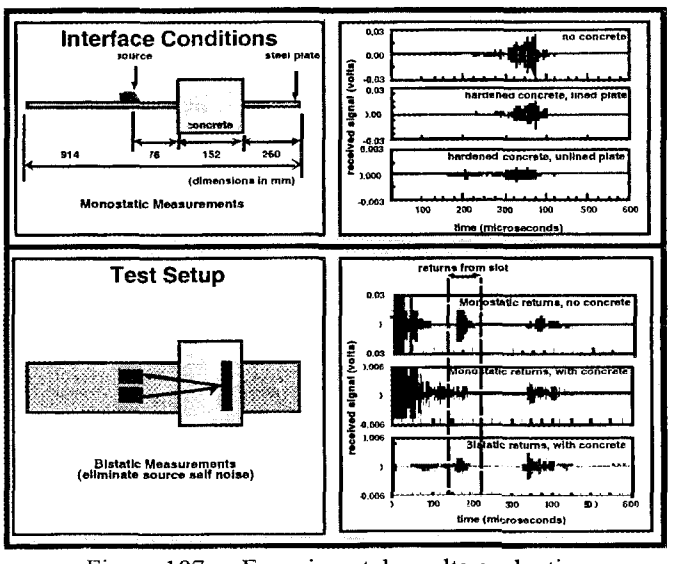

Figure 107. Experimental results evaluating interface conditions and test setup.

Magnetostrictive sensors are devices that launch guided waves and detect elastic waves in ferromagnetic materials electromagnetically to determine the location and severity of a defect based on timing and signal amplitude. The technique is noncontact, couplant free, and

requires no surface preparation. In addition, it has a sensing and inspection range from a single sensor that can exceed several hundred feet on bare metals, the sensor can detect defects on the inside and outside diameters of pipe surfaces, and it can inspect structures whose surfaces are not directly accessible due to the presence of paint or insulation. Its primary application has been to piping systems [91]. A preliminary study has been conducted to investigate the feasibility of applying magnetostrictive sensor technology to inspection of plate type materials and evaluate its potential for detecting and locating thickness reductions in the containment metallic pressure boundary resulting from corrosion [92]. Figure 108 presents the experimental setup used to demonstrate the capability of guided wave generation and detection in plate-type materials. Pulse-echo magnetostrictive sensor data for notches ranging from 10- to 30-cm long are presented in Fig. 108. The notches were placed into a 6.11 m long by 1.23 m wide by 6.35-mm thick plate at a

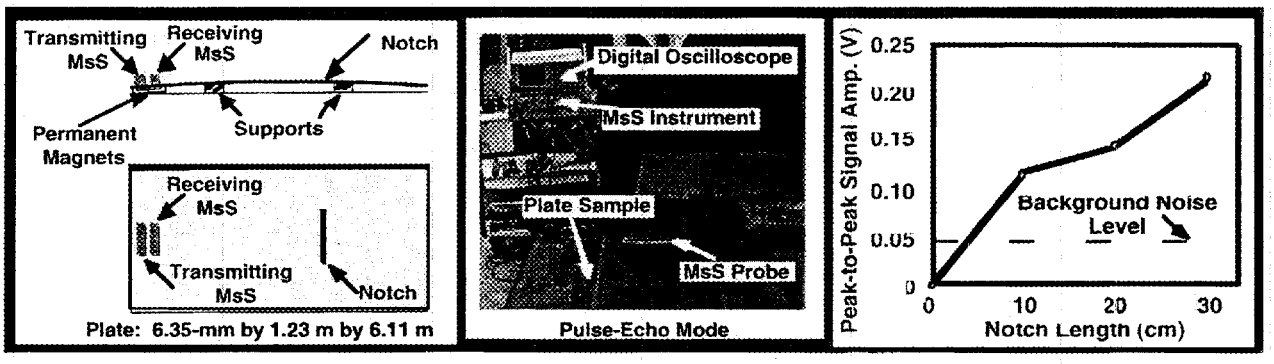

Figure 108. Magnetostrictive sensor test setup used to generate and detect waves.

distance equal to 4.06 meters from the probe end on the plate. As noted in the figure, the peak-to-peak signal amplitude increased as the notch length increased. In addition, potential approaches for guided-wave inspection, modeling of guided-wave dispersion in plates with different boundary conditions (e.g., free standing and backed by concrete on one or both sides), and assessment of magnetostrictive sensor-based system requirements for practical implementation were evaluated. It was concluded that guided waves provide an effective means of inspection of the metallic pressure boundary in a nuclear plant and are capable of performing global, long-range inspection of plates, including areas that are difficult to access because of the presence of other equipment or attachments, or the presence of concrete on one or both sides. Limited modeling studies suggest that a low-frequency A_0 mode wave would be best suited for inspection of containment pressure boundaries that are either backed on one or both sides by concrete. Other frequencies or modes such as S_0 would have the inspection range significantly reduced because of the increased wave attenuation due to the concrete presence. As a result of development of this technology for commercial applications related to piping systems, tailoring an existing system to containment pressure boundary inspection should be straight-forward. Field validation of the technique is required, however.

The guided wave technique (multi-mode guided plate waves) is more sensitive than techniques which utilize shear waves (e.g., electromagnetic acoustic transducers), provides a global inspection technique for characterizing corrosion damage, follows the contour of the structure, can travel long distances (e.g., 100 m depending on frequency and mode characteristics), and can interrogate different regions or cross sections (i.e., depths) of the component inspected [93-97]. The guided plate waves can be excited at one point on the structure, propagate over considerable distances, and be received at a remote point on the structure. This technique has been used with success to detect defects in piping materials, but its applicability to plate-type materials until recently has not been demonstrated. As a result, a limited investigation was conducted to demonstrate the feasibility of the guided wave technique for identification and location of thickness reductions in the metallic pressure boundary of nuclear

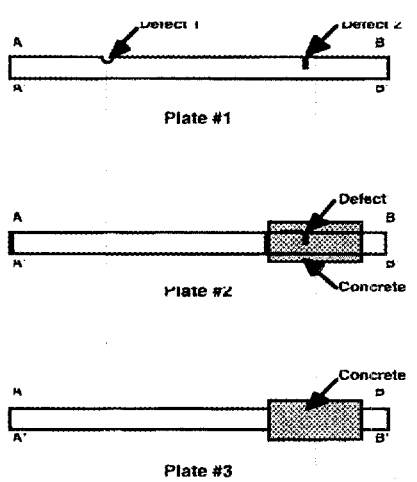

Figure 109. Schematics of plate specimens used to benchmark several aspects of guided wave inspection.

power plant containments [98]. The specimens are shown in Fig. 109 and include a bare plate with two defects, a plate coated with concrete with one defect, and a plate with concrete but no defects. Each plate was 25-mm thick by 203-mm wide by 914-mm long. The fabricated specimens provided a benchmark for studying several aspects of guided wave inspection, including sensitivity, transmission ability across defects, inspection reliability, and penetration ability. The plates were interrogated using both horizontal shear and Lamb guided waves.

Horizontal shear (SH) guided waves have particle displacements in the shear horizontal direction, which is perpendicular to the propagation direction. SH waves are sensitive to the transverse boundary conditions. Therefore, transducer couplant for SH waves should be a highly viscous material. The coupling problems once limited the applications of SH waves. With the advancements of electomagnetic acoustic transducers (EMATs), however, SH waves once again are receiving a lot of attention because of the couplant-free advantage of EMATs. The grid distance of the EMATs used in the experiment was 12.7 mm, which determines that the corresponding frequency for generating the non-dispersive SH wave mode is around 200-250 kHz. The non-dispersive SH wave mode has the same phase velocity as the SH bulk wave velocity (200 m/s), and a uniform energy distribution across the plate thickness. The obtained RF waveforms are shown in Fig. 110 for the plate containing two defects and the plate containing a defect embedded in concrete. The reflected echoes for the bare plate with two defects indicates that both defects can be detected by using the SH waves. Because the non-dispersive SH wave mode has a uniform particle displacement distribution, some energy can pass the first defect and be reflected by the second defect. The backwall echo shows a good penetration ability of the SH wave mode. Also shown in the figure is the defect echo for the plate embedded in concrete.

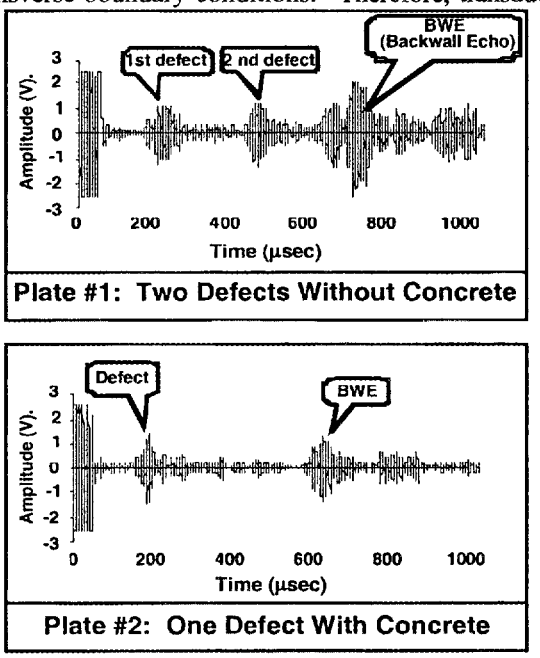

Figure 110. Experimental results using horizontal shear waves

Unlike SH waves, Lamb waves have particle displacements in both parallel and perpendicular directions to the propagation direction. Lamb waves are sensitive to both transverse and normal boundary conditions. Common couplant can be used for generating Lamb waves. The frequency and wedge angle determines the generated Lamb wave mode. Two wedge angles were considered at the frequency of 565 kHz. When the wedge was set to 62 degrees, it generated the A_0 and S_0 modes simultaneously, which have the same phase velocity (3030 m/s) at the working frequency and then degenerates into pseudo-surface waves. As the pseudo-surface wave has energy distribution close to the plate boundary, it is very sensitive to the defect close to the boundary, however, it is not sensitive to the defects on the other side of the plate. If the transducer is placed on the opposite side of the plate to the defects (bottom) both defects are ignored and only a backwall echo is received. If the transducer is placed on the same side of the plate as the defects, only the first defect echo is received because most of the energy close to the plate boundary is reflected by the first defect. This is a different case than for SH waves because of the uniform energy distribution of the SH wave mode. In order to obtain a fairly uniform energy distribution across the plate thickness for Lamb waves, the wedge angle was changed to 38 degrees. Once again, the tone burst frequency was 565 kHz. Figure 111 presents the pulse echo signals for the plate with two defects and the plate containing one defect embedded in concrete. The phase velocity and group velocity of the generated Lamb waves are 4385 m/s and 2220 m/s, respectively. For the plate embedded in concrete but without defects, multiple echoes are received from the plate-concrete interface before the backwall echo (Fig. 111). This indicates one of the disadvantages of this Lamb wave mode in that it is sensitive to the plate-concrete interface. However, this problem could be overcome by setting a threshold for a defect call (e.g., echoes from defects less than 30% of the cross-section thickness are ignored).

In-service monitoring. In-service monitoring involves examination of a component while it remains in service. It is generally used for repeated examinations of a flawed component or suspect area to monitor change with time. Data collection can be performed on a case-by-case basis at irregular intervals or at prescribed times using a computer-controlled data acquisition system. Results from in-service monitoring can provide valuable information for

assessing the current condition of a degraded component, estimating its remaining useful service life, and making informed aging-management decisions. An example of in-service monitoring would be on-line electrochemical measurements to establish the average degradation rate of a component caused by corrosion, or the cumulative metal loss or the instantaneous corrosion rate of a component under actual service conditions.

Repair practices. Whenever damage is detected, corrective actions are taken to identify and eliminate the source of the problem and thereby halt the degradation process. When significant wall thinning, cracking, surface defects, or leakage is detected and containment structural or leak-tight integrity is potentially jeopardized, defective areas are evaluated, repaired, or replaced before the plant is returned to service. The primary mechanism of concern to the containment pressure boundary is corrosion. Methods to prevent the occurrence of corrosion primarily include the application (or maintenance) of coatings to exposed steel that is at risk, and use of cathodic protection systems (i.e., impressed current or sacrificial anode). Repair methods generally include: (1) defect removal by mechanical means in which the unacceptable flaw is reduced and the resultant section thickness created by the removal process remains equal to at least the minimum design thickness; (2) repair welding in which the design section thickness is reestablished (e.g., cladding); and (3) component replacement with items that meet acceptance standards. Repair options for restoring damaged bellows include replacement of penetration assembly, bellows replacement, installation of new enveloping bellows, in-place welding repairs, removal of severe dents, and blending the surface. Detailed information on repair of the containment pressure boundary components is available [99].

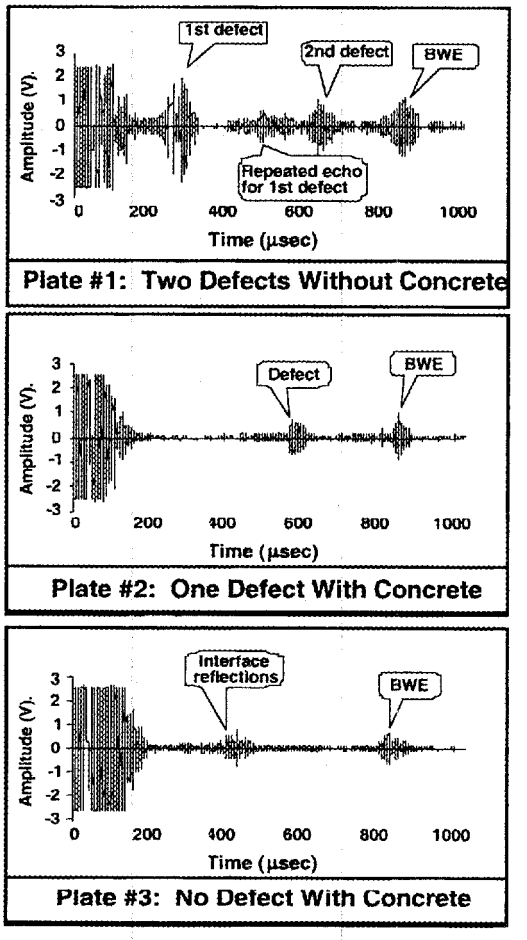

Figure 111. Experimental results using Lamb guided waves.

3.7.4.2 Reliability-based condition assessments

The objectives of this task are to (1) identify mathematical models from principles of structural mechanics to evaluate degradation in strength of containment pressure boundary structures over time; (2) recommend statistically-based sampling plans for inspection of steel structures to ensure that any damage present will be detected with a specified level of confidence; and (3) develop reliability-based methods to assess the probability that steel containment capacity has degraded below a specified level. This task is aimed at providing quantitative evidence that the strength of the containment pressure boundary is sufficient to withstand operating and environmental events with a level of reliability that is sufficient for public health and safety.

Structural aging may cause the integrity of the containment pressure boundary to evolve over time. In particular, a hostile service environment may cause structural strength and stiffness to degrade from corrosion, fatigue, chemical attack, or internal material changes. Any evaluation of the reliability or safety margin of the containment during its service life must take into account these effects, plus any previous challenges to its integrity that may have occurred. The stochastic nature of degradation also must be taken into account: in structural condition assessment, in evaluations of proposals for service life extension, and in development of risk management policies and procedures. Numerous uncertainties complicate the evaluation of aging effects in structures. Among these are inherent randomness in structural loads, lack of in-service records of performance, epistemic uncertainties in available models for quantifying time-dependent material changes and their contribution to pressure boundary degradation, inaccuracies of nondestructive evaluation techniques applied in difficult field circumstances, and shortcomings in existing methods for repair and retrofit.

Predictive models of structural performance should be based on principles of structural mechanics, supported by experimental data, to enable the changes in the structure that occur over time to be evaluated in terms of initial conditions, applied load history, and the operating environment. Unfortunately, state-of-the-art mechanics methods and finite-element modeling generally have not been sufficiently utilized by developers of fragility curves and much work still needs to be done in this area. For some mechanisms of degradation, such as stable crack growth under cyclic load, the mechanics of deterioration are reasonably well established. The behavioral models of other mechanisms are less certain or even unsuitable for structural analysis purposes. In some cases the models currently available for structural evaluation purposes are phenomenological in nature.

Surveys of steel containments and liners indicates that corrosion is the most significant damage mechanism affecting the nuclear power plant containment pressure boundary [81]. Uniform corrosion causes a thinning of the shell, leading eventually to gross inelastic deformations or instability of the shell. Pitting corrosion is a localized effect, leading to leakage or loss of the pressure boundary. In either case, the penetration, X(t), of the corrosion can be modeled by the kinetic equation,

$$X(t) = C\,(t-T_I)^m \tag{14}$$

in which C = rate parameter, m = time-order parameter, and T_I = random corrosion initiation period. The units in Eqn. (14) are such that X(t) is in μm when t and T_I are in years. The rate parameter depends on the nature of the environment, and must be determined experimentally. Typical values for uniform corrosion are in the range 100 to 200 μm. Similarly, T_I depends on the nature of the environment, and the effectiveness of protective coatings or electrochemical devices. The time-order parameter, m, typically is about 2/3 for carbon steels, and may be treated as deterministic. Statistics of the parameters C and T_I must be determined from experimental data, and depend on whether the corrosion mechanism gives rise to uniform or pitting corrosion. One must be cautious about extrapolating laboratory data to a prototype. Two examples will be considered: a time-dependent reliability analysis of an axisymmetric cylindrical steel ring-stiffened shell and a fragility assessment of a steel containment subjected to internal pressurization.

Structural aging and deterioration (due, e.g., to corrosion) cause the reliability of that structure to deteriorate with time. This can be illustrated with a time-dependent reliability analysis of an axisymmetric cylindrical steel ring-stiffened shell, structurally similar to a steel containment. The shell has a radius, r, and thickness, h_o, with a hemispherical end closure of the same thickness. It has ring stiffeners of cross-sectional area, A_1, placed circumferentially at intervals of S_1, and vertical stringers of area A_2 placed at intervals S_2 circumferentially in the cylindrical portion of the shell. While a finite-element analysis of shell behavior often is required, particularly when the shell contains changes in thickness or penetrations, a simpler limit analysis is conservative and sufficient for purposes of this illustration. The shell is fabricated of SA516/Grade 70 steel, which has a specified yield strength of 262 MPa and a tensile strength of 483 MPa.

The design equation for this shell is [100],

$$S_{mc} = F_{yn}/SF = \sigma_d + \sigma_{pa} \tag{15}$$

in which S_{mc} = allowable stress, F_{yn} = specified yield strength (here, 262 MPa), SF = 1.97 is the safety factor at first yield, and σ_d and σ_{pa} = stresses caused by dead load and accidental pressure load, respectively. Assuming that $\sigma_d \ll \sigma_{pa}$, the design thickness of the shell (based on an elastic analysis for design purposes) is,

$$h_o = P_a r/S_{mc} \tag{16}$$

Using the nominal (design) values in Table 4, h_o = 35 mm.

Accidental pressure loads due to loss-of-coolant accidents are accompanied by a rise in pressure (and temperature) within the containment. As the shell begins to deform due to pressure buildup, attachments begin to fail well before general shell rupture. Thus, the governing limit state is one of excessive general inelastic deformation. The limit pressure, P_o, corresponding to the onset of critical deformation for an axisymmetric shell is,

$$P_o = F_y(h(t)/r)\gamma \tag{17}$$

in which F_y = (random) yield strength, γ is a factor that takes into account the plastic deformation of the shell and

Table 4. Statistical data for steel cylinder.

Variable	Nominal	Mean	Coefficient of Variation	Probability Distribution Function
Radius, r	17m	17m	-	-
Thickness, h_o	35 mm	35 mm	-	-
Stringer area, A_1	155 cm^2	155 cm^2	-	-
Stringer spacing, S_1	3 m	3 m	-	-
Yield strength, F_y	262 MPa	288 MPa	0.07	Lognormal
Corrosion rate, C	-	300 μm/yr	0.30	Lognormal
Initiation time, T_I	-	10 yr	0.30	Lognormal
Peak pressure, P_a	0.28 MPa	0.22 MPa	0.20	Type I

the contributions of the stiffness [101]:

$$\gamma = (2\sqrt{3}) + A_1/(S_1 h(t)). \tag{18}$$

The parameter h(t) is the random thickness of the shell at time, t, taking into account any corrosion loss: $h(t) = h_o - X(t))$ (cf Eqn. 14). The margin of safety at any time thus is,

$$M(t) = P_o(t) - P(t) \tag{19}$$

in which P(t) = random pressure arising from the accident. Substituting Eqn. (17) into Eqn. (19) yields,

$$M(t) = F_y(h(t)/r)\gamma - P(t). \tag{20}$$

With the margin of safety thus defined, the time-dependent reliability analysis can proceed using stochastic methods similar to those already developed for the analysis of degrading reinforced concrete structural components and systems [67,102,103]. The probability of surviving interval of time (0,t) is defined by the reliability function, L(t):

$$L(t) = P[M(t_1) > 0,\ M(t_2) > 0, \ldots,\ M(t_N) > 0] \tag{21}$$

in which $t_1, t_2, \ldots, t_N$ are the times at which the extreme loads occur. Accidents are extremely rare and, for purposes of reliability analysis, their occurrence can be modeled as a Poisson process [104]. Table 4 summarizes statistical data on other parameters required to evaluate Eqns. (20) and (21). The corrosion rate parameter C = 300 μm/yr leads to a loss of 10% of the shell thickness in 60 years. Dimensional variabilities are insignificant in nuclear power plant construction, and thus structural dimensions are assumed to be deterministic.

Figure 112 shows the effect of corrosion rate and mean rate of occurrence of accidental pressurization on cumulative failure probability (CFP), defined as 1–L(t). The reliability of the shell is found to depend significantly on the corrosion rate, severe corrosion causing an increase in the CFP of four orders of magnitude. Sensitivity studies conducted with this simple model allow insights and perspectives that can guide and channel subsequent finite-element analyses of degraded steel containments, which are computationally more involved. For example, preliminary results indicate that the random corrosion initiation period, T_I, in Eqn. 14, is more significant for structural reliability assessment than the corrosion rate parameter, C, for steel plates with thicknesses that are typical in nuclear power plants (25 – 35 mm). Moreover, as observed earlier with nuclear power plant concrete structures [48], the conditional failure rate of an aging structure increases nonlinearly with time. Finally, curves such as those presented in Fig. 112 can be used to schedule in-service inspection and repair, once a target reliability goal is identified.

In contrast to corrosion, some damage mechanisms, such as fatigue crack initiation, elevated temperature creep, and irradiation effects involve microstructural changes in the steel that either may not become detectable with common nondestructive examination methods until significant damage has already occurred, or may become evident only at the point at which damage is accelerating rapidly. Continuum damage mechanics (CDM) deals with the characterization and analysis of growth of strength-reducing microstructural defects with the help of macroscopic state variables [105]. CDM makes it possible to predict the effects of damage processes on structures prior to the development of detectable flaws. Expressions for damage can be developed from principles of thermodynamics, and have been validated with limited experimental data [106]. Damage accumulation can be described by a stochastic differential equation, which can be solved numerically [107]. Statistical data are necessary to support the predictive damage models and reliability analyses described above. Quantification of uncertainties in loads, degradation mechanisms, and structural response is essential.

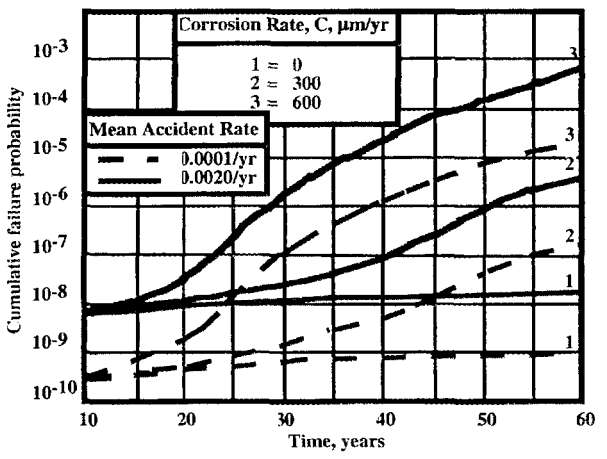

Figure 112. Time-dependent reliability of steel cylindrical shell: effect of corrosion and load rate.

The second example addresses a fragility assessment of a steel containment subjected to internal pressurization. Fragility analysis is an essential ingredient of a fully coupled risk analysis. A probabilistic safety assessment (PSA) is a structured framework for evaluating uncertainty, performance, and reliability of an engineered facility. The move toward quantitative risk assessment has accelerated in recent years as the benefits have become increasingly apparent in many fields [108]. The recently issued Regulatory Guide 1.174 [109] defines the NRC's position on risk-informed decision-making regarding proposed changes to the licensing bases of operating nuclear plants.

The PSA process is initiated with the identification of limit states (LS) or conditions in which the system ceases to perform its intended function(s) in some way. For structural components and systems in nuclear power plants, such limit states may be either strength or deformation-related, as large (inelastic) deformations affect the integrity or operability of mechanical or electrical systems that are attached to or otherwise interface with the structure. With the limit states identified, the limit state probability is expressed as,

$$P[LS] = \sum P[LS|D = x]\, P[D = x] \tag{22}$$

in which D describes the intensity of demand on the system (hazard), and $P[LS|D = x]$ is the conditional limit state probability, or the fragility, of the system.

The fragility displays, in probabilistic terms, the capability of an engineered system to withstand a specified event with intensity x (sometimes referred to as a review-level event), one that often is well in excess of the design-basis event. Thus, it defines safety margins against specific identified events probabilistically for decision and regulatory purposes in a manner that effectively uncouples the system analysis from the hazard analysis. The fragility modeling process leads to a median-centered estimate of system performance, coupled with an estimate of the uncertainty in performance. The fragility of a structural component or system often is modeled by a lognormal cumulative distribution function (CDF), described by,

$$FR(x) = \Phi\ [\ln\ (x/m_C)/\beta_C] \tag{23}$$

in which $\Phi(\ )$ = standard normal probability integral, m_C = median capacity (expressed in units that are consistent with the demand, x, in Eqn. (22), and β_C = logarithmic standard deviation, which is approximately equal to the coefficient of variation (COV) in capacity, V_C, when $V_C < 0.3$ and provides a measure of uncertainty in capacity.

The strengths of steel and concrete structural materials and components are random variables, and their median (or mean) strengths are well in excess of the nominal values specified for nuclear power plant design [110]. If these median strengths are used in structural analysis in lieu of specified nominal strengths, one often can obtain a reasonable estimate of the median capacity, m_C, in Eqn. (23) [111]. The uncertainty in capacity displayed by Eqn. (23) arises from numerous sources. Some of these uncertainties (denoted by COV β_R) are inherent (aleatory) in nature, and are essentially irreducible under current engineering analysis procedures. Other uncertainties (denoted by COV β_U) arise from assumptions made in the analysis of the system and from limitations in the supporting databases. Such knowledge-based (epistemic) uncertainties depend on the quality of the analysis and data, and generally can be reduced, at the expense of more comprehensive (and costly) analyses. The role of epistemic uncertainty on fragility can be displayed in one of two ways. In the first, a family of fragilities is generated, one for each modeling assumption. In the second (and simpler) approach, the aleatory and epistemic uncertainties are combined in the form $\beta_C^2 = \beta_R^2 + \beta_U^2$, and only one (mean) fragility curve is generated The second approach is taken herein.

The fragility assessment is illustrated using a PWR ice condenser steel containment, which has been modeled to be somewhat similar to one of the reference plants in the NUREG-1150 risk study [112] and has been thoroughly analyzed in several independent studies. The steel containment is designed for an internal pressure of 74 kPa, has an internal diameter of 35 m, springline height of 35 m, and the elevation of the apex of the spherical dome is 53 m. The steel in the shell is A516/Grade 60 plate, varying in thickness from 35 mm at the basemat to 12 mm at the springline. Vertical and circumferential stringers are welded to the exterior of the shell at approximately 1.2 m vertical and 3 m horizontal intervals.

The containment must confine radioactive material in the event of an accident, so the performance limit is loss of shell integrity or ability to perform this essential function [113]. This performance limit must be related to structural limit states that can be identified from nonlinear finite-element analysis, along with local or general structure or material failure criteria. Tests of internally pressurized scaled model containments have indicated that the governing failure mode invariably is one of tensile instability. In a recently published study [111], the tensile instability limit state for containment fragility analysis was defined by,

$$\varepsilon_p = \varepsilon_f \, f_1 \, f_2 \, f_4 \tag{24}$$

in which ε_p = effective plastic strain, ε_f = uniaxial limit strain, f_1 = factor to correct uniaxial limit strain for triaxiality effects, f_2 = factor that accounts for bias and uncertainty in the finite element analysis, and f_4 = factor to account for the reduction in steel ductility as a result of corrosion. The commercially available nonlinear finite-element program ABAQUS was used to perform the numerical experiments of the pressurized containment, and appropriate post-processing of these experiments led to the fragilities.

First, the containment fragility in the undegraded (uncorroded) condition is considered to establish a benchmark. This analysis is compared to results obtained from previous containment analyses [114,115] and in the Individual Plant Examination [116]. Then, corrosion patterns consistent with field inspection findings in similar containments are postulated (e.g., 10 % and 25% loss of containment shell thickness behind the ice basket, and the 50% loss adjacent to an upper floor). The fragilities are reassessed for each corrosion pattern and compared to the undegraded benchmark condition. Uncertainties are propagated using a Latin Hypercube sampling plan and points of failure are identified through post-processing the structural response data calculated by ABAQUS. The analysis is described in more detail elsewhere [111].

The fragility of the containment in the as-built condition is shown in Fig. 113. The mean (and median) capacity is 455 kPa, and the logarithmic standard deviation β_C is 0.04. The median is consistent with values obtained elsewhere by other investigators. The estimated 5-percent and 2-percent exclusion limits are 427 kPa and 421 kPa, respectively. For comparison, median fragilities based on simplified criteria such as first yielding or 2% strain in the circumferential direction, which

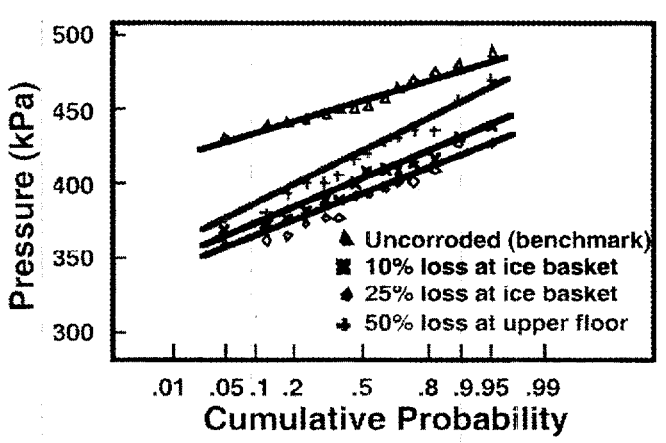

Figure 113. Containment fragilities for postulated corrosion.

can be modeled by simple yield analysis of the shell, are 290 kPa and 365 kPa, respectively. These simplified analyses lead to conservative estimates of the margin of safety. Fragilities for the other cases are also presented in the figure. In comparison, for a postulated 25% loss of shell thickness behind the ice basket the mean (median) capacity is 386 kPa, and the logarithmic standard deviation has increased to 0.06. The 5-percent and 2-percent exclusion limits for this postulated degraded condition have decreased to 352 kPa and 345 kPa, respectively, or by approximately 18% from the as-built condition.

3.7.4.3 Application of results

Information developed can be used in evaluations of (1) in-service inspection techniques and methodologies that have been utilized as part of an overall program to ensure that the containment pressure boundary will continue to provide the required safety margins, and (2) root-cause resolution practices that have been applied to restore containment pressure boundary components that have been damaged or degraded in service. Methods established under the reliability-based condition assessment activity will provide a means of establishing the current capacity margin for the pressure boundary components of a structure or estimating future residual capacity margins. Program results also can be used to address the significance of incidences of reported containment degradation. Potential regulatory applications of this work include (1) improved predictions of long-term material and structural performance and available safety margins at future times; (2) evaluation criteria for safety assessment of issues related to containment degradation incidents; (3) capability for assessment of structural integrity through a combination of reliability-based condition assessment and inspection/surveillance (pre- or post-accident) with possible lengthening of inspection frequencies for some components; and (4) improvements in damage inspection methodology through potential incorporation of results into national standards that could be referenced by standard review plans.

3.8 TECHNICAL COMMITTEE ACTIVITIES

Internationally, about 25% of nuclear power plants have been operating for over 20 years, with some having been in operation for over 30 years. Although the individual national programs (e.g., United Kingdom, France, and Switzerland) focus on the plants within each country, there are common generic aging effects. Issues presented by aging nuclear power plants are therefore of international interest and experience and information has been exchanged with a view of determining best practice. The principal organizations that have involved in these activities include Réunion Internationale des Laboratoires d'Essais et de Recherches sur les Matériaux (RILEM), Organization for Economic Co-operation and Development - Nuclear Energy Agency (OECD-NEA), and International Atomic Energy Agency (IAEA). Program personnel have been heavily involved in each of these activities.

RILEM Committee TC-160 MLN, "Methodology for Life Prediction of Concrete Structures in Nuclear Power Plants," was established in 1994 as a result of a proposal prepared by ORNL personnel to review existing guidelines and procedures used to monitor and evaluate concrete structures in nuclear power plants as well as their performance history. In order to provide the basis for development of a life prediction methodology, a series of state-of-the-art papers related to current practices for aging management of concrete structures in nuclear power plants has been prepared (e.g., service life, instrumentation systems, creep methodologies, and probabilistic methods) [117]. The committee also organized an international conference [118] and a workshop [119] on life prediction and aging management of concrete structures.

The Committee on the Safety of Nuclear Installations (CSNI) of the OECD-NEA has established a task group to study aging of nuclear power plant concrete structures. The basic mandate of this task group is to review current international (and, where appropriate, national) activities in the area of aging (both structural and functional), and to formulate recommendations for a medium-to-long term program of work. A task group report has been prepared that addresses the mandated items [120]. Recommendations of this group are being implemented through a series of workshops addressing specific issues associated with aging: prestress losses in nuclear power plant containments, development priorities for non-destructive examination of concrete structures, response of degraded structures (including finite-element analysis techniques), instrumentation and monitoring of concrete structures, and repair and condition assessment of concrete structures. Recently a second task group report has been published that addresses aging of concrete structures used to construct nuclear power plant fuel cycle facilities [121]. ORNL personnel have been major contributors to each of these reports and have participated in several of the workshops.

To assist Member States in understanding aging of structures, systems, and components important to safety, the Safety Division of the International Energy Agency (IAEA) initiated pilot studies related to evaluation and management of the safety aspects of nuclear power plant aging. Concrete containment buildings were included in these studies. Under Phase I, assessments of the current knowledge on age-related degradation, and its detection and mitigation, were

conducted, and recommendations developed for Phase II studies. Phase II activities (comprehensive aging studies) were implemented through IAEA Co-ordinated Research Programs (CRPs) that took place over a three- to five-year period. Under the CRP involving nuclear power plant concrete containment buildings two primary activities took place. The first activity developed a questionnaire that was sent to approximately 200 plant owners/operators to obtain information regarding aging and its management (i.e., general plant information; inspection, investigation, and preventative maintenance; and age-related degradation experience). Responses representing over 150 nuclear power units were provided from 15 countries. General conclusions resulting from responses were that over half the plants responding had some form of aging management program in place, but only about 10% addressed the concrete structures; visual examinations, leakage-rate testing, and testing of post-tensioning systems were the commonly used methods of inspection; utilities whose containments were instrumented generally used longer inspection intervals; and concrete cracking was the most common form of degradation. Under the second activity results of the questionnaire and experience of the CRP participants were used to identify current practices for detecting and mitigating the effects of aging, and to provide the technical basis for developing and implementing a systematic aging management program for concrete containment buildings. Drawing on international experience and best practice, a framework for an aging management program for concrete containment buildings was developed that is based on an understanding of the issues involved [122]. In a related activity, an aging management program for metal components of boiling-water reactor systems was also developed [123]. ORNL personnel have been major contributors to both these reports.

ORNL personnel have also been actively involved in a number of American Concrete Institute and American Society of Mechanical Engineers technical committees. This has included Chairpersons of two committees (ACI 361, "Composite Concrete and Steel Pressure Vessels for General Industrial Use," and ACI 126, "Database Formats for Concrete Materials Properties") and Secretary of ACI 365, "Service Life Prediction." ORNL have been one of the primary authors of several technical reports issued by these committees [ACI 361 R-86, "Composite Concrete and Steel High-Pressure Vessels for General Industrial Use;" ACI 365.1 R-00 "State-of-the-Art Report on Service Life of Concrete;" ACI 126.1R-97, "Guide to a Recommended Format for the Identification of Concrete in a Materials Property Database;" and ACI 126.3-99, "Guide to Recommended Format for Concrete in a Materials Property Database"). Work conducted under the Structural Aging Program has been incorporated into ACI 349.3R-96, "Evaluation of Existing Nuclear Safety-Related Concrete Structures." ORNL also participates in American Society of Mechanical Engineers Section XI technical committees (Working Group on Containment and Subgroup on Plant Life Extension).

4. REFRENCES

1. C.P. Tan, *Prestressed Concrete in Nuclear Pressure Vessels, A Critical Review of Current Literature*, ORNL-4227, Oak Ridge National Laboratory, Oak Ridge, Tenn. (May 1968).

2. C.P. Tan, *A Study of the Design and Construction Practices of Prestressed Concrete and Reinforced Concrete Containment Vessels*, Final Report F-C2121, ORNL Subcontract No. 2997, Franklin Institute Research Laboratories, Philadelphia (August 1969).

3. W.L. Greenstreet, C.B. Oland, J.P. Callahan and D.A. Canonico, *Feasibility Study of Prestressed Concrete Pressure Vessels for Coal Gasification*, ORNL-5312, Oak Ridge National Laboratory, Oak Ridge, Tenn. (1977).

4. V.V. Bertero and M. Polivka, "Influence of Thermal Properties on Mechanical Characteristics of Concrete," Paper SP 34-28 in ACI Special Publication SP-34, *Concrete for Nuclear Reactors*, Vol. I, American Concrete Institute, Detroit (1972).

5. C.B. Oland and J.P. Callahan, *Bond Between Concrete and Steel Reinforcement at Temperatures to 149°C (300°F)*, ORNL/TM-6086, Oak Ridge National Laboratory, Oak Ridge, Tenn. (April 1978).

6. J.P. Callahan and G.C. Robinson, "Uniaxial Compressive Strengths of Concrete for Temperatures Reaching 1033 K", *Nuclear Engineering and Design* 45, pp. 439-448, North-Holland Publishing Company (1978).

7. C.B. Oland, D.J. Naus and G.C. Robinson, *Final Report of Comprehensive Testing Program for Concrete at Elevated Temperatures*, ORNL/BRP-80/5, Oak Ridge National Laboratory, Oak Ridge, Tenn. (October 1980).

8. H.C. Hirth, Jr., M. Polivka and D. Pirtz, *Final Report on Thermal Properties of Concrete at Elevated Temperatures*, ORNL/BRP-81/1/R1, University of California at Berkeley (August 1984).

9. T.W. Kennedy, *An Evaluation and Summary of a Study of the Long-Term Multiaxial Creep Behavior of Concrete*, Research Report 3899-2, ORNL Subcontract No. 3661, University of Texas at Austin (December 1975).

10. J.E. McDonald, *Time-Dependent Deformation of Concrete Under Multiaxial Stress Conditions*, ORNL/TM-5052, Oak Ridge National Laboratory, Oak Ridge, Tenn. (October 1975).

11. J.M. Corum and J.E. Smith, *Use of Small Models in Design and Analysis of Prestressed-Concrete Reactor Vessels*, ORNL-4346, Oak Ridge National Laboratory, Oak Ridge, Tenn. (May 1970).

12. G.D. Whitman, J.P. Callahan and J.M. Corum, "An Investigation of the Time-Dependent Behavior of Prestressed Concrete Pressure Vessels," Paper SP 34-39 in ACI Special Publication SP-34, *Concrete for Nuclear Reactors*, Vol. II, American Concrete Institute, Detroit (1972).

13. J.D. Reins, J.L. Quiros, Jr., W.C. Schnobrich, and M.A. Sozen, *Shear Strength of End Slabs of Prestressed Concrete Nuclear Reactor Vessels*, ORNL/SUB/4164-1, Oak Ridge National Laboratory, Oak Ridge, Tenn. (July 1976).

14. H.O. Abdulrahman, M.A. Sozen and W.C. Schnobrich, *An Analytical Model for Shear Strength of End Slabs of Prestressed Concrete Nuclear Reactor Vessels*, Report No. UILU-ENG-78-2026, ORNL Subcontract 4164, University of Illinois, Urbana (April 1979).

15. J.E. McDonald, *Moisture Migration in Concrete*, ORNL-TM-5051, Oak Ridge National Laboratory, Oak Ridge, Tenn. (May 1975).

16. W.G. Dodge, G.C. Robinson and J.P. Callahan, *GCFR 1/15-Scale PCRV Steam Generator Cavity Closure Model Test*, ORNL/TM-6005, Oak Ridge National Laboratory, Oak Ridge, Tenn. (April 1978).

17. G.C. Robinson, W.G. Dodge and J.P. Callahan, *GCFR 1/15-Scale PCRV Steam-Generator Cavity Closure Half-Thickness Model Test*, ORNL/TM-6461, Oak Ridge National Laboratory, Oak Ridge, Tenn. (December 1978).

18. G.C. Robinson, J.R. Dougan and D.J. Naus, "Test of Small-Scale Central Core Cavity Closure Model for a 300 MW(e) GCFR," in *Proc. of Sixth International Conference on Structural Mechanics in Reactor Technology*, Paper H4/5, Paris, France (August 1981).

19. D.J. Naus, *Structural Model Testing for Prestressed Concrete Pressure Vessels: A Study of Grouted vs Nongrouted Posttensioned Prestressing Tendon Systems*, ORNL/TM-6478, Oak Ridge National Laboratory, Oak Ridge, Tenn. (April 1979).

20. D.J. Naus, *An Evaluation of the Effectiveness of Selected Corrosion Inhibitors for Protection of Prestressing Steels in PCPVs*, ORNL/TM-6479, Oak Ridge National Laboratory, Oak Ridge, Tenn. (March 1979).

21. D.J. Naus, "Acoustic Emission Monitoring of Steel and Concrete Structural Elements with Particular Reference to Primary Nuclear Containment Structures," *Proc. of International Conference on Acoustic Emission*, Anaheim, California, Dunhart Publishers, September 10-13, 1979.

22. *ASME Boiler and Pressure Vessel Code*, The American Society of Mechanical Engineers, New York, New York, 2001.

23. D.J. Naus, *Test Plan for High-Strength Concrete Evaluations in Support of HTGR-SC/C Prestressed Concrete Reactor Vessel Design*, ORNL/GCR-83/3, Oak Ridge National Laboratory, Oak Ridge, Tenn. (May 1983).

24. D.J. Naus and C.B. Oland, *Final Report: Phase I Development and Evaluation of High-Strength Concrete Mix Designs in Support of the HTGR Prestressed Concrete Reactor Vessel Design*, HTGR-85-046(ORNL/GCR-85/7), Oak Ridge National Laboratory, Oak Ridge, Tenn. (July 1985).

25. C.B. Oland, "Testing of Plain and Fibrous Concrete Single-Cavity Prestressed Concrete Reactor Vessel Models," in *Proc. of 8th International Conference on Structural Mechanics in Reactor Technology*, Paper H1/1, Brussels, Belgium (August 19-23, 1985).

26. D.J. Naus, *A Review of Prestressed Concrete Reactor Vessel Related Structural Model Tests*, ORNL/GCR-80/10, Oak Ridge National Laboratory, Oak Ridge, Tenn. (June 1980).

27. C.B. Oland, *Structural Response Testing of Thermal Barrier Hard Ceramic Materials*, ORNL/GCR-82/10, Oak Ridge National Laboratory (June 1982).

28. C.B. Oland and D.J. Naus, *Room-Temperature Testing of Fused Silica Thermal Barrier Hard Ceramic Pad Materials*, ORNL/GCR-84/7, Oak Ridge National Laboratory, Oak Ridge, Tenn. (September 1984).

29. R.K. Nanstad, *A Review of Concrete Properties for Prestressed Concrete Pressure Vessels*, ORNL/TM-5497, Oak Ridge National Laboratory, Oak Ridge, Tenn. (October 1976).

30. D.J. Naus, *Task 2: Concrete Properties in Nuclear Environment - A Review of Concrete Material Systems for Application to Prestressed Concrete Pressure Vessels*, ORNL/TM-7632, Oak Ridge National Laboratory, Oak Ridge, Tenn. (May 1981).

31. D.J. Naus, *Steel Reinforcement and Prestressing for Prestressed Concrete Pressure Vessels*, ORNL/GCR-80/28, Oak Ridge, Tenn. (December 1980).

32. D.J. Naus, *Liner, Cooling, and Insulation Systems for Prestressed Concrete Pressure Vessels*, ORNL/GCR-81/4, Oak Ridge National Laboratory (April 1981).

33. D.J. Naus, *Monitoring of Prestressed Concrete Pressure Vessels. 1. An Overview of Concrete Embedment Strain Instrumentation and Calibration Test Results for Selected Concrete Embedment Strain Meters*, ORNL/TM-6191/V1, Oak Ridge National Laboratory, Oak Ridge, Tenn. (June 1978).

34. D.J. Naus, *Monitoring of Prestressed Concrete Pressure Vessels. 2. Performance of Selected Concrete Embedment Strain Meters Under Normal and Extreme Environmental Conditions*, ORNL/TM-6191/V2, Oak Ridge National Laboratory, Oak Ridge, Tenn. (October 1978).

35. H.L. Gotschall, J.E. Roberts and J.P. Callahan, *Plan for Development of an Optimized PCRV for HTGR Power Plant*, ORNL/TM-6606, Oak Ridge National Laboratory, Oak Ridge, Tenn. (June 1979).

36. D. J. Naus, "Section 3.0, Structural Component Development and Testing," pp. 35-44; and "Section 9.3.3, Evaluation of Pressure Vessels for Modular HTRs (with H. I. Bowers)," pp. 210-211 in *Gas-Cooled Reactor Programs, High-Temperature Gas-Cooled Reactor Base Technology Program Progress Report for Period Ending December 31, 1983*, ORNL-5960, Oak Ridge National Laboratory (June 1983).

37. D.J. Naus, *An Evaluation of Pressure Vessel Concepts for Application to High-Temperature Gas-Cooled Modular Reactor Systems*, ORNL/GCR-82/12, Oak Ridge National Laboratory, Oak Ridge, Tenn. (July 1982).

38. *Code of Federal Regulations*, 10 CFR Part 50, Office of Federal Register Washington, D.C. (1995).

39. J.R. Dougan, *Evaluation of Inservice Inspections of Greased-Prestressing Tendons*, ORNL/TM-8278, Oak Ridge National Laboratory, Oak Ridge, Tenn. (September 1982).

40. D. J. Naus, *Regulatory Analysis of Regulatory Guide 1.35 (Revision 3, Draft 2)- In-Service Inspection of Ungrouted Tendons in Prestressed Concrete Containments*, NUREG/CR-4712 (ORNL/TM-10163), Oak Ridge National Laboratory, Oak Ridge, Tenn. (February 1987).

41. *Requirements for Class CC Concrete Components of Light-Water Cooled Plants*, Section XI, Subsection IWL in *American Society of Mechanical Engineers Boiler and Pressure Vessel Code*, 1992 edition with Addenda, New York, 1995.

42. American National Standards Institute, "Containment System Leakage Testing Requirements," ANSI/ANS-56.8, sponsored by American Nuclear Society, LaGrange Park, Illinois, February 1981.

43. J.R. Dougan, *Evaluation of Containment Leak Rate Testing Criteria*, ORNL/TM-8909, Oak Ridge National Laboratory, Oak Ridge, Tenn. (March 1984).

44. F.E. Gregor and C.J. Hookham, "Remnant Life Preservation of LWR Plant Structures,: Transactions of 12 International Conference on Structural Mechanics in Reactor Technology, Paper DH06/2, Elsevier, Amsterdam, The Netherlands, pp. 453-45, (August 1993).

45. H. Ashar, D.J. Naus and C.P. Tan, "Prestressed Concree in U.S. Nuclear Power Plants," Concrete International 16(5), pp. 30-34, Farmington Hills, Michigan (1994).

46. D.J. Naus, *Concrete Material Systems in Nuclear Safety Related Structures - A Review of Factors Relating to their Durability, Degradation Detection and Evaluation, and Remedial Measures of Areas of Distress*," Appendix B in The Longevity of Nuclear Plant Systems by I. Spiewak and R. S. Livingston, EPRI NP-4208, Electric Power Research Institute, Palo Alto, CA, pp. B1-B6 (August 1985).

47. D.J. Naus, *Concrete Component Aging and Its Significance Relative to Life Extension of Nuclear Power Plants*, NUREG/CR-4652 (ORNL/TM-10059), Oak Ridge National Laboratory, Oak Ridge, Tenn. (September 1986).

48. D.J. Naus, C. B. Oland, and B.R. Ellingwood, *Report on Aging of Nuclear Power Plant Reinforced Concrete Structures*, NUREG/CR-6424 (ORNL/TM-13148), Lockheed Martin Energy Research Corp., Oak Ridge National Laboratory, Oak Ridge, Tenn. (March 1996).

49. C.B. Oland, *The Structural Materials Information Center and Its Potential Applications*, ORNL/NRC/LTR-92/8, Martin Marietta Energy Systems, Inc., Oak Ridge National Laboratory, Oak Ridge, Tenn. (May 1992).

50. C.B. Oland, and D.J. Naus, *Summary of Materials Contained in the Structural Materials Information Center*, ORNL/NRC/LTR-94/22, Martin Marietta Energy Systems, Inc., Oak Ridge National Laboratory, Oak Ridge, Tenn. (November 1994) .

51. J.R. Clifton, *Predicting the Remaining Service Life of Concrete*, NISTIR 4712, National Institute of Standards and Technology, U.S. Department of Commerce, Gaithersburg, Maryland (November 1991).

52. H.T. Hill, *Concrete Containment Posttensioning System Aging Study,* ORNL/NRC/LTR-95/13, Lockheed Marietta Energy Systems, Inc., Oak Ridge National Laboratory, Oak Ridge, Tenn. (August 1995).

53. D.J. Naus and C.B. Oland, "An Investigation of Tendon Sheathing Filler Migration Into Concrete," NUREG/CR-6598 (ORNL/TM-13554), Lockheed Martin Energy Research Corp., Oak Ridge National Laboratory, Oak Ridge, Tenn. (March 1998).

54. C.J. Hookham, *Structural Aging Assessment Methodology for Concrete Structures in Nuclear Power Plants,* ORNL/NRC/LTR-90/17, Multiple Dynamics Corporation, Southfield, Michigan (Subcontract Report 11X-SD343V), Oak Ridge National Laboratory, Oak Ridge, Tenn. (March 1991).

55. T.M. Refai and M.K. Lim, *Inservice Inspection and Structural Integrity Assessment Methods for Nuclear Power Plant Concrete Structures,* ORNL/NRC/LTR-90/29 (Subcontract Report 17X-SE611V from Construction Technology Laboratories, Inc., Skokie, Illinois), Martin Marietta Energy Systems, Inc., Oak Ridge National Laboratory, Oak Ridge, Tenn. (September 1991).

56. K.A. Snyder, J.R. Clifton and N.J. Carino, *Nondestructive Evaluation of the In-Place Compressive Strength of Concrete Based Upon Limited Destructive Testing,* NISTIR 4874, National Institute of Standards and Technology, U.S. Department of Commerce, Gaithersburg, Md (July 1992).

57. W.F. Price et al., *Review of European Repair Practice for Corrosion Damaged Reinforced Concrete,* Report No. 1303/91/5823 (Subcontract No. 31X-SH469V), Taywood Engineering Ltd., London, England (April 1993).

58. P.D. Krauss, *Repair Materials and Techniques for Concrete Structures in Nuclear Power Plants,* ORNL/NRC/LTR-93/28 (Subcontract90X-SJ024C with Wiss, Janney, Elstner, and Associates, Inc. Northbrook, Illinois), Martin Marietta Energy Systems, Inc., Oak Ridge National Laboratory, Oak Ridge, Tenn. (March 1994).

59. C.J. Hookham, *In-Service Inspection Guidelines for Concrete Structures in Nuclear Power Plants,* ORNL/NRC/LTR-95/14, Lockheed Marietta Energy Systems, Inc., Oak Ridge National Laboratory, Oak Ridge, Tenn. (December 1995).

60. *Guidelines for Structural Condition Assessment of Existing Buildings,* ANSI/ASCE 11-90, American Society of Civil Engineers, New York, New York (August 1, 1991).

61. American Concrete Institute, "Guide for Making a Condition Survey of Concrete In-Service," pp. 905–918 in *Proceedings of American Concrete Institute,* 65(11), Farmington Hills, Michigan (November 1968).

62. Y. Mori and B.R. Ellingwood, "Maintaining Reliability of Concrete Structures I: Role of Inspection/Repair," pp. 824-845 in *Journal of Structural Engineering,* 120(3), American Society of Civil Engineers, New York (1994).

63. Y. Mori and B.R. Ellingwood, "Maintaining Reliability of Concrete Structures II: Optimum Inspection/Repair Strategies," pp. 846-862 in *Journal of Structural Engineering,* 120(3), American Society of Civil Engineers, New York (1994).

64. Y. Mori, *Reliability-Based Condition Assessment and Life Prediction of Concrete Structures,*" thesis presented to The Johns Hopkins University, Baltimore, Maryland, in partial fulfillment of the requirements for the degree of Doctor of Philosophy, (1992).

65. *Building Code Requirements for Reinforced Concrete,* ACI Standard 318-71, American Concrete Institute, Farmington Hills, Michigan (November 1971).

66. *Code Requirements for Nuclear Safety Related Concrete Structures,* ACI Standard 349–85(90), Farmington Hills, Michigan (1990).

67 B.R. Ellingwood, and Y. Mori, "Probabilistic Methods for Condition Assessment and Life Prediction of Concrete Structures in Nuclear Power Plants," pp. 155-166 in *Nuclear Engineering and Design* 142, Elsevier Science S.A., North-Holland, Amsterdam. The Netherlands (1993).

68. Y. Mori and B.R. Ellingwood, *Reliability Assessment of Degrading Concrete Shear Walls,* ORNL/NRC/LTR-94/6, Martin Marietta Energy Systems, Inc., Oak Ridge National Laboratory, Oak Ridge, Tennessee, 1994c.

69. F. Barda, J.M. Hanson, and W.G. Corley, "Shear Strength of Low-Rise Walls with Boundary Element," in *Reinforced Concrete Structures in Seismic Zones,* ACI SP-53, American Concrete Institute, Farmington Hills, Michigan (1977).

70. I. Shiraishi, N. Shirai, T. Murakami, and K. Minami, "Macroscopic Models for R/C Shear Walls," pp. 271 280 in *Proc. of Structural Congress, Structural Design, Analysis, and Testing*, American Society of Civil Engineers, New York, New York,(1989).

71. R. Shohara, N. Shirai, and H. Noguchi, "Verification of Macroscopic Models for R/C Walls," pp. 281-290 in *Proc. of Structural Congress, Structural Design, Analysis, and Testing*, American Society of Civil Engineers, New York, New York (1989).

72. F. Watanabe, and T. Ichinose, "Strength and Ductility Design of RC Members Subjected to Combined Bending and Shear," pp. 429-438 in *Concrete Shear in Earthquake,* Eds. T. C. C. Hsu and S. T. Mau, Elsevier Applied Science, New York, New York (1992).

73. W.F. Chen, and D.J. Han, *Plasticity for Structural Engineers,* Spring-Vartag, New York (1988).

74. F.P. Vecchio and M.P. Collins, "The Modified Compression-Field Theory for Reinforced Concrete Elements Subjected to Shear," American Concrete Institute 83(2), pp. 219-231 (1986).

75. A.E. Cardenas et al., "Design Provisions for Shear Walls," *Journal American Concrete Institute* 70(3), pp. 221 -230, 4, Farmington Hills, Michigan,(1973).

76. J.G. MacGregor, A. Mirza, and B.R. Ellingwood, "Statistical Analysis of Resistance of Reinforced and Prestressed Concrete Members," pp. 167-176 in *Journal of American Concrete Institute* 80(3), Farmington Hills, Michigan (1983).

77. G.W. Washa, J.C. Saemann, and S.M. Cramer, "Fifty-Year Properties of Concrete Made in 1937," pp. 367 371 *in ACI Materials Journal* 86(4), American Concrete Institute, Farmington Hills, Michigan (1989).

78. H. Madsen, J.D. Sorenson, and R. Olesen, "Optimal Inspection Planning for Fatigue Damage of Offshore Structures," pp. 2099-2106 in *Proceedings of ICOSSAR '89, Vol.* III, American Society of Civil Engineers, New York, New York (1989).

79. J. Yang, "Application of Reliability Methods to Fatigue, Quality Assurance, and Maintenance," pp. 3-18 in *Proceedings of ICOSSAR '93, Vol.* I, A. A. Balkema, Rotterdam, The Netherlands (1994).

80. C.B. Oland, "Nuclear Power Plant Containment Metallic Pressure Boundary Materials and Plans for Collecting and Presenting Their Properties," ORNL/NRC/LTR-95/2, Martin Marietta Energy Systems, Inc., Oak Ridge National Laboratory, Oak Ridge, Tennessee (1995).

81. D.J. Naus and H.L. Graves, III, "Detection of Aging of Nuclear Power Plant Structures," *Workshop on the Instrumentation and Monitoring of Concrete Structures*, Nuclear Safety NEA/CSNI/R(2000)15, pp. 19-58, Nuclear Energy Agency, Issy-les-Moulineaux, France (22-23 March 2000).

82. M. F. Marchbanks and C. B. Oland, *Considerations in the Formulation of a Customized Data Base for Structural Materials,* ORNL/NRC/LTR-94/20, Martin Marietta Energy Systems, Inc., Oak Ridge National Laboratory, Oak Ridge, Tennessee (November 1994).

83. C.B. Oland and D.J. Naus, *Degradation Assessment Methodology for Application to Steel Containments and Liners of Reinforced Concrete Structures in Nuclear Power Plants*, ORNL/NRC/LTR-95/29, Lockheed Martin Energy Research Corporation, Oak Ridge National Laboratory, Oak Ridge, Tennessee (1996).

84. American Society of Mechanical Engineers "Rules for Inservice Inspection of Nuclear Power Plant Components," *ASME Boiler and Pressure Vessel Code*, Section XI, Division 1, Subsection IWE, Requirements for Class MC and Metallic Liners of Class CC Components of Light-Water Cooled Power Plants, American Society of Mechanical Engineers, New York, New York (1995).

85. W.E. Norris, D.J. Naus and H.L. Graves, III, "Inspection of Nuclear Power Plant Containment Structures," *Nuclear Engineering and Design* 192, pp. 303-329 (1999).

86. R.E. Beissner and A.S. Birring, "Nondestructive Evaluation Methods for Characterization of Corrosion," NTIAC-88-1, Nondestructive Testing Information Analysis Center, San Antonio, Texas (December 1988).

87. "Corrosion," *ASM Handbook*, ASM International, Materials Park, Ohio (1992).

88. D.J. Naus and C.J. Hookham, "Condition Assessment of Concrete Structures in Nuclear Power Plants," in *State-Of-The-Art: Considerations for Use In Managing the Aging of Nuclear Power Plant Concrete Structures*, Report No. 19, International Union of Testing and Research Laboratories for Materials and Structures (RILEM), Cachan Cedex, France (1999).

89. J.E. Bondaryk, C.N. Corrado and V. Godino, *Feasibility of High Frequency Acoustic Imaging for Inspection of Containments*, NUREG/CR-6614, U.S. Nuclear Regulatory Commission, Washington, DC (1998).

90. J. Rudzinsky, J. Bondarek and M. Conti, *Feasibility of High Frequency Acoustic Imaging for Inspection of Containments: Phase II,"* ORNL/NRC/LTR-99/11, Oak Ridge National Laboratory, Oak Ridge, Tennessee (1999).

91. H. Kwun, "Long-Range Volumetric Inspection of Tubing Using the Magnetostrictive Sensor Technique," *4th EPRI Balance of Plant Nondestructive Evaluation Symposium*, Jackson Hole, Wyoming (1996).

92. H. Kwun, *Feasibility of Magnetostrictive Sensor Inspecion of Containments*, NUREG/CR-5724, U.S. Nuclear Regulatory Commission, Washington, DC (1999).

93. D.N. Alleyne and P. Cawley, "The Interaction of Lamb Waves with Defects," *IEEE Transactions on Ultrasonics, Ferro Electrics, and Frequency Control* 39(3), pp. 381-397 (1992).

94. D.N. Alleyne and P. Cawley, "The Long-Range Detection of Corrosion in Pipes Using Lamb Waves," *Review of Progress in Quantitative NDE*, pp. 2075-2080, Plenum Press. (1995).

95. Y. Cho, Y. and J.L. Rose, "Guided Waves in Water Loaded Hollow Cylinder," *Nondestructive Testing & Evaluation* 12, pp. 323-339 (1996).

96. J.L. Rose, D. Jiao and J. Spanner, Jr., "Ultrasonic Guided Wave NDE for Piping," *Materials Evaluation* 54(11), pp. 1310-1313 (1996).

97. M. Quarry and J.L. Rose, "Multimode Guided Wave Inspection of Piping Using Comb Transducers," *Materials Evaluation* 57(10), pp. 1089-1090 (1999).

98. J. Li and J.L. Rose, *Guided Wave Inspection of Containment Structures*, Engineering Science and Mechanics Department, The Pennsylvania State University, University Park, Pennsylvania (2000).

99. C.B. Oland and D.J. Naus, *A Survey of Repair Practices for Nuclear Power Plant Containment Metallic Pressure Boundaries*, NUREG/CR-6615, U.S. Nuclear Regulatory Commission, Washington, DC (1998).

100. B.R.Ellingwood, et al., *Reliability-Based Condition Assessment of Steel Containments and Liners*, NUREG/CR-5442, U.S. Nuclear Regulatory Commission, Washington, DC (1996).

101. L.G. Greimann, et al., *Reliability Analysis of Steel Containment Strength*, NUREG/CR-2442, U.S. Nuclear Regulatory Commission, Washington, DC (1982).

102. D.J. Naus, C.B. Oland, B. Ellingwood, Y. Mori and D.G. Arndt, "An Overview of the ORNL/NRC Program to Address Aging of Concrete Structures in Nuclear Power Plants," pp. 327-339 in *Nuclear Engineering and Design* 142, Elsevier, North-Holland (1993).

103. B.R. Ellingwood and B. Bhattacharya, "Reliability-Based Condition Assessment and Service Life Prediction of Steel Containments and Liners." pp. 39-46 in *Trans. of 14th International Conference on Structural Mechanics in Reactor Technology*, Vol. 10 (1997).

104. H. Hwang, H., et al., "Probability-Based Design Criteria for Nuclear Plant Structures," pp. 925-942 in *Journal Structural Engineering*, American Society of Civil Engineers, New York, New York, 113(5) (1985).

105. J. Lemaitre, "How to Use Damage Mechanics," pp. 233-245 in *Nuclear Engineering and Design* 80, Elsevier, North-Holland (1984).

106. B.R. Ellingwood and B. Bhattacharya, (1996). "A Damage Mechanics-Based Approach to Structural Deterioration." pp. 588-591 in *Proceedings llth Engineering Mechanics Specialty Conference*, American Society of Civil Engineers, New York, New York (1996).

107. B. Bhattacharya and B.R. Ellingwood, "A CMD-Based Approach to Stochastic Damage Growth." pp. 772-775 in *Proceedings 7th Specialty Conf. on Probabilistic Methods and Structural Reliability*, American Society of Civil Engineers, New York, New York (1996).

108. B.R. Ellingwood, "Probability-Based Codified Design: Past Accomplishments and Future Challenges." *Strucural. Safety* 13(3), pp. 159-176 (1994).

109. USNRC. *An Approach for Using Probabilistic Risk Assessment in Risk-Informed Decisions on Plant-Specific Changes to the Licensing Basis*, Regulatory Guide 1.174, U.S. Nuclear Regulatory Commission, Washington, DC (1998).

110. B.R. Ellingwood and H. Hwang, "Probabilistic Descriptions of Resistance of Safety-Related Structures in Nuclear Plants." *Nuclear Engineering and Design* 88(2), pp. 169-178 (1986).

111. B.R. Ellingwood, J.L. Cherry and D.J. Naus, D.J., "Fragility Modeling of a Steel Containment with Localized Corrosion," *Proceedings of Computer Technology-1999*, ASME PVP-385, American Society of Mechanical Engineers, New York, New York, pp. 101-105 (1999).

112. USNRC. *Severe Accident Rates: An Assessment for Five U.S. Nuclear Power Plants*, NUREG-1150, U.S. Nuclear Regulatory Commission, Washington, DC (1989).

113. W.A. Von Riesemann and M.B. Parks, M.B., "Current State of Knowledge on the Behavior of Steel Liners in Concrete Containments Subjected to Overpressurization Loads," *Nuclear Engineering and Design* 157, pp. 481-487 (1995).

114. J.D. Miller, *Analysis of Shell-Rupture Failure Due to Hypothetical Elevated-Temperature Pressurization of the Sequoyah Unit 1 Steel Containment Building*, NUREG/CR-5405, U.S. Nuclear Regulatory Commission, Washington, DC (1990).

115. J.L. Cherry, "Analyses of Containment Structures With Corrosion Damage," *Proceedings of 24th Water Reactor Safety Information Meeting*, NUREG/CP-0157, U.S. Nuclear Regulatory Commission, Washington, DC (1997)

116. M.W. Pilch, M.D. Allen and E.W. Klamerus, *Resolution of the Direct Containment Heating Issue for All Westinghouse Plants With Large Dry Containments or Subatmospheric Containments*, NUREG-6338, U.S. Nuclear Regulatory Commission, Washington, DC (1995).

117. D. J. Naus (Editor), *State-Of-The-Art: Considerations for Use In Managing the Aging of Nuclear Power Plant Concrete Structures*, Report No. 19, International Union of Testing and Research Laboratories for Materials and Structures (RILEM), Cachan Cedex, France (September 1999).

118. T. Jávor (Editor), *RILEM-IMEKO International Conference on Diagnosis of Concrete Structures,* EXPERTCENTRUM CZECHOSLOVAKIA, Slovak Technical University, Bratislava, Slovakia (1999).

119. D. J. Naus (Editor), *Proc. of International RILEM Workshop on Aging Management and Life Prediction of Concrete Structures*, Cannes, France, PRO 16, RILEM Publications S.A.R.L., Cachan, France (2000).

120. "Report of the Task Group Reviewing International Activities in the Area of Ageing of Nuclear Power Plant Concrete Structures,"NEA/CSNI/R(95)19, Nuclear Energy Agency of the Organisation of Economic Cooperation and Development, Issy-les-Moulineaux, France (November 1995).

121. "Report of Task Group Reviewing Activities in the Area of Ageing of Concrete Structures Used to Construct Nuclear Power Plant Fuel Cycle Facilities," NEA/CSNI/R(2002)14, Nuclear Energy Agency, Organization for Economic Cooperation and Development, Paris, France (10 July 2002).

122. Assessment and Management of Ageing of Major Nuclear Power Plant Components Importantto Safety: *Concrete Containment Buildings*, IAEA-TECDOC-1025, International Atomic Energy Agency, Vienna, Austria (June 1998).

123. *Assessment and Management of Ageing of Major Nuclear Power Plant Components Important to Safety: Metal Components of BWR Containment Systems,* IAEA-TECDOC-1181, InternationalAtomic Energy Agency, Vienna, Austria (October 2000).

Internal Distribution

1. E. E. Bloom
2. J. M. Corum
3. E. Lara-Curzio
4. L. Dole
5. E. C. Fox
6. R. G. Gilliland
7. G. E. Michaels
8. D. J. Naus
9. C. B. Oland
10. A. E. Pasto
11. C. E. Pugh
12. J. B. Roberto
13. J. J. Simpson
14. R. E. Ziegler
15. ORNL Patent Section
16. Central Research Library
17. Document Reference Section
18. Laboratory Records

External Distribution

19. S. Ali, NRC
20. C. Andrade, IETCC
21. H. G. Ashar, NRC
22. G. Bagchi. NRC
23. G. Barslivo, SwedPower AB
24. G. B. Batson, Clarkson College
25. Z. P. Bazant, Northwestern University
26. G. S. Bedi, NRC
27. A. Bentur, Israel Institute of Technology
28. Z. Bittnar, Czech Technical University
29. J. H. Bungey, Liverpool University
30. J. Carey, EPRI
31. A. Chockie, Chockie Consulting
32. T-Y. Chang, NRC
33. N. C. Chokshi, NRC
34. Commander and Director, USAE Waterways Experiment Station
27. P. Contri, IAEA
28. J. F. Costello, NRC
29. K. Cozens, NEI
30. R. Danisch, Framatome
31. M. A. Daye, Royal Comm. for Jubail and Yanbu
32. R. K. Dhir, University of Dundee
33. C. W. Dolan, University of Wyoming
32. D. H. Dorman, NRC
33. B. R. Ellingwood, Georgia Tech
34. S. W. Forster, Federal Highway Administration
35. W. L. Gamble, University of Illinois
36. M. Geiker, Technical University of Denmark
37. B. Gerard, OXAND
38. H. L. Graves, III, NRC
39. F. E. Gregor, LCM Engineering
40. W. Heep, NOK
41. H. K. Hilsdorf, Consultant
42. G. Imbro, NRC
43. D. C. Jeng, NRC
44. P-T Kuo, NRC
45. K. D. Lauer, University of Notre Dame
46. P. Lenki, Janus Pannonius University
47. T. C. Liu, U.S. Army Corps of Engineers

48. W. D. Magwood, IV, DOE
49. S. Mahadevan, Vanderbilt University
50. K. Manoly, NRC
51. G. Marcus, DOE
52. A. Marchertas, Northern Illinois University
53. E. Mathet, OECD-NEA
54. H. W. Massie, DNFSB
55. M. E. Mayfield, NRC
56. T. McNulty, HSE
57. P. K. Mehta, University of California Berkeley
58. P. K. Mukherjee, INSAAR Services Ltd.
59. H. Müller, Universität Karlsruhe
60. A. J. Murphy, NRC
61. W. E. Norris, NRC
62. R. S. Orr, Westinghouse
63. T. J. Pasko, Jr., Federal Highway Administration Ret.
64. J. Philip, NRC
65. C. D. Pomeroy, Consultant
66. G. D. Reed, UTK
67. H. W. Reinhardt, Stuttgart University
68. D. M. Roy, The Pennsylvania State University
69. A. Sarja, VTT Building Technology
70. V. Schmitz, IzfP
71. U. Schneider, Technical University Wien
72. M. Schupack, Schupask and Associates
73. S. P. Shah, Northwestern University
74. P. Shaw, Force Institute
75. R. E. Shewmaker, NRC
76. L. Smith, British Energy Generation
77. H. Stephens, EPRI
78. J. D. Stevenson, Stevenson and Associates
79. M. G. Stewart, University of Newcastle
81-231. Strategic Development Council – American Concrete Institute
232. P. J. E. Sullivan, Sullivan and Associates
233. R. N. Swamy, University of Sheffield
234. D. Terao, NRC
235. S. Thelandersson, Technical University of Lund
236. M. Velez, University of Missouri Rolla
237. R. M. Versluis, DOE
238. J. P. Vora, NRC
239. A. Y. Wang, Stone and Webster
240. S. Weiner, PNNL
241. R. E. Weyers, Virginia Polytechnic University
242. H. Wiggenhauser, BAM
243. Office of Assistant Manager for Energy Research and Development, DOE-OR
244. Office of Scientific and Technical Information